TR 76-3
Vol. I

Storm Surge Simulation in Transformed Coordinates

VOLUME I

Theory and Application

by

John J. Wanstrath, Robert E. Whitaker,
Robert O. Reid, and Andrew C. Vastano

TECHNICAL REPORT NO. 76-3
NOVEMBER 1976

Approved for public release;
distribution unlimited.

Prepared for
U.S. ARMY, CORPS OF ENGINEERS
COASTAL ENGINEERING
RESEARCH CENTER
Kingman Building
Fort Belvoir, Va. 22060

UNCLASSIFIED

SECURITY CLASSIFICATION OF THIS PAGE *(When Data Entered)*

REPORT DOCUMENTATION PAGE

READ INSTRUCTIONS BEFORE COMPLETING FORM

1. REPORT NUMBER: TR 76-3

2. GOVT ACCESSION NO.:

3. RECIPIENT'S CATALOG NUMBER:

4. TITLE *(and Subtitle)*: STORM SURGE SIMULATION IN TRANSFORMED COORDINATES
VOLUME I. THEORY AND APPLICATION
VOLUME II. PROGRAM DOCUMENTATION

5. TYPE OF REPORT & PERIOD COVERED: Technical Report

6. PERFORMING ORG. REPORT NUMBER:

7. AUTHOR(s): John J. Wanstrath, Robert E. Whitaker, Robert O. Reid, and Andrew C. Vastano

8. CONTRACT OR GRANT NUMBER(s): DACW72-73-C-0014

9. PERFORMING ORGANIZATION NAME AND ADDRESS:
Texas A&M Research Foundation
F.E. Box H
College Station, Texas 77843

10. PROGRAM ELEMENT, PROJECT, TASK AREA & WORK UNIT NUMBERS: A31231

11. CONTROLLING OFFICE NAME AND ADDRESS:
Department of the Army
Coastal Engineering Research Center
Kingman Building, Fort Belvoir, Virginia 22060

12. REPORT DATE: November 1976

13. NUMBER OF PAGES: Vol. I, 166 Vol. II, 176

14. MONITORING AGENCY NAME & ADDRESS *(if different from Controlling Office)*:

15. SECURITY CLASS. *(of this report)*: UNCLASSIFIED

15a. DECLASSIFICATION/DOWNGRADING SCHEDULE:

16. DISTRIBUTION STATEMENT *(of this Report)*

Approved for public release, distribution unlimited.

17. DISTRIBUTION STATEMENT *(of the abstract entered in Block 20, if different from Report)*

18. SUPPLEMENTARY NOTES

19. KEY WORDS *(Continue on reverse side if necessary and identify by block number)*

Computer program
Coordinate transformation
Hurricane Camille
Hurricane Carla
Hurricane Gracie
Numerical modeling
Orthogonal curvilinear coordinates
Storm surge

20. ABSTRACT *(Continue on reverse side if necessary and identify by block number)*

A two-dimensional time-dependent numerical storm surge model using orthogonal curvilinear coordinates is presented. The curvilinear coordinate system is based on a conformal mapping of the interior region bounded by the actual coast, the seaward boundary (taken as the 180-meter depth contour) and two parallel lateral boundaries into a rectangle in the image plane. Three regions of the Continental Shelf of the Gulf of Mexico and two regions of the eastern seaboard of the United States are mapped.

(Continued)

DD FORM 1 JAN 73 1473 EDITION OF 1 NOV 65 IS OBSOLETE

UNCLASSIFIED

SECURITY CLASSIFICATION OF THIS PAGE *(When Data Entered)*

Since the transformation is conformal, the associated modifications of the vertically integrated equations of motion and mass continuity are minimized. The coast, seaward boundary, and the lateral boundaries of the computing grid are straight lines in the image plane thus facilitating the application of the boundary conditions. The final coordinates allow for the greatest resolution near the coast in a central area of principal storm surge development and modification.

The model is employed in the simulation of the storm surge induced by Hurricanes Carla (1961) and Camille (1969) which crossed the gulf coast of the United States and Hurricane Gracie (1959) which crossed the east coast. Analytical interpretations of the wind and atmospheric pressure-forcing functions are used in the computations.

PREFACE

This report is published to provide coastal engineers with the results of a study to develop an operational program for numerical simulation of storm surges on a given segment of the Continental Shelf, using a curvilinear coordinate system. The report consists of two volumes. Volume I discusses the theory and application of the transformation procedure for generating the curvilinear shelf coordinate system for particular regions, and the theory, numerical algorithm, and application of the storm surge program for simulation of Hurricanes Carla (1961), Camille (1969), and Gracie (1959). Volume II presents the program documentation and the coded programs for carrying out the coordinate transformation (CONFORM), for establishing the spatial lattice (GRID), and for carrying out the storm surge calculations on the shelf (SSURGE). The work was carried out under the wave mechanics program of the U.S. Army Coastal Engineering Research Center (CERC).

Volume I of the report was prepared by John J. Wanstrath (who also authored Volume II), Robert E. Whitaker, Robert O. Reid, and Andrew C. Vastano, Department of Oceanography, Texas A&M University, College Station, Texas, under CERC Contract No. DACW72-73-C-0014. Most of the computational work in the development and application was carried out at the National Center for Atmospheric Research which is supported by the National Science Foundation.

The authors express their appreciation to Thomas J. Reid for assistance in program coding, and to Dr. D. Lee Harris, CERC, for very constructive comments on the draft of this report.

Dr. D. Lee Harris, Chief, Oceanography Branch, was the CERC technical monitor of the report, under the general supervision of Mr. R.P. Savage, Chief, Research Division.

Comments on this publication are invited.

Approved for publication in accordance with Public Law 166, 79th Congress, approved 31 July 1945, as supplemented by Public Law 172, 88th Congress, approved 7 November 1963.

JOHN H. COUSINS
Colonel, Corps of Engineers
Commander and Director

CONTENTS

CONTENTS

TABLES

FIGURES

CONTENTS

FIGURES-Continued

CONTENTS

FIGURES-Continued

CONTENTS

FIGURES-Continued

FIGURES-Continued

CONVERSION FACTORS, U. S. CUSTOMARY TO METRIC (SI) UNITS OF MEASUREMENT

U.S. customary units of measurement used in this report can be converted to metric (SI) units as follows:

Multiply	by	To obtain
inches	25.4	millimeters
	2.54	centimeters
square inches	6.452	square centimeters
cubic inches	16.39	cubic centimeters
feet	30.48	centimeters
	0.3048	meters
square feet	0.0929	square meters
cubic feet	0.0283	cubic meters
yards	0.9144	meters
square yards	0.836	square meters
cubic yards	0.7646	cubic meters
miles	1.6093	kilometers
square miles	259.0	hectares
acres	0.4047	hectares
foot-pounds	1.3558	newton meters
ounces	28.35	grams
pounds	453.6	grams
	0.4536	kilograms
ton, long	1.0160	metric tons
ton, short	0.9072	metric tons
degrees (angle)	0.1745	radians
Fahrenheit degrees	5/9	Celsius degrees or Kelvins[1]

[1] To obtain Celsius (C) temperature readings from Fahrenheit (F) readings, use formula: $C = (5/9)(F - 32)$. To obtain Kelvin (K) readings, use forumla: $K = (5/9)(F - 32) + 273.15$.

STORM SURGE SIMULATION IN TRANSFORMED COORDINATES

Volume I. Theory and Application

by

John J. Wanstrath, Robert E. Whitaker, Robert O. Reid, and Andrew C. Vastano

I. INTRODUCTION

1. Background.

Storm surges are transient fluctuations in the sea level induced by atmospheric disturbances, notably those due to extra-tropical storms and hurricanes and to a less frequent extent pressure jumps associated with line squalls. The rise of the water and circulation caused by a hurricane can be considerable and is of special practical importance with respect to loss of lives and property not only adjacent to the coast but also well inland. Statistical studies of hurricanes of record provide a means of predicting the surge height along an open coast. The empirical formulas developed from these studies relate the maximum expected surge height to meteorological parameters and effective coastal bathymetry (Donn, 1958). However, all such studies do not provide the time history or even the time scale of the forcing function which is necessary as input for bay-response studies (Reid and Bodine, 1968).

More recently, time-dependent models based upon the physics of the storm surge phenomena have been developed to study the generation or modification of the surge as it leaves deep water and moves over the Continental Slope and Shelf. These models, like the one proposed herein, involve the vertically integrated equations of motion and mass continuity. The greatest difficulty in utilizing these models has been the manner in which the shoreline has been portrayed and the application of realistic boundary conditions at the specified shore. Jelesnianski (1967, 1972) takes the shoreline as a vertical plane of infinite height, thereby facilitating the mathematical representation of the shore boundary. More general portrayal of the shoreline is achieved by the schemes of Miyazaki (1963) and Platzman (1963) in which the coastline is represented as a series of straight-line segments connected at right angles. Specifying the shoreline in this stairstep manner results in greater numerical programing complexity for the shore boundary condition in that the algorithm must possess the ability to search for and substantiate the location of land. A more serious objection is that this approximation may inject spurious oscillations into the calculations. This adverse effect is more than academic since the concentration of energy is near its maximum at the coast, and further, this is precisely the region from which water level observations are usually available for model verification.

Clearly, these difficulties are avoided or minimized if a curvilinear coordinate system is employed which will map the interior region bounded by the actual coastline, the seaward boundary (taken as the 180-meter depth contour) and two lateral straight lines. Thus, the transformation is such that the coast, as well as the 180-meter isobath, is mapped as a straight line in the image plane. In order to minimize the associated modification of the differential equations governing the storm surge, an orthogonal curvilinear system is employed in the present study, the desired mapping being carried out via a conformal transformation.

2. Objectives.

The objectives are twofold: (a) to develop a method which will conformally map the interior region bounded by two arbitrarily shaped curves each beginning and ending on parallel straight lines drawn between the two curves; (b) to develop and verify a numerical model of a hurricane-induced surge on the Continental Shelf employing the transformed equations of motion in the orthogonal curvilinear coordinate system.

II. CONFORMAL MAPPING

1. Development.

The selection of appropriate conformal mapping and error functions is of principal concern in achieving the first stated objective. We desire to map a region R of the Z-plane into a rectangle in the ζ-plane (Figure 1), in which the seaward boundary and coastline curves are specifically transformed into the image plane as constant values of η. Furthermore, the curves in the negative x region are required to be the mirror image of those in the positive x region. As an artifice to assure that the lateral boundaries of the mapped region represent straight parallel lines normal to the shoreline and the seaward boundary, symmetry about one of these boundaries ($x = 0$) is imposed and the whole range in x ($-\lambda$ to λ) is considered to be one wavelength of a periodic function. Thus only the range $0 < x < \lambda$ in the top panel of Figure 1 corresponds to the real region of the shelf.

The conformal mapping relation is taken in the form:

$$Z = F(\zeta) , \tag{1}$$

where

$$Z = x + iy , \tag{2}$$

$$\zeta = \xi + i\eta , \tag{3}$$

and

$$i = \sqrt{-1} . \tag{4}$$

An appropriate form of the transformation for the mapping considered in Figure 1 is:

$$F(\zeta) = P_o + Q_o\zeta + \sum_{n=1}^{N} (P_n \cos nk\zeta + Q_n \sin nk\zeta) , \tag{5}$$

where

$$k = \pi/\lambda , \tag{6}$$

and λ is half the horizontal extent of the region in the Z, or ζ plane. The coefficients P_n and Q_n, $n=0,1...N$, are, in general, complex and independent of ξ or η. Let

$$P_n = A_n + iB_n , \tag{7}$$

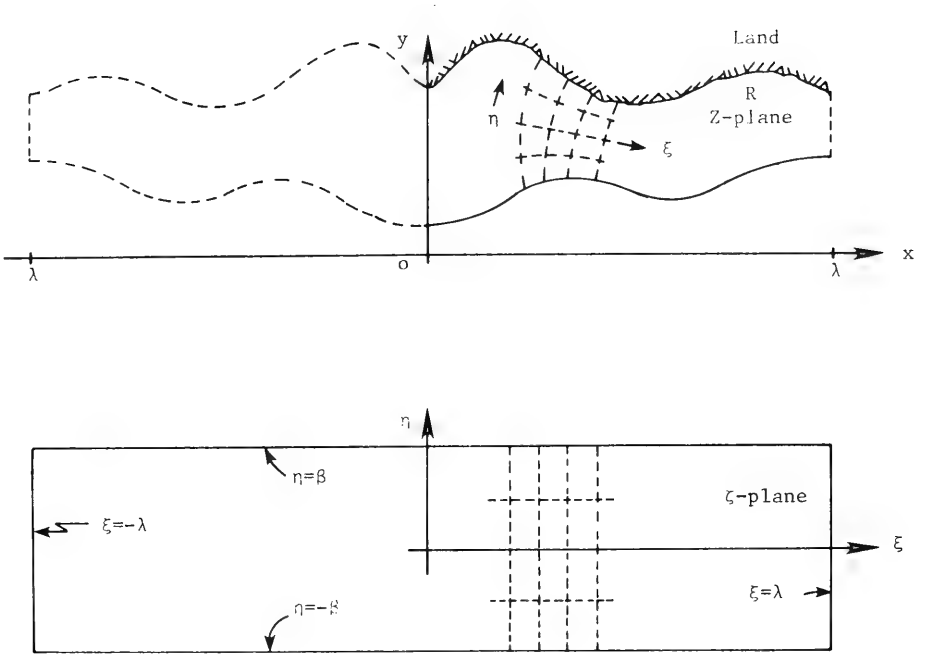

Figure 1. Conformal mapping planes for transforming the interior region of the Z-plane into the interior region of the ζ-plane.

and

$$Q_n = C_n + iD_n \ , \tag{8}$$

where the coefficients A_n , B_n , C_n , and D_n are real quantities. However, the symmetry condition about $x = 0$ (or $\xi = 0$) requires that all A_n and D_n be zero. The resulting relations for x and y in terms of ξ and η are:

$$x(\xi,\eta) = C_o\xi + \sum_{n=1}^{N} (B_n \sinh nk\eta + C_n \cosh nk\eta) \sin nk\xi \ , \tag{9}$$

and

$$y(\xi,\eta) = B_o + C_o\eta + \sum_{n=1}^{N} (B_n \cosh nk\eta + C_n \sinh nk\eta) \cos nk\xi \ . \tag{10}$$

The condition that the range of x and ξ be the same requires that $C_o = 1$. The remaining N values of C_n and $N+1$ values of B_n are determined by matching the coastal and seaward boundary curves at $\eta = \pm \beta$, respectively, β also being a parameter to be determined.

The coordinates X,Y of the given coast or seaward boundary curves are specified parametrically in terms of arc length measured along each curve from some fixed point. The functions X^s , Y^s , X^c , and Y^c are *single-valued* functions of this parameter where the superscript s or c represents the seaward boundary or coastline curve, respectively. This property is essential since a Fourier series-type representation is employed in determining the coefficients. The problem is to determine β , B_o , and the set of coefficients, B_n and C_n , for a given N such that equations (9) and (10) give a best fit to the given curves, in the sense of minimizing an appropriate mean square error function. Since the specified curves are not known directly in terms of ξ , but, rather in terms of arc length, the bicurve fitting equations require an iterative process starting from some initial estimate of arc length in terms of ξ for each curve.

It is found that a convergent iterative procedure results if one chooses the following as the $i+1$ approximation of the coefficients:

$$\beta^{i+1} = \frac{1}{2\lambda}\left[\int_o^\lambda Y^c(\Delta^i)\, d\xi - \int_o^\lambda Y^s(\Delta^i)\, d\xi\right] , \tag{11}$$

$$B_o^{i+1} = \frac{1}{2\lambda}\left[\int_o^\lambda Y^c(\Delta^i)\, d\xi + \int_o^\lambda Y^s(\Delta^i)\, d\xi\right] , \tag{12}$$

$$B_n^{i+1} = (\Psi_n \Omega_n - \Gamma_n \Phi_n)/(T_n \Omega_n - (\Phi_n)^2) \ , \qquad (13)$$

and

$$C_n^{i+1} = (\Gamma_n T_n - \Gamma_n \Phi_n)/(T_n \Omega_n - (\Phi_n)^2) \ , \qquad (14)$$

where i=1,2... denotes the iteration number, Δ is the transform generated arc length and

$$T_n = \left(\frac{W_x^{c,i}+W_x^{s,i}}{2}\right) \sinh^2 nk\beta^{i+1} + \left(\frac{W_y^{c,i}+W_y^{s,i}}{2}\right) \cosh^2 nk\beta^{i+1} \ , \qquad (15)$$

$$\Phi_n = \frac{(W_x^{c,i}-W_y^{s,i})\ (W_y^{c,i}-W_y^{s,i})}{4} \sinh 2nk\beta^{i+1} \ , \qquad (16)$$

$$\Omega_n = \left(\frac{W_y^{c,i}+W_y^{s,i}}{2}\right) \sinh^2 nk\beta^{i+1} + \left(\frac{W_x^{c,i}+W_x^{s,i}}{2}\right) \cosh^2 nk\beta^{i+1} \ , \qquad (17)$$

$$\Psi_n = \frac{\sinh nk\beta^{i+1}}{\lambda} \left[W_x^{c,i} \int_0^{\lambda} (X^c(\Delta^i) - \xi) \sin nk\xi \, d\xi \right.$$

$$\left. - W_x^{s,i} \int_0^{\lambda} (X^s(\Delta^i) - \xi) \sin nk\xi \, d\xi \right]$$

$$+ \frac{\cosh nk\beta^{i+1}}{\lambda} \left[W_y^{c,i} \int_0^{\lambda} Y^c(\Delta^i) \cos nk\xi \, d\xi \right.$$

$$\left. + W_y^{s,i} \int_0^{\lambda} Y^s(\Delta^i) \cos nk\xi \, d\xi \right] \ , \qquad (18)$$

$$\Gamma_n = \frac{\cosh nk\beta^{i+1}}{\lambda} \left[W_x^{c,i} \int_0^{\lambda} (X^c(\Delta^i) - \xi) \sin nk\xi \, d\xi \right.$$

$$\left. + W_x^{s,i} \int_0^{\lambda} (X^s(\Delta^i) - \xi) \sin nk\xi \, d\xi \right]$$

$$+ \frac{\sinh nk\beta^{i+1}}{\lambda} \left[W_y^{c,i} \int_0^{\lambda} Y^c(\Delta^i) \cos nk\xi \, d\xi \right.$$

$$\left. - W_y^{s,i} \int_0^{\lambda} Y^s(\Delta^i) \cos nk\xi \, d\xi \right] . \qquad (19)$$

The W terms are weighting factors used to distribute the error proportionally between the components of the transform generated and specified curves.

It can be shown that the above relations result from minimizing the following error function:

$$E_{i+1} = W_x^{s,i} E_x^{s,i+1} + W_y^{s,i} E_y^{s,i+1}$$

$$+ W_x^{c,i} E_x^{c,i+1} + W_y^{c,i} E_y^{c,i+1} , \qquad (20)$$

where

$$E_x^{s,i+1} = \frac{1}{2\lambda} \int_{-\lambda}^{\lambda} [X^s(\Delta^i(\xi,-\beta)) - x^{i+1}(\xi,-\beta)]^2 \, d\xi , \qquad (21)$$

$$E_y^{s,i+1} = \frac{1}{2\lambda} \int_{-\lambda}^{\lambda} [Y^s(\Delta^i(\xi,-\beta)) - y^{i+1}(\xi,-\beta)]^2 \, d\xi , \qquad (22)$$

$$E_x^{c,i+1} = \frac{1}{2\lambda} \int_{-\lambda}^{\lambda} [X^c(\Delta^i(\xi,+\beta)) - x^{i+1}(\xi,+\beta)]^2 \, d\xi , \qquad (23)$$

and

$$E_y^{c,i+1} = \frac{1}{2\lambda} \int_{-\lambda}^{\lambda} [Y^c(\Delta^i(\xi,+\beta)) - y^{i+1}(\xi,+\beta)]^2 \, d\xi \ . \qquad (24)$$

The transform generated arc length and weighting factors are determined relative to the results of the previous iteration by:

$$W_x^s = E_x^s/\bar{E} \ , \qquad (25)$$

$$W_y^s = E_y^s/\bar{E} \ , \qquad (26)$$

$$W_x^c = E_x^c/\bar{E} \ , \qquad (27)$$

$$W_y^c = E_y^c/\bar{E} \ , \qquad (28)$$

where $\bar{E}$ is the average value of equations (21) through (24). The arc length functions are given by:

$$\Delta(\xi^\dagger,-\beta) = \gamma^s \int_o^{\xi^\dagger} [(\frac{\partial x}{\partial \xi})^2 + (\frac{\partial y}{\partial \xi})^2]^{\frac{1}{2}} \, d\xi \ , \qquad (29)$$

and

$$\Delta(\xi^\dagger,\beta) = \gamma^c \int_o^{\xi^\dagger} [(\frac{\partial x}{\partial \xi})^2 + (\frac{\partial y}{\partial \xi})^2]^{\frac{1}{2}} \, d\xi \ , \qquad (30)$$

for $0 \leq \xi^\dagger \leq \lambda$ and γ^s and γ^c are prorating factors taken such that $\Delta(\lambda,\eta)$ is exactly the known length of the given curve. Two levels of approximation are involved in the error function. The ith approximation of these quantities is involved in the interpolation of the given curves. This approximation is mandatory in deriving a deterministic form for these quantities relative to the i+1 level.

The iterative procedure is initiated by setting all coefficients to zero, all weighting factors to unity, and equations (29) and (30) are given by $\gamma^s\xi^\dagger$ and $\gamma^c\xi^\dagger$, respectively. The first estimates of β, B_o and the Fourier-type coefficients

are determined from equations (11) through (14), respectively. Having the first approximation for these quantities, the transform-generated arc length for each curve and weight factors may be determined thus permitting a second approximation. This procedure is repeated for given N until β, B_0 and the transform coefficients have converged as indicated by successive values of the error function. The error function approaches a constant value governed by N and the inherent errors in estimating the various integrals by numerical methods. The trapezoidal rule employing M values of ξ at equal increments over the interval $0 \leq \xi \leq \lambda$ is used to estimate all integrals. Given the value of ξ, the appropriate values of X^S, Y^S, X^C and Y^C are computed by an interpolational subroutine called CURV, which was obtained from Dr. Alan Cline, National Center for Atmospheric Research. This routine is based on a numerical analogy to a spline under tension (for example, see Schweikert, 1966). In all applications of the conformal mapping procedure, the total number of terms of the series, N, is taken as M or smaller. The limitation on N is imposed since, for a determinate system, the total number of Fourier-type coefficients cannot exceed the number of data points. The selection of N is governed by the desired degree of fit of the functions X^S, Y^S, X^C and Y^C. The procedure outlined above follows the rudiments of a conformal mapping technique developed by Reid and Vastano (1966).

2. Applications.

Three regions of the Continental Shelf of the Gulf of Mexico and two regions of the eastern seaboard of the United States have been mapped. These regions are:

(a)	western gulf coast:	Laguna Madre, Mexico, to Marsh Island, Louisiana;
(b)	central gulf coast:	Matagorda Bay, Texas, to Timbalier Bay, Louisiana;
(c)	eastern gulf coast:	Atchafalaya Bay, Louisiana, to Apalachee Bay, Florida;
(d)	lower east coast:	Cape Kennedy, Florida, to Pamlico Sound, North Carolina;
(e)	upper east coast:	Pamlico Sound, North Carolina, to Penobscot Bay, Maine;

and are shown in Figures 2 through 6. The top and bottom curve in each figure represents the coastline and the 180-meter isobath, respectively. The latter is taken to correspond approximately to the shelf break, seaward of which the depths increase abruptly; the 180-meter contour may not always be the most appropriate one for the outer limit of the Continental Shelf. The chart scale, orientation of the region, and location of cities and bays along the coast are indicated on each figure. The x's represent the location where

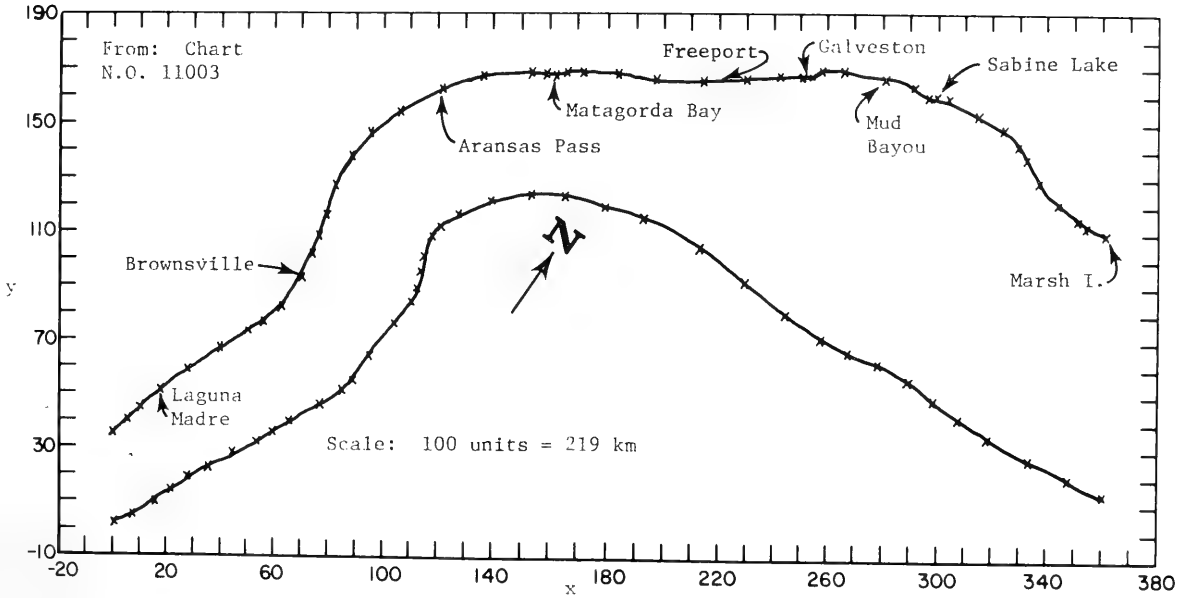

Figure 2. Coastline (top) and seaward boundary curve (bottom), western gulf coast.

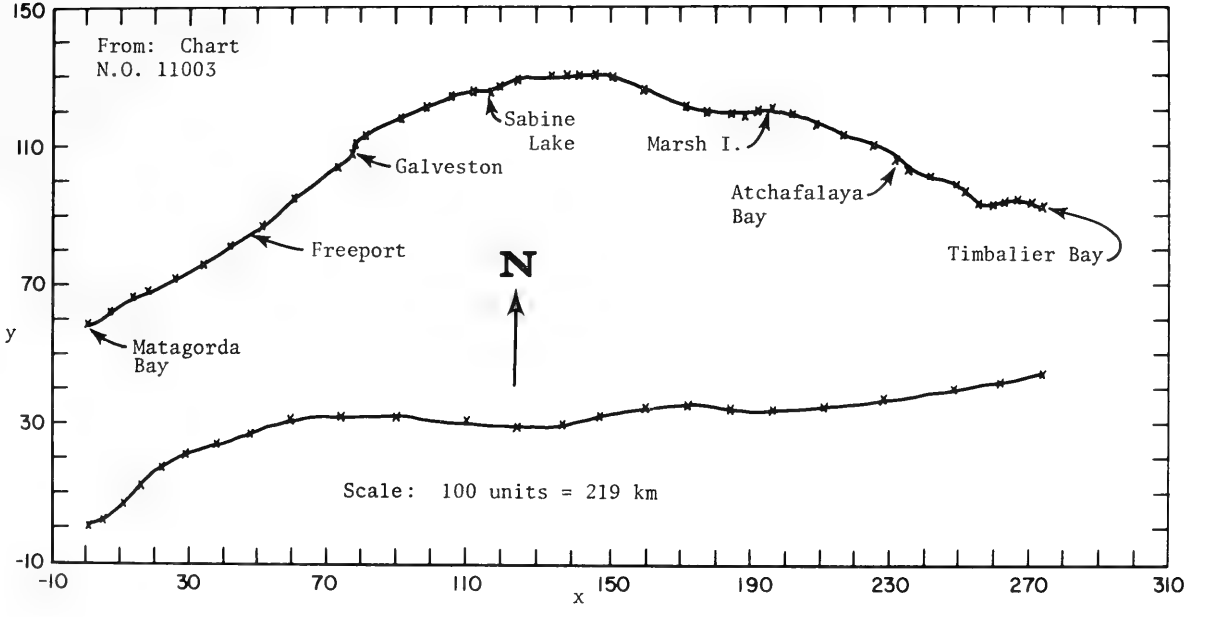

Figure 3. Coastline (top) and seaward boundary curve (bottom), central gulf coast.

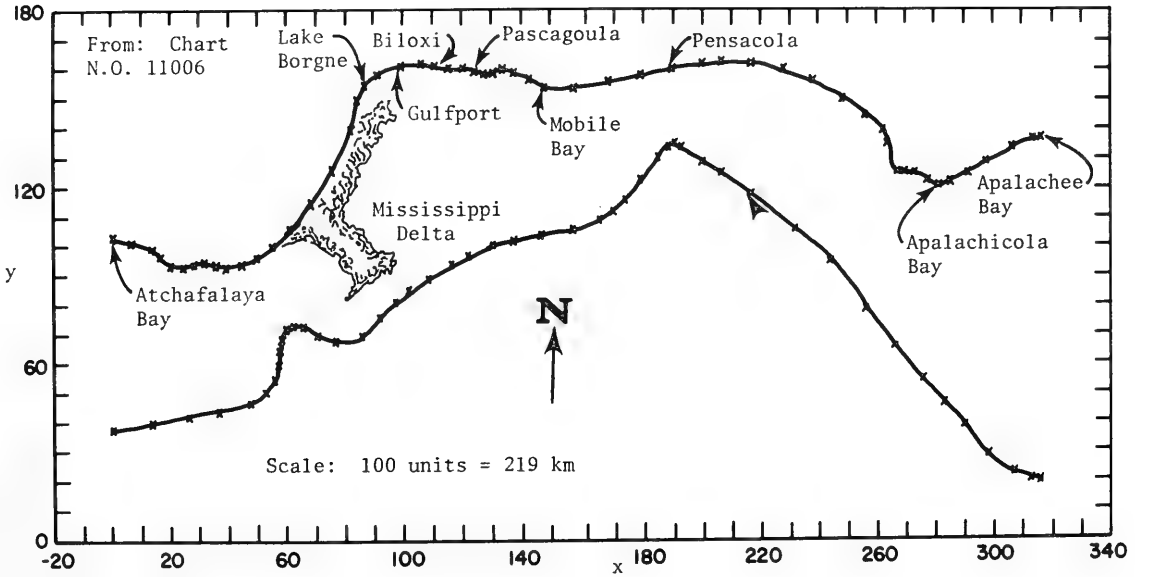

Figure 4. Coastline (top) and seaward boundary curve (bottom), eastern gulf coast.

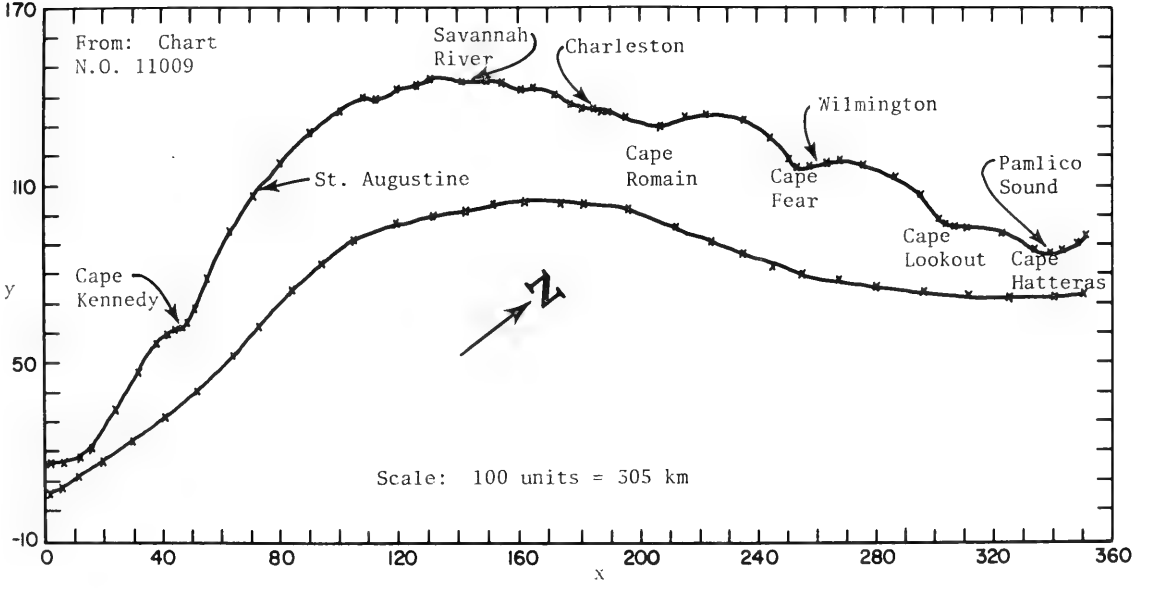

Figure 5. Coastline (top) and seaward boundary curve (bottom), lower east coast.

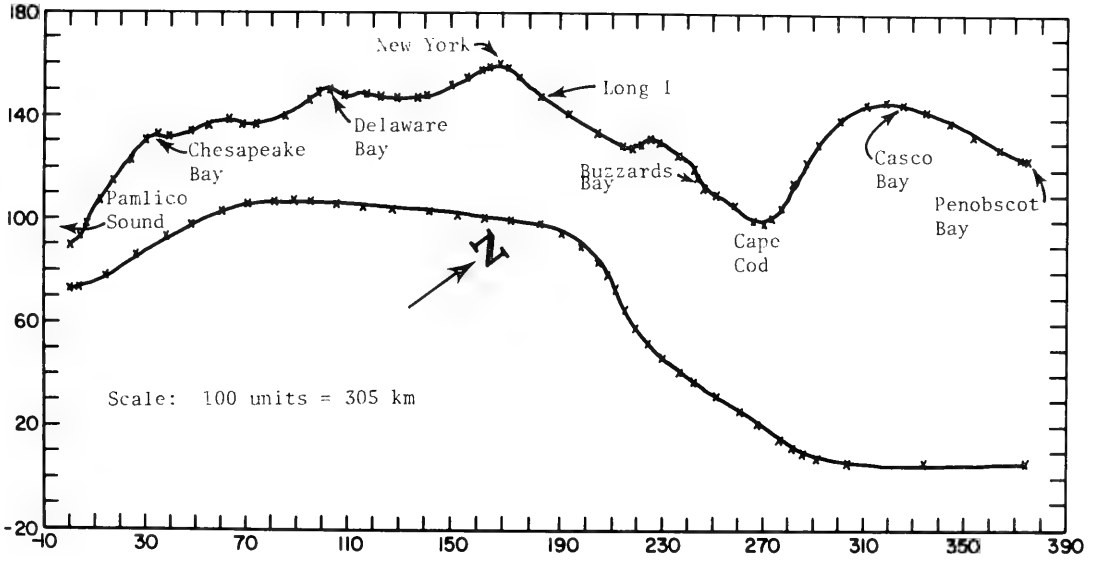

Figure 6. Coastline (top) and seaward boundary curve (bottom), upper east coast.

the coast and the 180-meter contour were digitized from an overlay of bathymetric charts for the regions concerned. The smooth curve is the result of applying the numerical spline interpolation routine to these points. In reading the discrete positions, both the coastline and the 180-meter isobath have been smoothed subjectively to suppress variations with scale lengths less than the grid scale ultimately employed in the surge calculations. For example, narrow entrances to bays are replaced by a fictitious coastline across the entrance, and the cusp-shaped features are smoothed.

A method was adopted which minimizes the amount of computer time required to solve equations (9) and (10) by hastening the convergence of the iterative procedure. The method consisted of increasing N at selected iteration intervals. The iterative procedure used to determine the transformation coefficients was terminated if the convergence criterion was satisfied or if the available computer storage was exceeded because of increasing N. The convergence criterion was a mean variance of less than 1 square kilometer between the transform-generated curves and that specified. However, for development purposes, the iterative procedure for the western and central gulf coast and lower east coast areas was continued beyond this criterion to obtain a better fit.

It is convenient to discuss the mapping of the western and central gulf coast regions at the end of this section since additional testing of the solution to the mapping equations was performed with these areas. Figure 4 shows the shelf region for the eastern gulf coast where the Mississippi Delta is shown as the shaded area. Consideration of the numerical time step for the surge algorithm was the principle reason why the coastline to be mapped did not follow the delta. The reduction in the time step if the actual coastline had been followed would, probably, have been at least tenfold with respect to the one used in the simulation of the storm surge induced by Hurricane Camille (Section V). Since the delta, or really the levee adjacent to the Mississippi River, has a controlling influence on the circulation and surge caused by the hurricane, this geographical feature was included in the surge model as a wall protruding from the coast. The fit of the transform-generated coast and seaward boundary curves with respect to that specified after 1, 20, 40, 80, and 160 iterations is shown in Figures 7 through 11, respectively. The successively better agreement of the mapped curves with respect to that specified is obvious from the convergence table for the gulf coast region of Atchafalaya Bay to Apalachee Bay (Table 1). The table shows the variance and convergence behavior of selected transformation coefficients as the iteration and N increases. The coast variance in X, the third column of Table 1, is calculated by:

$$\frac{1}{M-1} \sum_{j=1}^{M} \left| X^c(\Delta^i(\xi_j,\beta)) - x^i(\xi_j,\beta) \right|^2 \qquad (31)$$

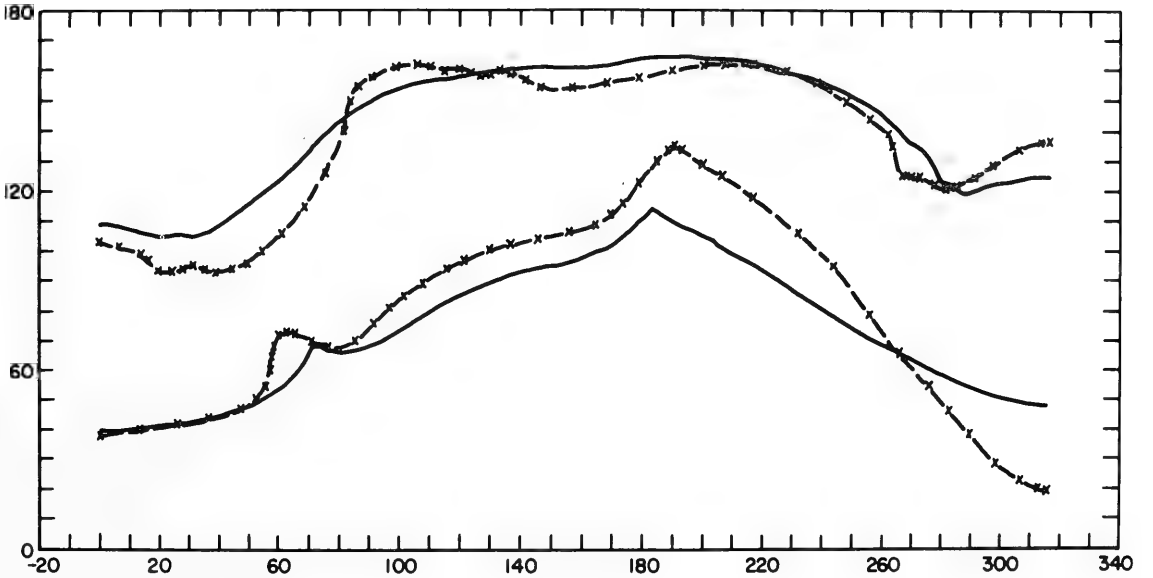

Figure 7. Transform-generated coastline and seaward boundary curve after one iteration (solid) and that specified (dashed), eastern gulf coast.

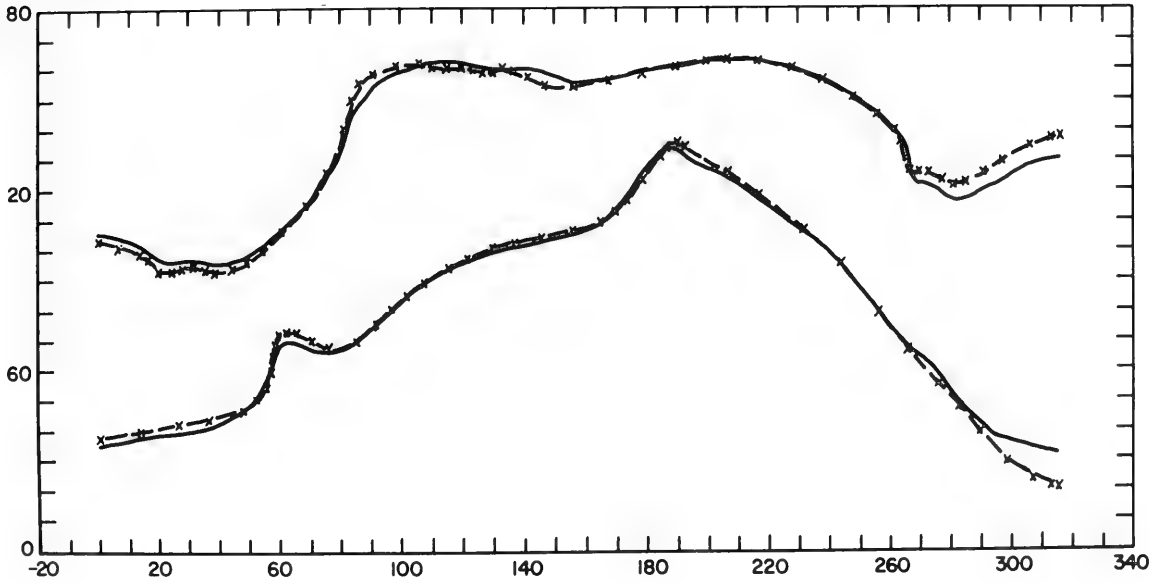

Figure 8. Transform-generated coastline and seaward boundary curve after 20 iterations (solid) and that specified (dashed), eastern gulf coast.

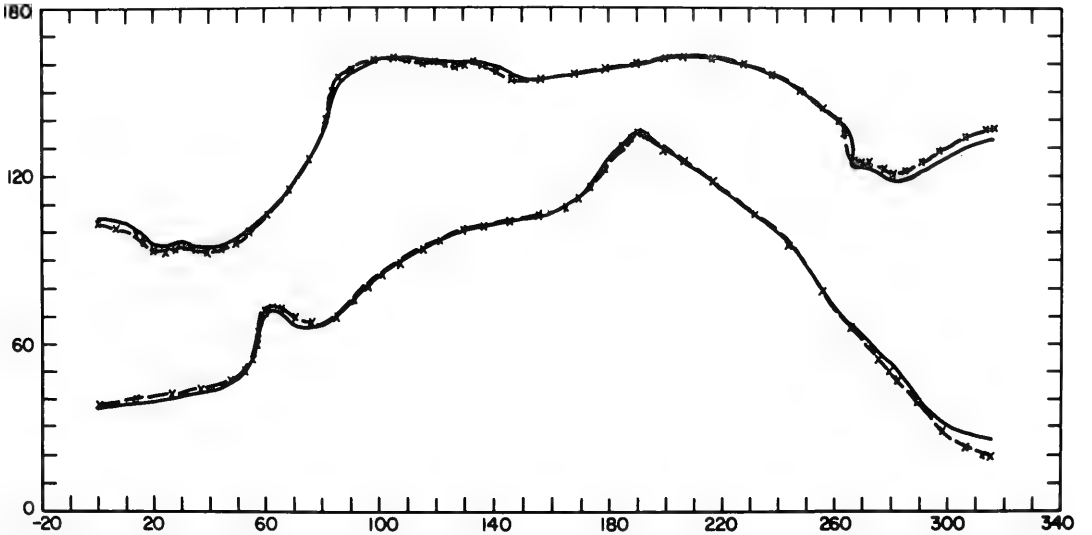

Figure 9. Transform-generated coastline and seaward boundary curve after 40 iterations (solid) and that specified (dashed), eastern gulf coast.

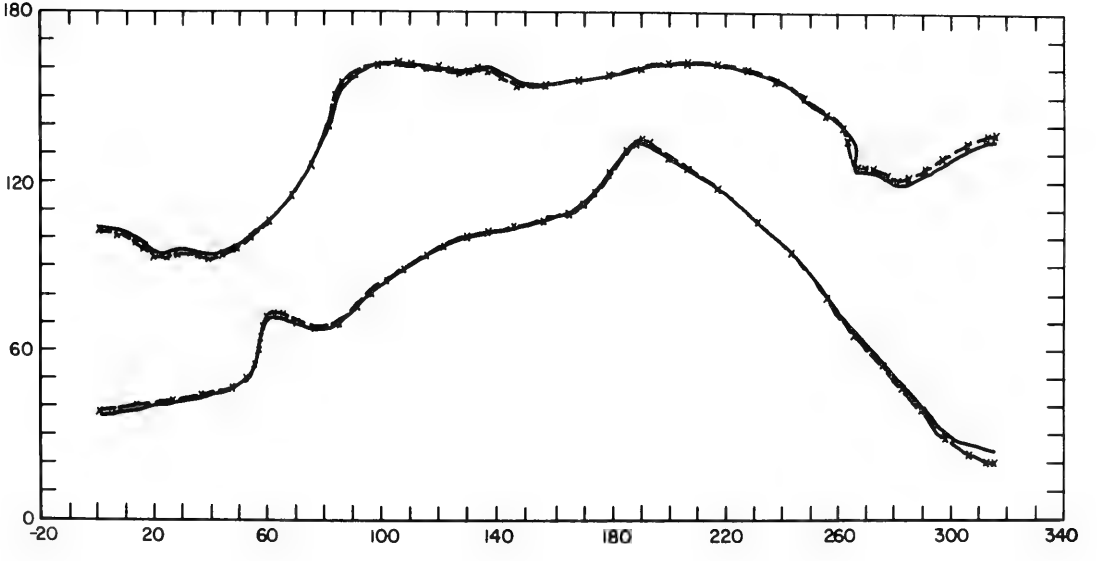

Figure 10. Transform-generated coastline and seaward boundary curve after 80 iterations (solid) and that specified (dashed), eastern gulf coast.

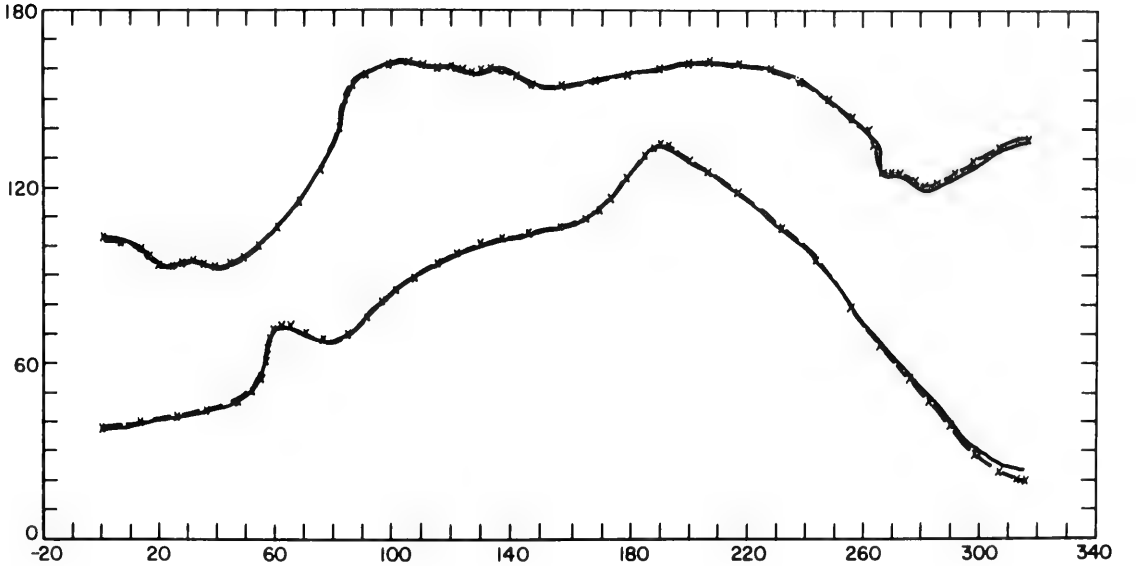

Figure 11. Transform-generated coastline and seaward boundary curve after 160 iterations (solid) and that specified (dashed), eastern gulf coast.

Table 1. Convergence table for the gulf coast region of Atchafalaya Bay to Apalachee Bay.

Iteration number	M	Coast variance		Seaward boundary variance		Transformation coefficients*					
		X (km^2)	Y (km^2)	X (km^2)	Y (km^2)	ℓ	B_0	B_1	B_2	C_1	C_2
1	40	$5.6055(10^1)$	$1.4926(10^2)$	$1.1138(10^2)$	$3.9184(10^2)$	28.857	108.25	-10.762	-23.765	-0.312	0.820
20	40	$1.3440(10^1)$	$1.4473(10^1)$	$1.3118(10^1)$	$1.6300(10^1)$	20.309	112.87	-15.799	-29.373	2.775	6.351
30	60	$9.3814(10^0)$	$8.9689(10^0)$	$8.2482(10^0)$	$9.8086(10^0)$	20.124	113.25	-16.348	-29.143	2.477	7.034
40	80	$6.3338(10^0)$	$5.1409(10^0)$	$3.8816(10^0)$	$4.8941(10^0)$	20.010	113.37	-17.086	-28.859	1.464	7.255
50	80	$3.6652(10^0)$	$4.0278(10^0)$	$3.9975(10^0)$	$4.7352(10^0)$	20.024	113.19	-17.401	-28.663	0.548	6.855
60	90	$3.1148(10^0)$	$2.8983(10^0)$	$3.1933(10^0)$	$3.5493(10^0)$	19.993	113.16	-17.715	-28.498	-0.074	6.824
70	100	$3.3957(10^0)$	$2.4113(10^0)$	$2.2394(10^0)$	$2.5457(10^0)$	19.972	113.16	-17.866	-28.443	-0.323	6.799
80	110	$2.8861(10^0)$	$2.2610(10^0)$	$1.7544(10^0)$	$2.1083(10^0)$	19.960	113.11	-17.938	-28.420	-0.455	6.657
100	110	$1.5027(10^0)$	$1.8287(10^0)$	$2.1875(10^0)$	$2.3649(10^0)$	19.970	113.02	-18.116	-28.272	-1.038	6.480
120	110	$2.4666(10^0)$	$1.9193(10^0)$	$1.7331(10^0)$	$1.9468(10^0)$	19.961	113.02	-18.088	-28.327	-0.903	6.493
125	120	$1.4062(10^0)$	$1.8438(10^0)$	$1.8247(10^0)$	$1.8511(10^0)$	19.959	113.02	-18.106	-28.288	-1.069	6.477
130	130	$2.0073(10^0)$	$1.7391(10^0)$	$1.3645(10^0)$	$1.5994(10^0)$	19.940	113.02	-18.161	-28.298	-0.984	6.481
135	140	$1.0719(10^0)$	$1.1581(10^0)$	$1.1742(10^0)$	$1.1707(10^0)$	19.929	113.04	-18.379	-28.154	-1.506	6.554
140	140	$1.2660(10^0)$	$1.2533(10^0)$	$1.0313(10^0)$	$1.2058(10^0)$	19.929	112.99	-18.356	-28.189	-1.397	6.423
150	150	$8.8417(10^{-1})$	$9.6646(10^{-1})$	$8.3174(10^{-1})$	$9.6572(10^{-1})$	19.921	112.95	-18.510	-28.105	-1.752	6.328
160	160	$6.9851(10^{-1})$	$8.0370(10^{-1})$	$6.9110(10^{-1})$	$8.0386(10^{-1})$	19.915	112.91	-18.619	-28.047	-2.014	6.240

* x,y units.

Similar expressions are employed for the other variances. Appendix A contains the transformation coefficients used to produce Figure 11.

The successful application of the mapping equations to the other shelf regions was accomplished. Tables 2 through 5 clearly indicate the successive convergence of the mapped curves with respect to that specified for the lower and upper east coast and the western and central gulf coast, respectively. Figures 12 through 15 show the fit of the transform-generated curves and that specified after the last iteration for the above regions. Appendixes B and C contain the mapping coefficients used to produce Figures 12 and 13, respectively. The bottom part of Tables 4 and 5 show the results of additional testing of the conformal mapping equations (9) and (10) with the western and central gulf coast regions. Another, less general, solution of equations (9) and (10) is possible if one minimizes the least square error function defined only in terms of the Y integrals. This solution for the transformation coefficients, hereafter referred to as an alternate solution, may be obtained from equations (13) through (19) with $W_x^s = W_x^c = 0$. The testing procedure was to continue the iterative process as outlined in the previous section with the initial approximation for the coefficients being those values determined from the 80th iteration. The alternate solution as applied to the western and central gulf coast regions was stable and, moreover, provided a better fit with N = 110 than the more general one. The fit of the mapped curves with respect to that specified after 1 and 40 (or, 81 and 120) iterations with the alternate solution is shown in Figures 16 and 17, respectively, for the western gulf coast and Figures 18 and 19, respectively, for the central gulf coast. Appendixes D and E contain the transformation coefficients used to produce Figures 17 and 19, respectively. In testing with the other three shelf regions, the alternate solution was nonconvergent in that the successive values of the error function do not decrease or approach a constant as outlined in the previous section. The reason for this behavior has not been investigated.

The total variance of x and y from a linear transform of the curvilinear coordinates may be defined as:

$$\sigma^2 = \sigma_x^2 + \sigma_y^2 \tag{32}$$

where

$$\sigma_x^2 = \frac{1}{2\beta\lambda} \int_{-\beta}^{\beta} \int_{o}^{\lambda} [x - \xi]^2 \, d\xi \, d\eta \; ; \tag{33}$$

and

Table 2. Convergence table for the east coast region of Camp Kennedy to Pamlico Sound.

Iteration number	N	Coast variance		Seaward boundary variance		Transformation coefficients*					
		X (km^2)	Y (km^2)	X (km^2)	Y (km^2)	β	B_0	B_1	B_2	C_1	C_2
1	40	$2.6405(10^1)$	$2.7256(10^2)$	$5.0073(10^0)$	$3.6144(10^1)$	15.589	89.525	-22.520	-33.927	-18.080	- 5.263
20	40	$4.6478(10^0)$	$5.9443(10^0)$	$3.3735(10^0)$	$1.6403(10^1)$	10.588	77.300	-33.209	-36.519	-25.428	-31.752
30	60	$2.3205(10^0)$	$4.3793(10^0)$	$1.3463(10^0)$	$8.5265(10^0)$	10.383	75.211	-25.921	-34.977	-34.676	-31.200
40	80	$1.4254(10^0)$	$3.0723(10^0)$	$9.3167(10^{-1})$	$4.5406(10^0)$	10.313	74.384	-37.558	-33.767	-41.867	-29.297
50	80	$1.0398(10^0)$	$2.2590(10^0)$	$6.4350(10^{-1})$	$2.6101(10^0)$	10.252	73.589	-38.870	-33.691	-47.263	-27.825
60	90	$6.8483(10^{-1})$	$1.5203(10^0)$	$3.7444(10^{-1})$	$1.4973(10^0)$	10.169	72.776	-39.993	-31.597	-51.967	-26.689
70	100	$4.8592(10^{-1})$	$1.0938(10^0)$	$2.5042(10^{-1})$	$9.1575(10^{-1})$	10.121	72.229	-40.782	-30.770	-54.858	-25.815
80	110	$3.7721(10^{-1})$	$7.1814(10^{-1})$	$1.5550(10^{-1})$	$5.8581(10^{-1})$	10.076	71.764	-41.400	-30.061	-57.315	-25.098
85	110	$3.5201(10^{-1})$	$6.0795(10^{-1})$	$1.2339(10^{-1})$	$4.4959(10^{-1})$	10.076	71.647	-41.562	-29.839	-58.112	-24.762
90	120	$2.5931(10^{-1})$	$5.4169(10^{-1})$	$1.1529(10^{-1})$	$4.0754(10^{-1})$	10.035	71.441	-41.821	-29.538	-59.071	-24.562
95	130	$1.8001(10^{-1})$	$5.1220(10^{-1})$	$8.7043(10^{-2})$	$3.1579(10^{-1})$	10.002	71.220	-42.031	-29.247	-59.903	-24.438
100	140	$1.7351(10^{-1})$	$3.6610(10^{-1})$	$6.2407(10^{-2})$	$2.7878(10^{-1})$	9.985	71.041	-42.247	-28.989	-60.648	-24.258
105	140	$1.6453(10^{-1})$	$3.0474(10^{-1})$	$4.9283(10^{-2})$	$2.3048(10^{-1})$	9.983	70.951	-42.362	-28.835	-61.145	-24.036
110	150	$1.2972(10^{-1})$	$2.7717(10^{-1})$	$4.4844(10^{-2})$	$2.0928(10^{-1})$	9.956	70.812	-42.515	-28.629	-61.745	-23.944
115	160	$9.2046(10^{-2})$	$2.8100(10^{-1})$	$3.6558(10^{-2})$	$1.7213(10^{-1})$	9.931	70.658	-42.671	-28.412	-62.379	-23.809
120	170	$8.0505(10^{-2})$	$2.2524(10^{-1})$	$2.8676(10^{-2})$	$1.5266(10^{-1})$	9.917	70.530	-42.827	-28.218	-62.954	-23.648

* x,y units.

Table 3. Convergence table for the east coast region of Pamlico Sound to Penobscot Bay.

Iteration number	N	Coast variance		Seaward boundary variance		Transformation coefficients*					
		X (km^2)	Y (km^2)	X (km^2)	Y (km^2)	β	B_0	B_1	B_2	C_1	C_2
1	40	$3.2165(10^1)$	$8.4764(10^2)$	$6.7486(10^1)$	$1.0543(10^3)$	34.332	97.42	23.194	-10.918	- 4.792	3.696
20	40	$4.5820(10^0)$	$8.0430(10^0)$	$4.9460(10^{-1})$	$4.4481(10^0)$	22.308	105.20	9.496	-25.276	-69.243	12.937
30	60	$2.8173(10^0)$	$3.7523(10^0)$	$9.5326(10^{-2})$	$3.0576(10^0)$	22.090	104.90	9.132	-25.502	-70.991	12.233
40	80	$2.0259(10^0)$	$2.3924(10^0)$	$6.1320(10^{-2})$	$2.0761(10^0)$	22.004	104.68	8.994	-25.611	-71.997	11.729
50	80	$2.0206(10^0)$	$2.1922(10^0)$	$5.0238(10^{-2})$	$1.9723(10^0)$	21.996	104.67	8.917	-25.625	-72.204	11.686
60	90	$1.8278(10^0)$	$1.9846(10^0)$	$3.8529(10^{-2})$	$1.7978(10^0)$	21.957	104.66	8.776	-25.664	-72.551	11.697
70	100	$1.6584(10^0)$	$1.7801(10^0)$	$4.6508(10^{-2})$	$1.6235(10^0)$	21.922	104.67	8.613	-25.686	-72.998	11.716
80	110	$1.5317(10^0)$	$1.6516(10^0)$	$3.6249(10^{-2})$	$1.5411(10^0)$	21.908	104.62	8.616	-25.697	-73.125	11.620
85	110	$1.5381(10^0)$	$1.5079(10^0)$	$3.7517(10^{-2})$	$1.5831(10^0)$	21,905	104.62	8.576	-25.705	-73.191	11.595
90	120	$1.5469(10^0)$	$1.5590(10^0)$	$3.9493(10^{-2})$	$1.5502(10^0)$	21.903	104.61	8.615	-25.696	-73.135	11.569
95	130	$1.5490(10^0)$	$1.4588(10^0)$	$3.4949(10^{-2})$	$1.5854(10^0)$	21.911	104.60	8.630	-25.698	-73.105	11.569
100	140	$1.3406(10^0)$	$1.5108(10^0)$	$2.9971(10^{-2})$	$1.3704(10^0)$	21.893	104.59	8.601	-25.711	-73.335	11.538
105	140	$1.3179(10^0)$	$1.3480(10^0)$	$3.1411(10^{-2})$	$1.3679(10^0)$	21.883	104.57	8.538	-25.721	-73.510	11.502
110	150	$1.2353(10^0)$	$1.3288(10^0)$	$2.9630(10^{-2})$	$1.2612(10^0)$	21.877	104.57	8.538	-25.722	-73.612	11.492
115	160	$1.2412(10^0)$	$1.2463(10^0)$	$2.8945(10^{-2})$	$1.2542(10^0)$	21.868	104.56	8.489	-25.730	-73.711	11.488
120	170	$1.2148(10^0)$	$1.2522(10^0)$	$3.0086(10^{-2})$	$1.2140(10^0)$	21.866	104.56	8.493	-25.728	-73.731	11.490
125	170	$1.2032(10^0)$	$1.2331(10^0)$	$3.0312(10^{-2})$	$1.1966(10^0)$	21.863	104.57	8.477	-25.727	-73.778	11.500
130	180	$1.1602(10^0)$	$1.1731(10^0)$	$3.0363(10^{-2})$	$1.1854(10^0)$	21.856	104.56	8.449	-25.734	-73.867	11.485
135	190	$1.1226(10^0)$	$1.1697(10^0)$	$3.0663(10^{-2})$	$1.1412(10^0)$	21.852	104.55	8.453	-25.734	-73.907	11.467

* x,y units.

Table 4. Convergence table for the gulf coast region of Laguna Madre to Marsh Island.

Iteration number	N	Coast variance		Seaward boundary variance		Transformation coefficients*					
		X (km^2)	Y (km^2)	X (km^2)	Y (km^2)	β	B_0	B_1	B_2	C_1	C_2
1	40	$4.4703(10^1)$	$6.1399(10^2)$	$1.5149(10^1)$	$5.9347(10^2)$	32.695	100.050	-19.772	-33.266	-14.339	- 0.198
20	40	$3.3362(10^0)$	$5.9192(10^0)$	$2.1040(10^0)$	$4.0178(10^0)$	21.305	96.781	-40.641	-34.152	-62.905	18.610
30	60	$1.2695(10^0)$	$1.0979(10^0)$	$1.3335(10^{-1})$	$1.1496(10^0)$	21.304	95.941	-42.274	-32.978	-65.080	18.413
40	80	$9.7655(10^{-1})$	$1.0520(10^0)$	$5.1013(10^{-1})$	$1.1103(10^0)$	21.281	95.928	-42.253	-33.119	-65.313	18.681
50	80	$9.3119(10^{-1})$	$9.5186(10^{-1})$	$1.9825(10^{-1})$	$9.5914(10^{-1})$	21.270	95.906	-42.311	-32.995	-65.437	18.673
60	90	$5.3540(10^{-1})$	$6.1508(10^{-1})$	$6.3537(10^{-2})$	$5.7841(10^{-1})$	21.236	95.725	-42.588	-32.682	-66.002	18.796
70	100	$3.9750(10^{-1})$	$4.1391(10^{-1})$	$5.5730(10^{-2})$	$4.3694(10^{-1})$	21.218	95.602	-42.737	-32.547	-66.335	18.891
80	110	$2.7778(10^{-1})$	$2.9846(10^{-1})$	$7.9148(10^{-2})$	$3.0390(10^{-1})$	21.196	95.547	-42.815	-32.456	-66.649	19.043
81**	110	$2.5786(10^0)$	$1.5554(10^0)$	$1.5174(10^0)$	$2.0078(10^0)$	21.195	95.543	-42.818	-32.440	-69.237	19.329
100**	110	$2.7283(10^{-1})$	$1.6763(10^{-2})$	$9.7561(10^{-2})$	$3.7868(10^{-2})$	21.146	95.146	-42.435	-31.835	-68.203	19.479
110**	130	$1.6539(10^{-1})$	$1.0869(10^{-2})$	$2.0403(10^{-2})$	$2.4804(10^{-2})$	21.141	95.133	-42.433	-31.780	-68.111	19.380
120**	150	$1.4947(10^{-2})$	$4.1681(10^{-3})$	$6.7609(10^{-2})$	$1.7859(10^{-2})$	21.110	95.079	-42.494	-31.662	-68.177	19.427

* x,y units.

** Alternate solution to the mapping equations (9) and (10).

Table 5. Convergence table for the Gulf coast region of Matagorda Bay to Timbalier Bay.

Iteration number	N	Coast variance		Seaward boundary variance		Transformation coefficients*					
		X (km^2)	Y (km^2)	X (km^2)	Y (km^2)	β	B_0	B_1	B_2	C_1	C_2
1	40	$7.9830(10^{0})$	$2.1422(10^{2})$	$1.7966(10^{1})$	$2.5237(10^{1})$	37.496	67.944	- 9.379	-6.528	- 4.428	- 4.489
20	40	$6.3380(10^{-1})$	$4.8899(10^{-1})$	$2.6871(10^{-1})$	$5.2789(10^{-1})$	32.194	64.194	-13.349	-9.338	-13.289	-11.863
30	60	$5.5068(10^{-1})$	$4.8121(10^{-1})$	$2.8623(10^{-1})$	$5.1662(10^{-1})$	32.729	64.074	-13.404	-9.210	-14.335	-11.894
40	80	$4.5343(10^{-1})$	$4.5954(10^{-1})$	$1.2039(10^{-1})$	$4.4980(10^{-1})$	32.683	63.986	-13.508	-9.161	-14.653	-11.993
50	80	$4.5553(10^{-1})$	$4.6773(10^{-1})$	$1.1890(10^{-1})$	$4.5879(10^{-1})$	32.682	63.983	-13.511	-9.161	-14.677	-11.993
60	90	$4.4845(10^{-1})$	$4.6106(10^{-1})$	$8.6362(10^{-2})$	$4.5014(10^{-1})$	32.676	63.971	-13.523	-9.159	-14.697	-12.006
70	100	$4.0931(10^{-1})$	$4.2744(10^{-1})$	$6.4145(10^{-2})$	$4.1463(10^{-1})$	32.670	63.962	-13.530	-9.160	-14.653	-12.034
80	110	$4.1086(10^{-1})$	$4.2171(10^{-1})$	$5.1257(10^{-2})$	$4.1125(10^{-1})$	32.669	63.959	-13.533	-9.161	-14.651	-12.038
81**	110	$9.0550(10^{-1})$	$3.9487(10^{-1})$	$1.5013(10^{-2})$	$3.5927(10^{-2})$	32.669	63.959	-13.589	-9.194	-13.327	-12.333
100**	110	$3.4458(10^{-1})$	$1.8250(10^{-3})$	$3.0168(10^{-2})$	$3.4018(10^{-3})$	32.666	64.031	-13.454	-9.307	-12.908	-12.537
110**	130	$3.0251(10^{-1})$	$1.0063(10^{-3})$	$1.8262(10^{-2})$	$1.7687(10^{-3})$	32.666	64.028	-13.455	-9.308	-12.897	-12.534
120**	150	$2.5897(10^{-1})$	$6.3789(10^{-4})$	$1.1498(10^{-2})$	$9.7215(10^{-4})$	32.666	64.025	-13.455	-9.309	-12.888	-12.532

* x,y units.

** Alternate solution to the mapping equations (9) and (10).

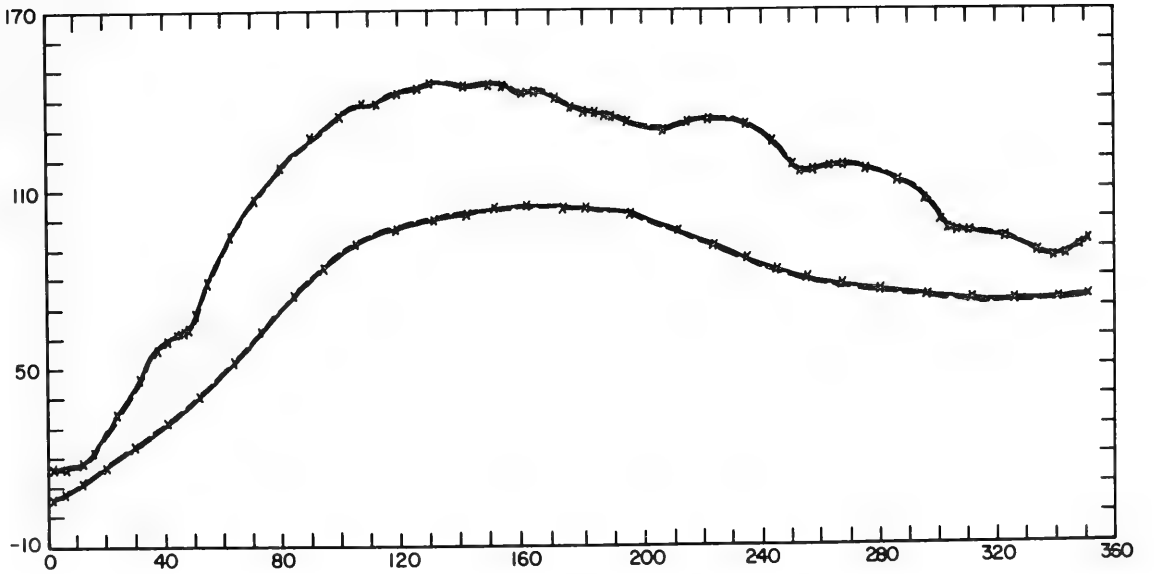

Figure 12. Transform-generated coastline and seaward boundary curve after 120 iterations (solid) and that specified (dashed), lower east coast.

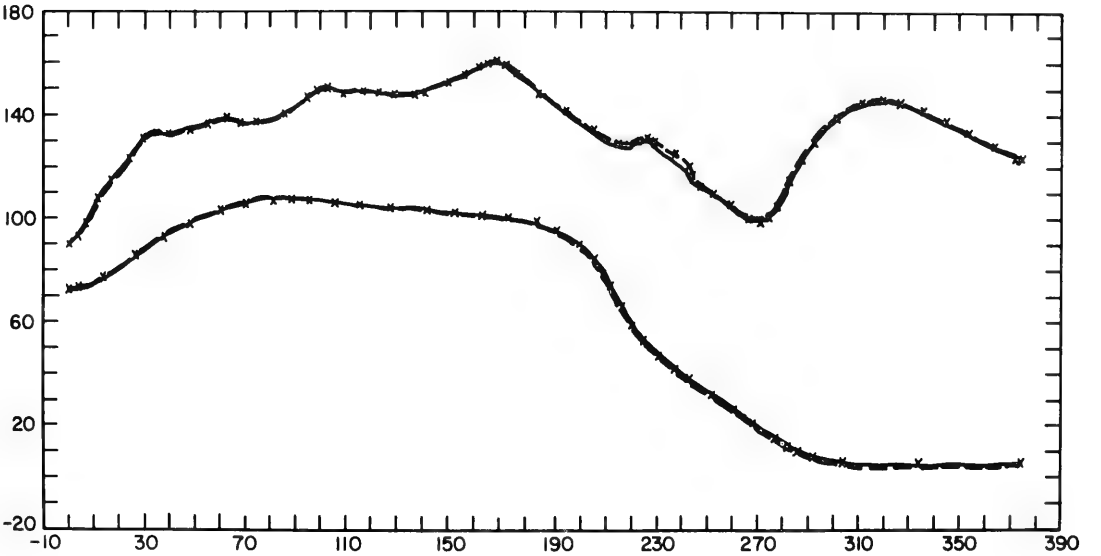

Figure 13. Transform-generated coastline and seaward boundary curve after 135 iterations (solid) and that specified (dashed), upper east coast.

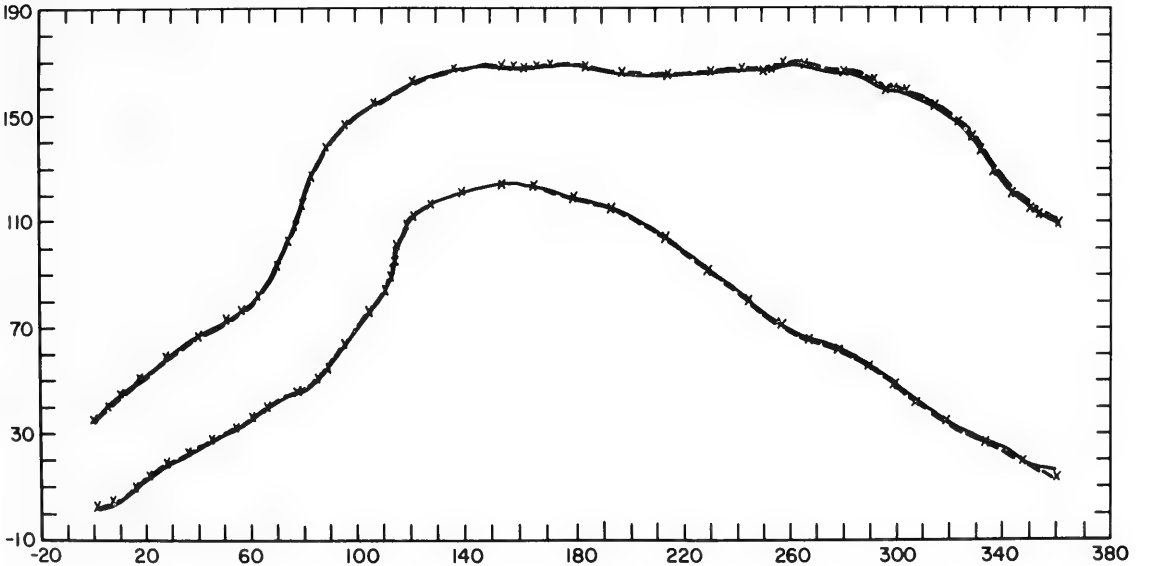

Figure 14. Transform-generated coastline and seaward boundary curve after 80 iterations (solid) and that specified (dashed), western gulf coast.

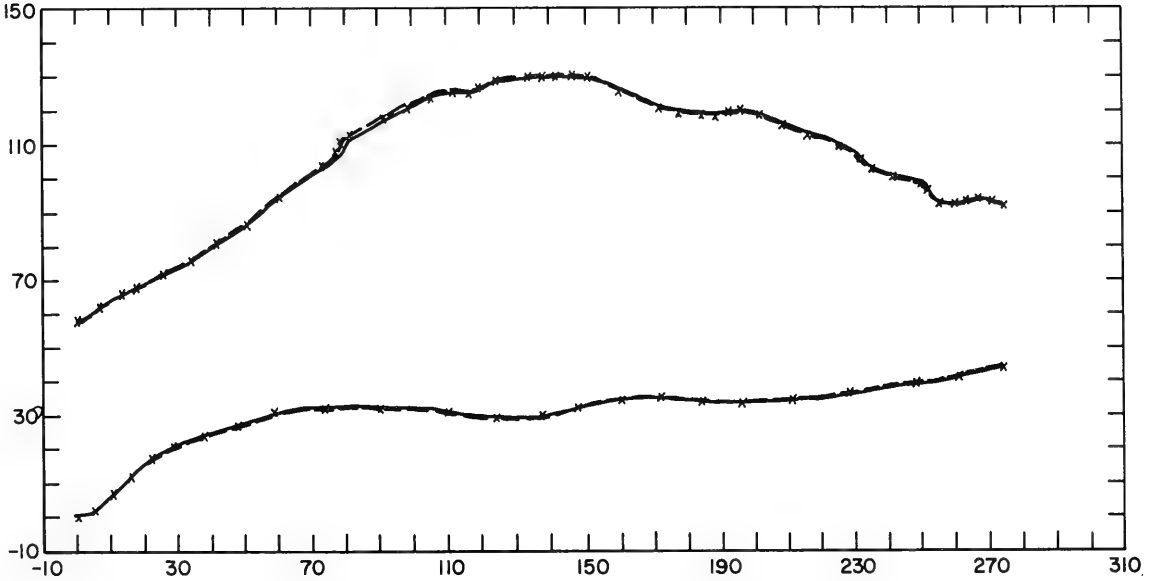

Figure 15. Transform-generated coastline and seaward boundary curve after 80 interations (solid) and that specified (dashed), central gulf coast.

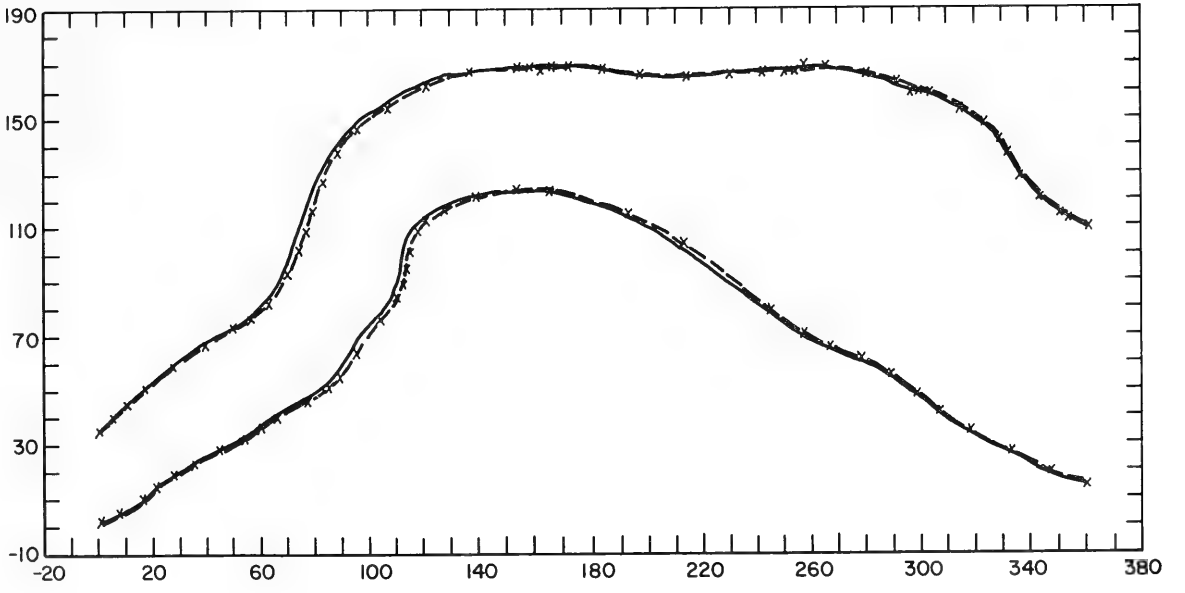

Figure 16. Transform-generated coastline and seaward boundary curve after one iteration with the alternate solution (solid) and that specified (dashed), western gulf coast.

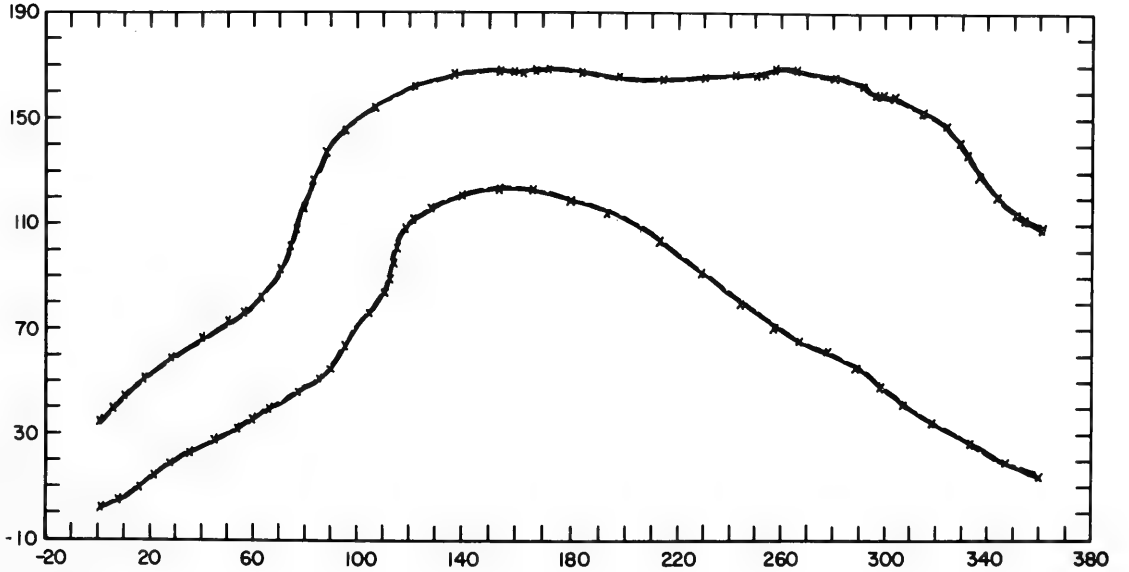

Figure 17. Transform-generated coastline and seaward boundary curve after 40 iterations with the alternate solution (solid) and that specified (dashed), western gulf coast.

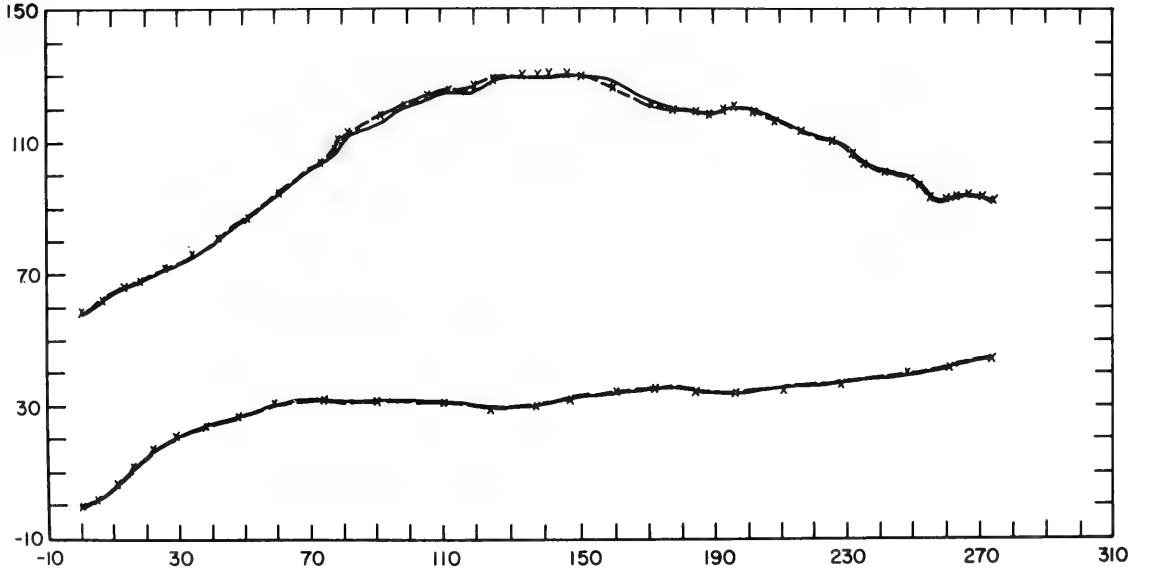

Figure 18. Transform-generated coastline and seaward boundary curve after one interation with the alternate solution (solid) and that specified (dashed), central gulf coast.

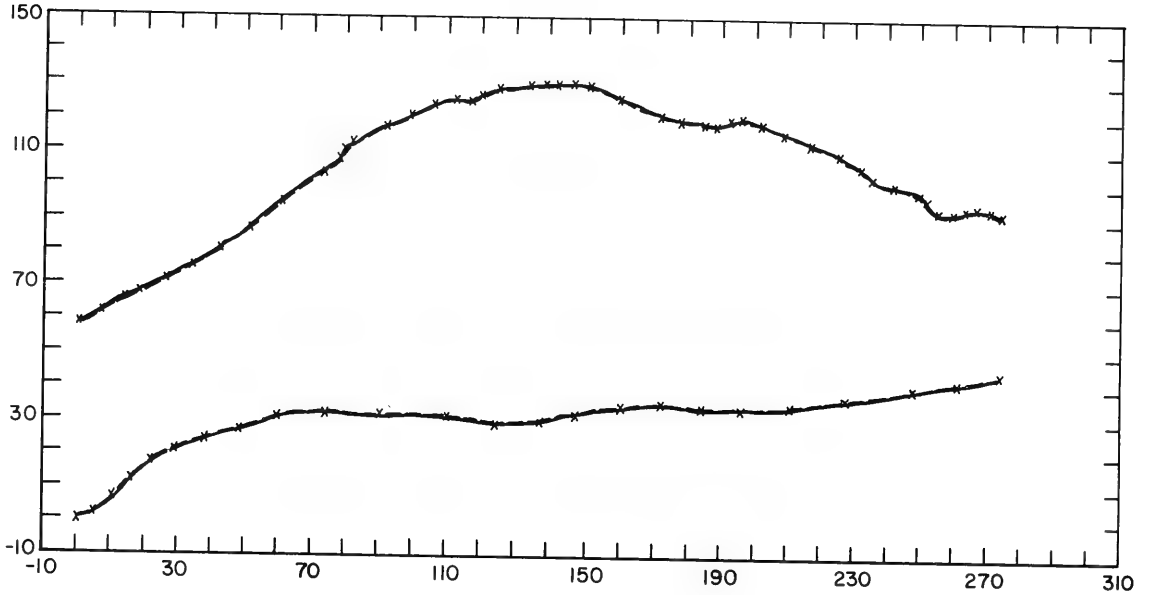

Figure 19. Transform-generated coastline and seaward boundary curve after 40 iterations with the alternate solution (solid) and that specified (dashed), central gulf coast.

$$\sigma_y^2 = \frac{1}{2\beta\lambda} \int_{-\beta}^{\beta} \int_{o}^{\lambda} [y - (B_o + \eta)]^2 \, d\xi \, d\eta \, . \qquad (34)$$

These expressions are measures of the "curvilinearity" of the transforms $x(\xi,\eta)$ and $y(\xi,\eta)$. From equations (9) and (10), it can be shown that

$$\sigma^2 = \sum_{n=1}^{N} \sigma_n^2 \, , \qquad (35)$$

where the contribution to the total curvilinearity variance due to the n^{th} term is:

$$\sigma_n^2 = \frac{(B_n^2 + C_n^2) \sinh 2nk\beta}{4nk\beta} \, . \qquad (36)$$

The value of σ_n^2/σ^2 is a more meaningful measure of the relative importance of the various terms in the transformation than the raw B_n, C_n coefficients. The curvilinearity variance spectrum given by σ_n^2/σ^2 as a function of n for the final transform of the five regions is shown in Figure 20. The values of σ^2 and σ/λ for the five regions are indicated in the figure. Each of the curves indicates a general inverse power law trend of about 4th degree. The variability of the spectrum in all but the middle curve is more pronounced in the higher harmonics than in the lower.

3. Limitations.

Testing of the conformal mapping equations was conducted with coastlines that varied in the degree of smoothness and regions that varied in λ. Another version of the coastline from Cape Kennedy to Pamlico Sound is shown in Figure 21. Comparing Figure 5 with this version, it can be seen that there are two small differences in the form of the coastline. Figure 21 shows the narrowing of the Continental Shelf in the area south of Cape Kennedy. Another difference is the slightly sharper vertex at Cape Kennedy, Cape Fear, and Cape Lookout. The (general) solution of the mapping equations proved unstable for this situation. It is not known which change in the coastline permitted the convergence of the iterative procedure for Figure 5.

One test of the mapping equations was conducted on the region from Matagorda Bay to Apalachee Bay (Figure 22). This region is the result of joining Figures 3 and 4 and represents in this study, the

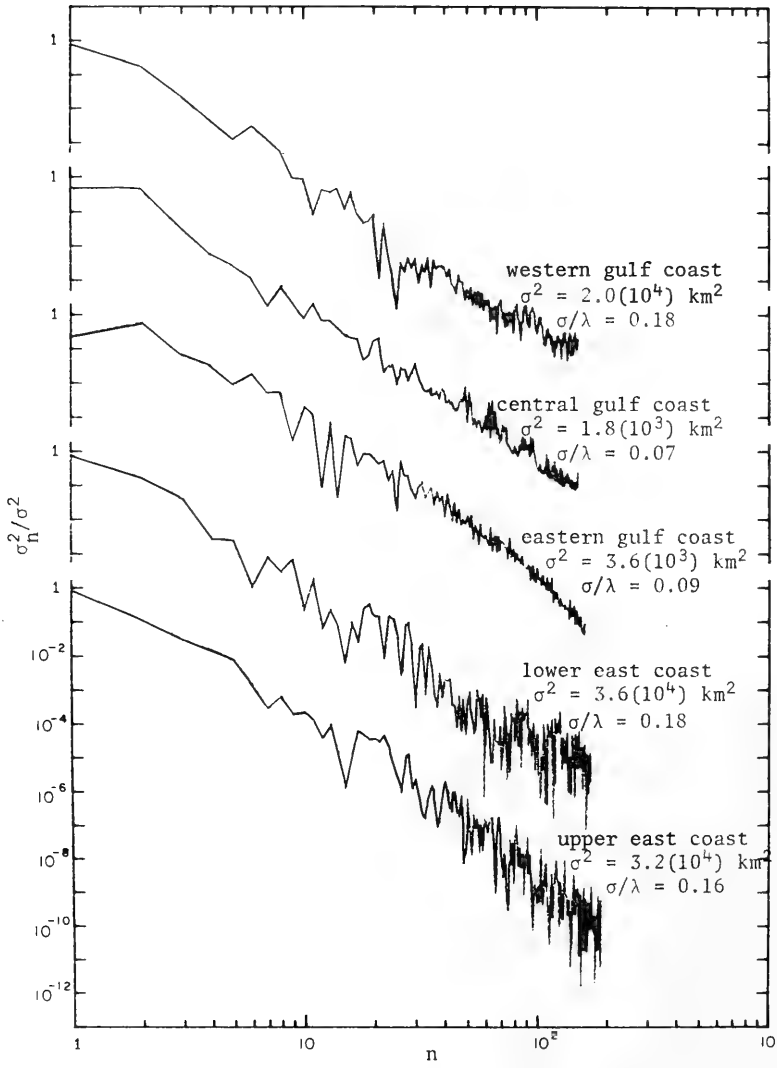

Figure 20. The "curvilinearity" variance spectra for the final transform of the five mapped regions.

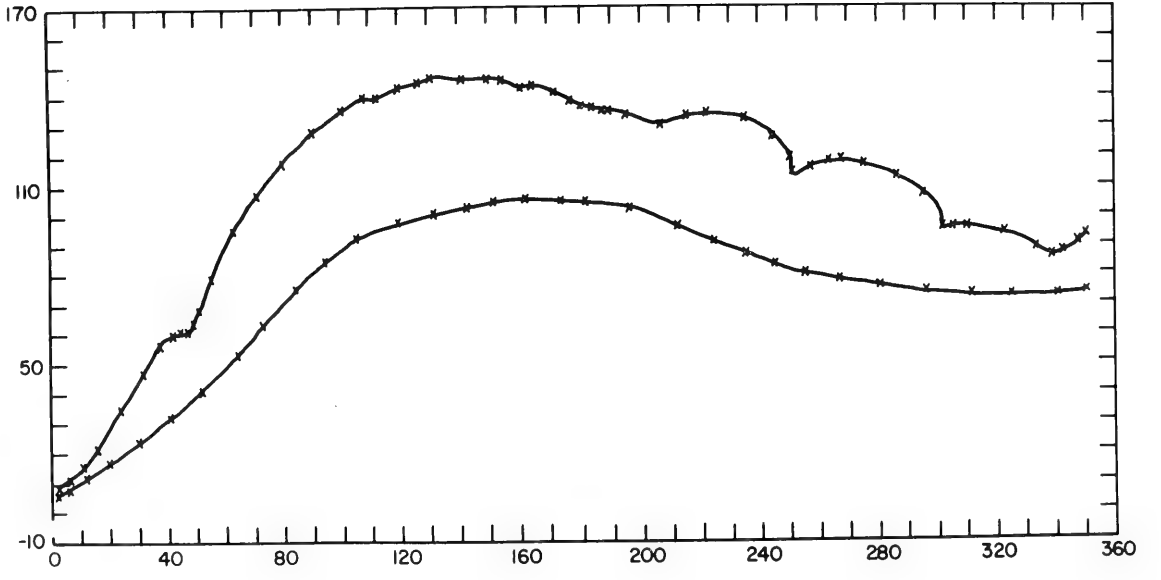

Figure 21. Coastline (top) and seaward boundary curve (bottom), lower east coast.

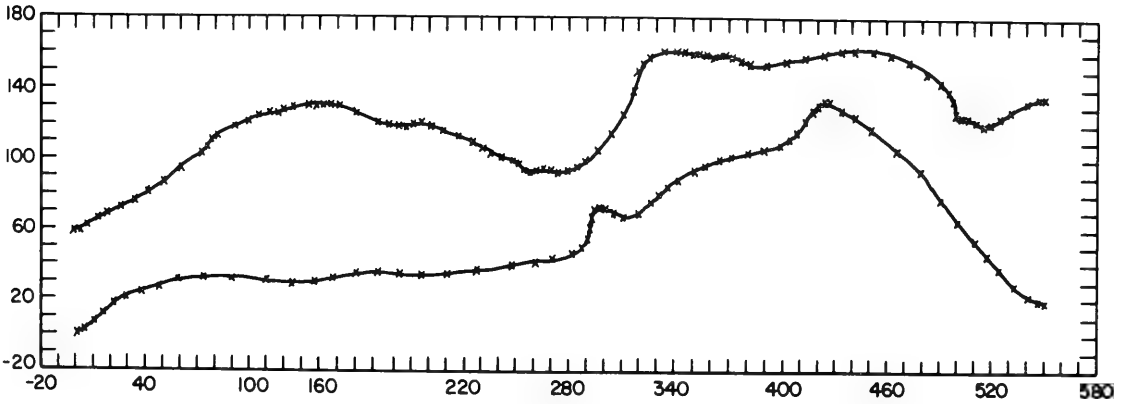

Figure 22. Coastline (top) and seaward boundary curve (bottom), central and eastern gulf coasts.

longest horizontal extent of a region to be mapped. The mean variance between the mapped curves and that specified after 120 iterations with n=140 was 4.4 square kilometers. The level of variance achieved indicates that the bicurve fitting equations are marginally successful in mapping this enlarged region. The change in the variance level over the last 10 iterations and limits on computer time were the bases for terminating the iterative procedure. The convergence criteria can be satisfied either by a shorter horizontal extent or smoother curves for a longer region.

III. THE STORM SURGE EQUATIONS IN THE SHELF COORDINATE SYSTEM

1. Stretched Shelf Coordinate System.

Consider the transform-generated coastline and seaward boundary curves as shown in Figure 23. The orthogonal curvilinear mesh associated with the coordinates (ξ,η) is designated the *shelf coordinate system.* Although the surge calculations can be performed in the shelf coordinate system (Figure 23b), a problem remains in obtaining the desired spatial resolution with the fewest possible computational points. The computing grid employed (Figure 23c) is the result of a second transformation which preserves the orthogonality property but allows independent stretching of ξ and of η. The grid resulting from the second transformation is termed the *stretched shelf coordinate system* (S^*,T^*).

The stretched shelf coordinate system is generated by independently transforming the ξ and η axes in the following manner:

(a) Given the hurricane storm track, the location where the storm crosses the coast and the coastline configuration, the values of ξ along the coastline are determined which will produce a constant relatively fine increment of coastline arc length, S_p. In this area of prime interest, line BC in Figure 23(a), the constant increment of arc length is equal to ΔS^*. However, regions AB and CD show that for the same ΔS^* as above, there is a relative expansion of the increment of the coastline arc length. The functional relationship between ξ and S^* is:

$$S^* = S^*(S_p(\xi)) \ , \tag{37}$$

where the expansion of S_p with respect to S^* is specified by an (arbitrary) analytical expression of the form $S_p = A + B(S^*)^C$ where A, B, and C are constants.

(b) For the shelf bathymetry along a particular centrally located isoline of ξ, the values of η are determined which will yield a constant change in the time, ΔT^*, required for a long wave traveling at the local free wave celerity to proceed from seaward boundary to the coast. The long wave travel time, T, is calculated by:

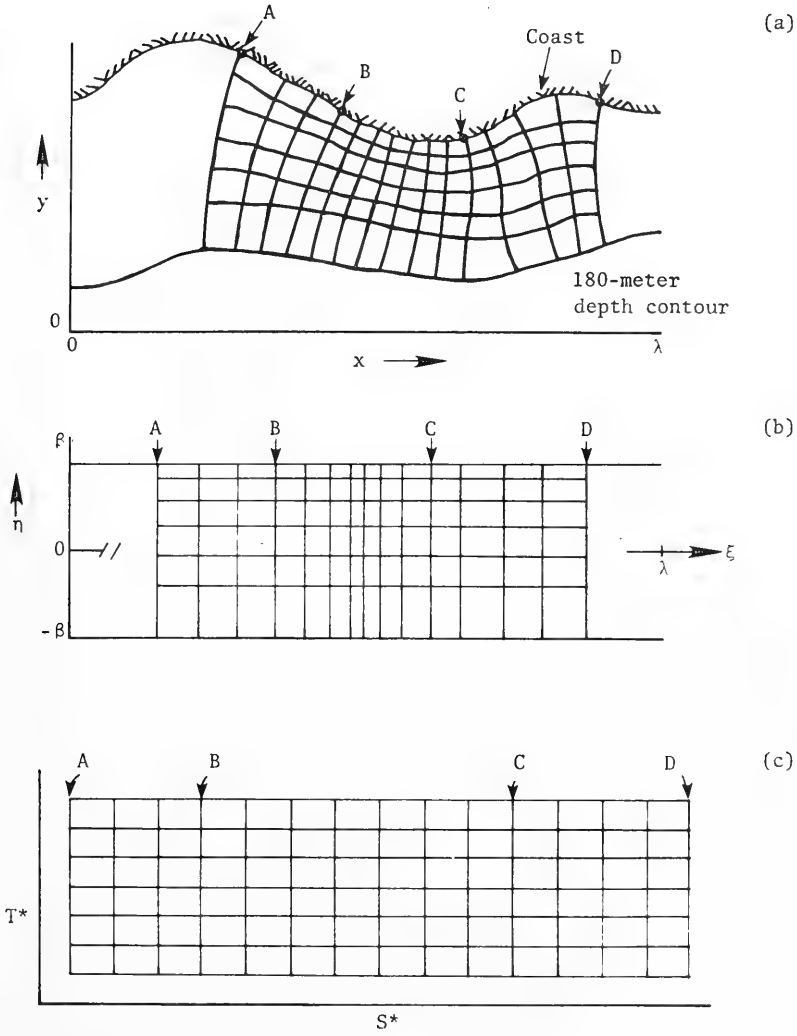

Figure 23. Orthogonal curvilinear grid system in the Z-plane (a), in the ζ-plane (b), and in the computing grid (c).

$$T = \int_{S_n(\eta)} \frac{ds}{\sqrt{gD_o}} \quad , \tag{38}$$

where S_n is the distance along the isoline of ξ, D_o is the local depth relative to mean sea level, and g is the acceleration due to gravity. The relation between η and T^* is given by:

$$T^* = T^*(T(S_n(\eta))) \quad , \tag{39}$$

The incremental values of T^* are determined from equation (38) subject to the (arbitrary) expansion relationship of $T^*(T)$. This relationship is a convenience which permits an additional degree of freedom in adjusting the relative spacing between isolines of η. However, if $T^* = T$, the value of ΔT^* is that which divides the total long wave travel time by an integer number of lines of η. The selection of the final ΔT^* is based upon a compromise for providing adequate resolution for the wind field and the resulting surge with a minimum number of points. The form chosen for the expansion is $T = A + B(T^*)^C$ where A, B, and C are constants.

The stretched shelf coordinate system provides a grid system with a finer resolution near the coast than at the 180-meter isobath. The expansion curve, $S^*(S_p)$, stretches the horizontal reach of the grid while maintaining a finer grid in the area of landfall of the hurricane. In this manner an economy is achieved in terms of the number of grid points required by the surge program. However, because the preferred expansion curves dictate the locations (in x,y space) of the depths required for the surge calculations, the depth field must be redefined for different pairs of stretching functions. Application of this procedure has been accomplished for the simulation of the storm surges caused by Hurricanes Carla, Camille, and Gracie. Figure 24 shows the transform-generated coastline and seaward boundary curves for the western gulf coast area. Also shown is the shelf coordinate system (ξ,η) which was employed in the Hurricane Carla surge simulation. The track of the hurricane is the dashline. The grid system extends over approximately 750 kilometers of coastline. The stretched shelf coordinate system (Figure 25) is attained through the functional relationships specified in Figure 26 for the S* axis and Figure 27 for the T* axis. The shelf coordinate system, the stretched shelf coordinate system, and similar transformation relationships are shown in Figures 28 through 31, for the grid used to simulate the storm surge caused by Hurricane Camille, and in Figures 32 through 35 for the grid associated with the Hurricane Gracie storm surge.

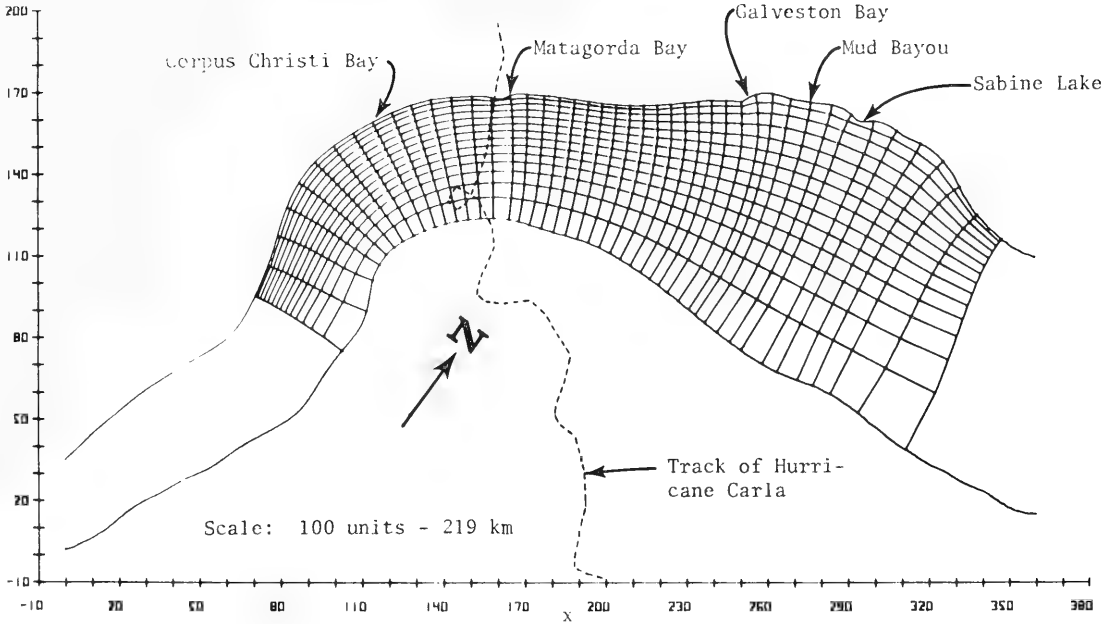

Figure 24. Shelf coordinate system (ξ,η) for Hurricane Carla surge simulation.

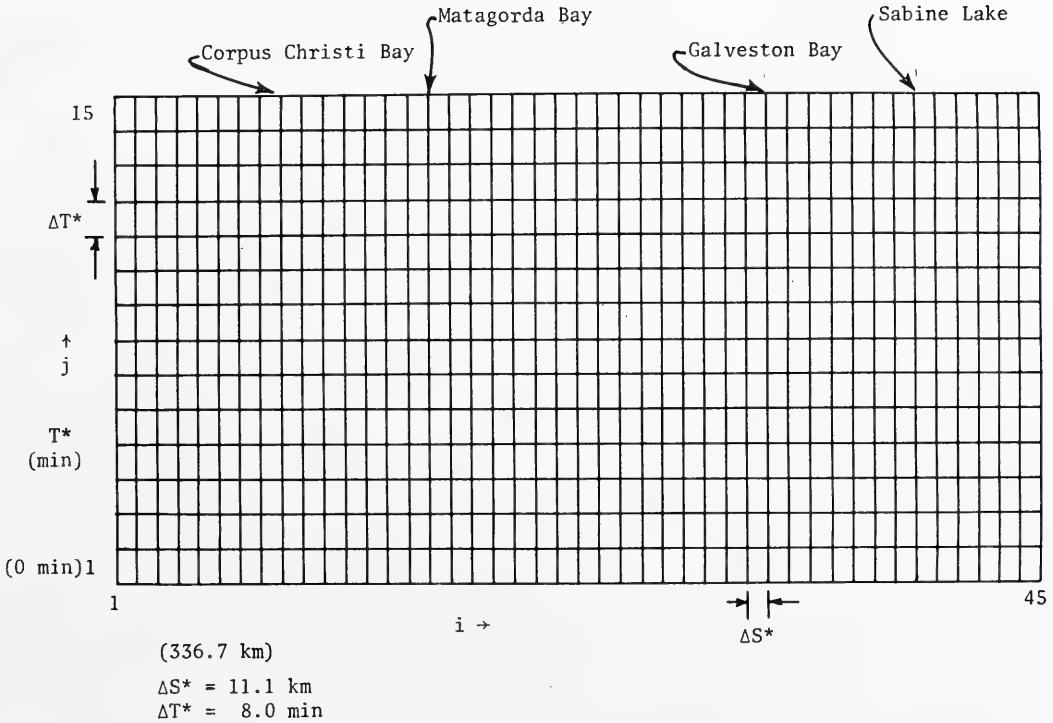

Figure 25. Stretched shelf coordinate system (S*,T*) for Hurricane Carla surge simulation.

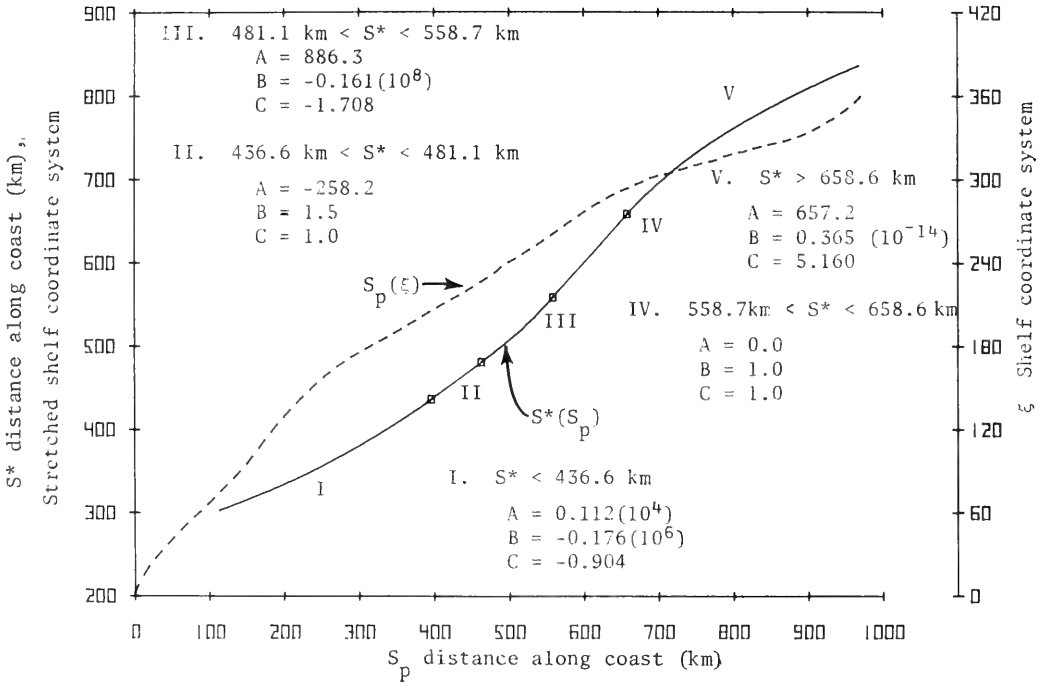

Figure 26. Functional relationships transforming ξ to S* for Hurricane Carla surge simulation.

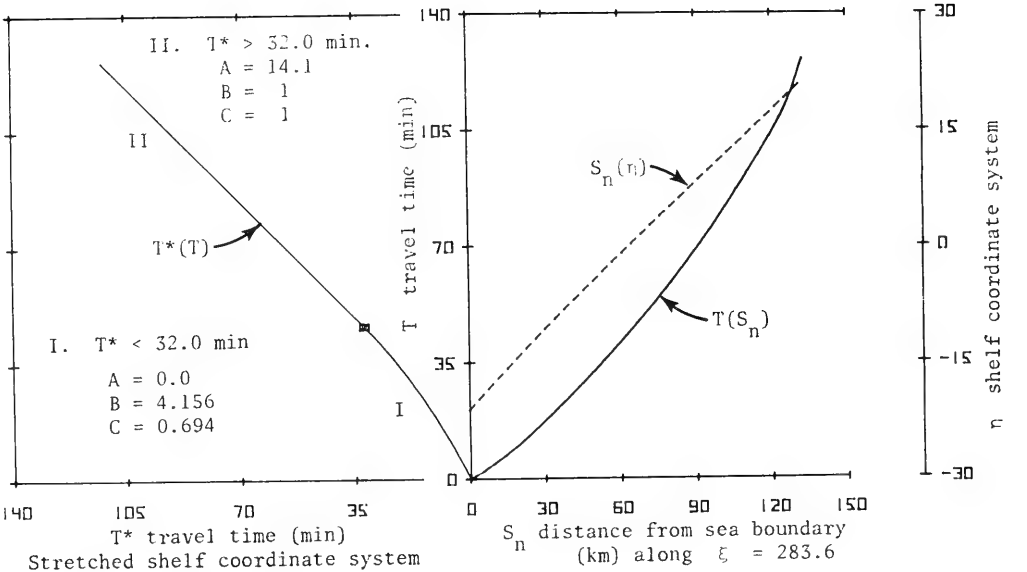

Figure 27. Functional relationships transforming η to T* for Hurricane Carla surge simulation.

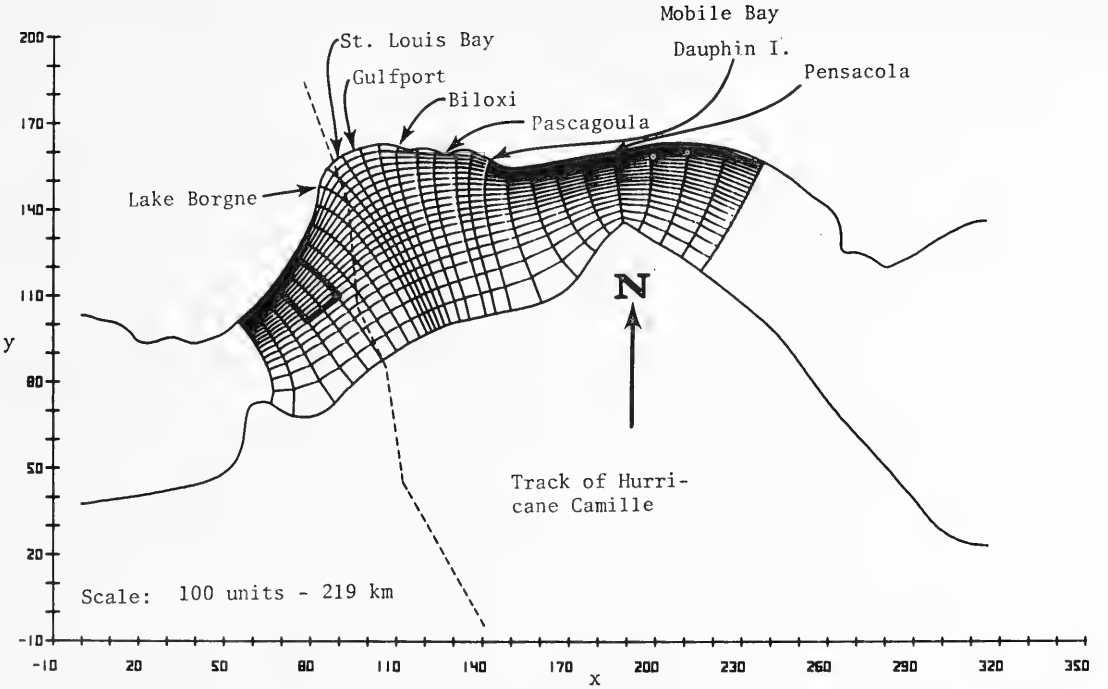

Figure 28. Shelf coordinate system (ξ,η) for Hurricane Camille surge simulation. Outline of simulated Mississippi Delta shown by heavy line (this extends only to the seaward end of the Mississippi River levee).

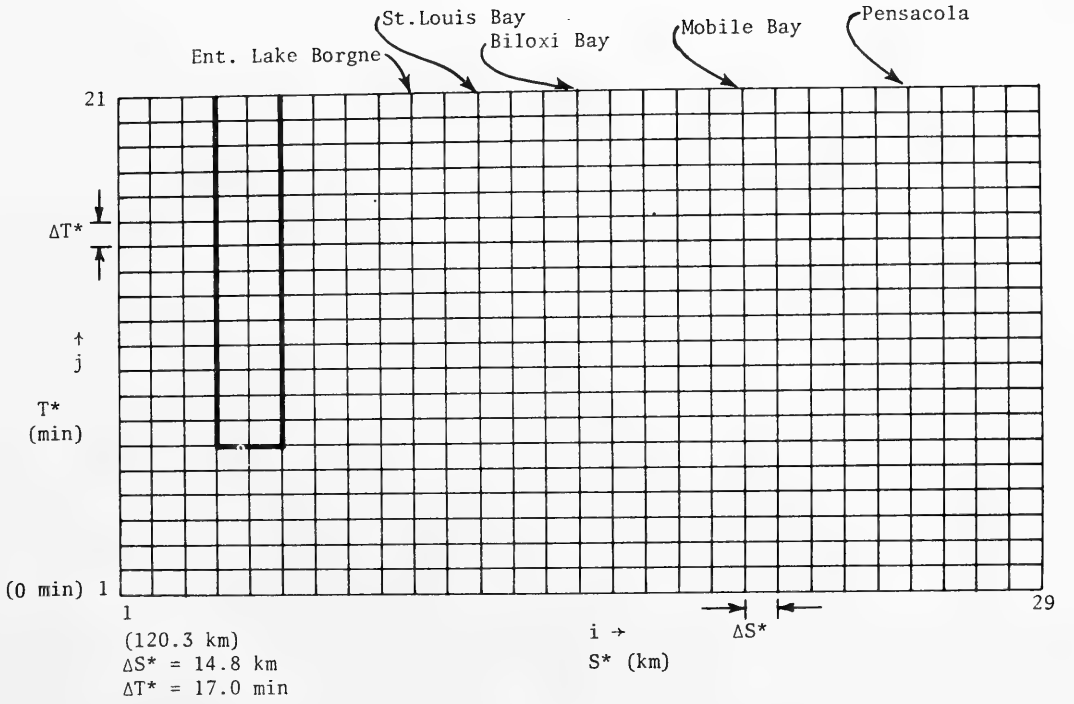

Figure 29. Stretched shelf coordinate system (S*,T*) for Hurricane Camille surge simulation.

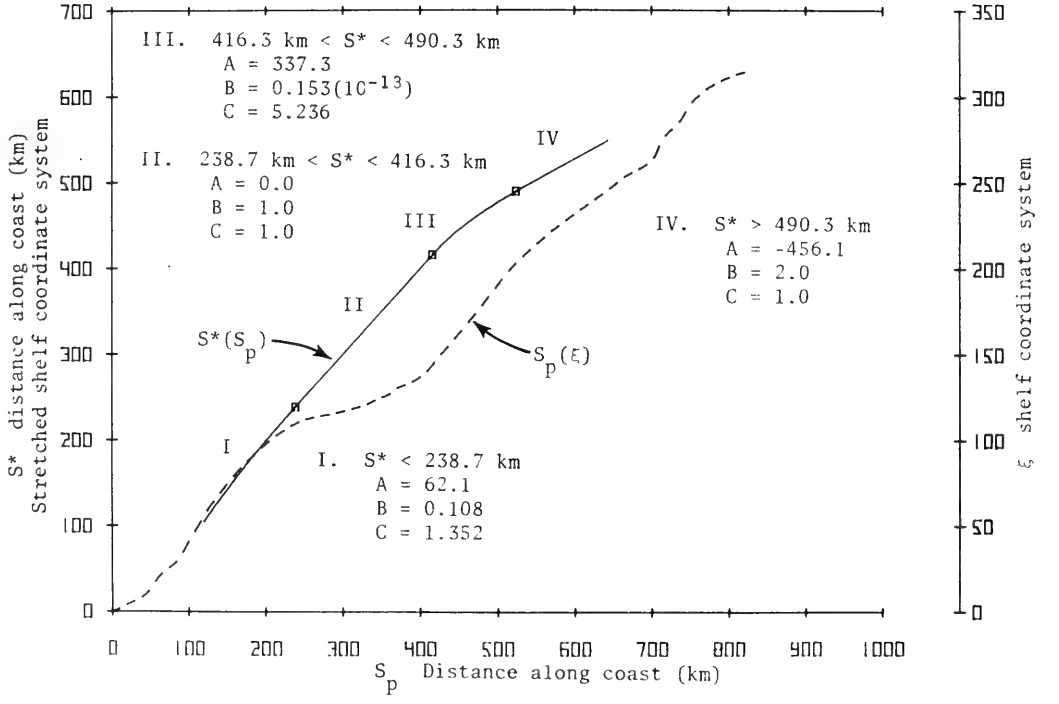

Figure 30. Functional relationships transforming ξ to S* for Hurricane Camille surge simulation.

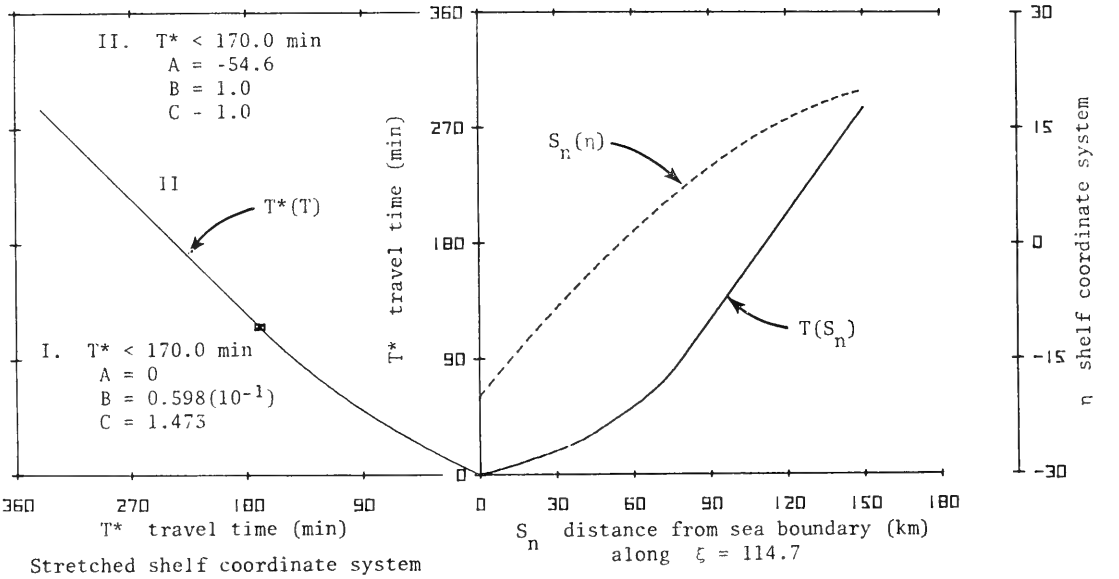

Figure 31. Functional relationships transforming η to T* for Hurricane Camille surge simulation.

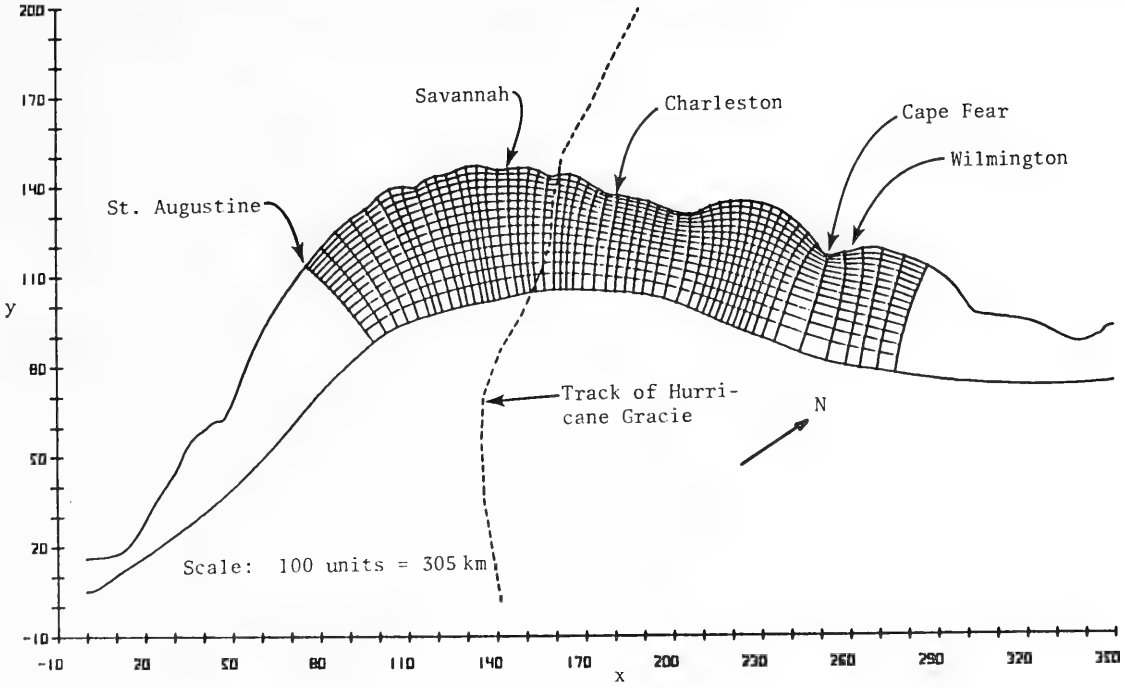

Figure 32. Shelf coordinate system (ξ,η) for Hurricane Gracie surge simulation.

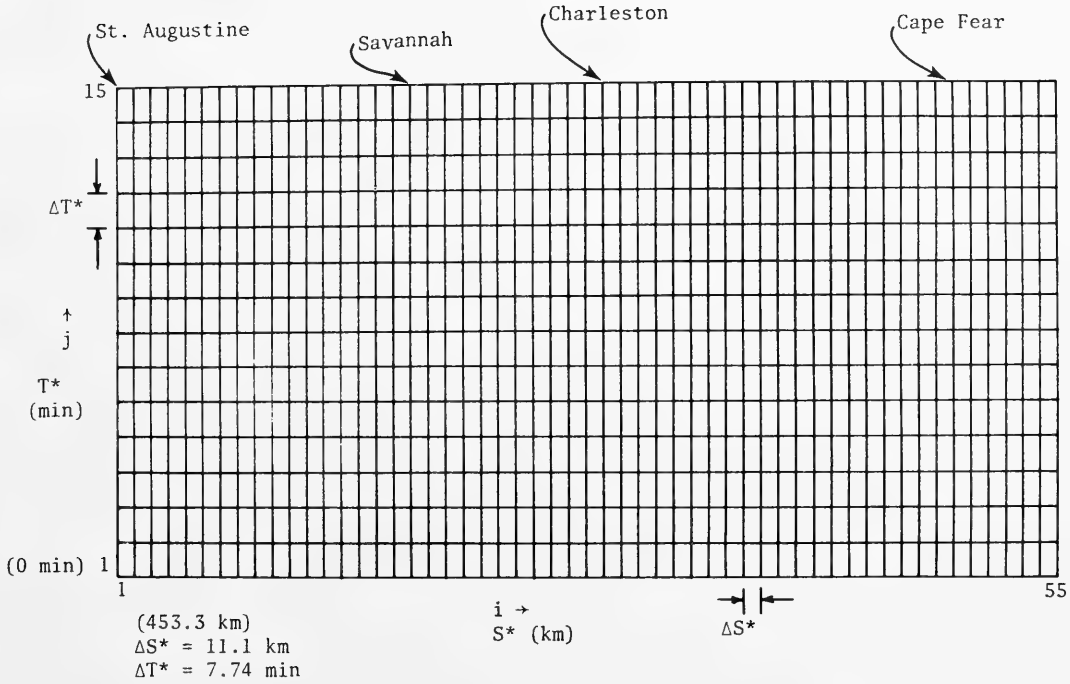

Figure 33. Stretched shelf coordinate system (S*,T*) for Hurricane Gracie surge simulation.

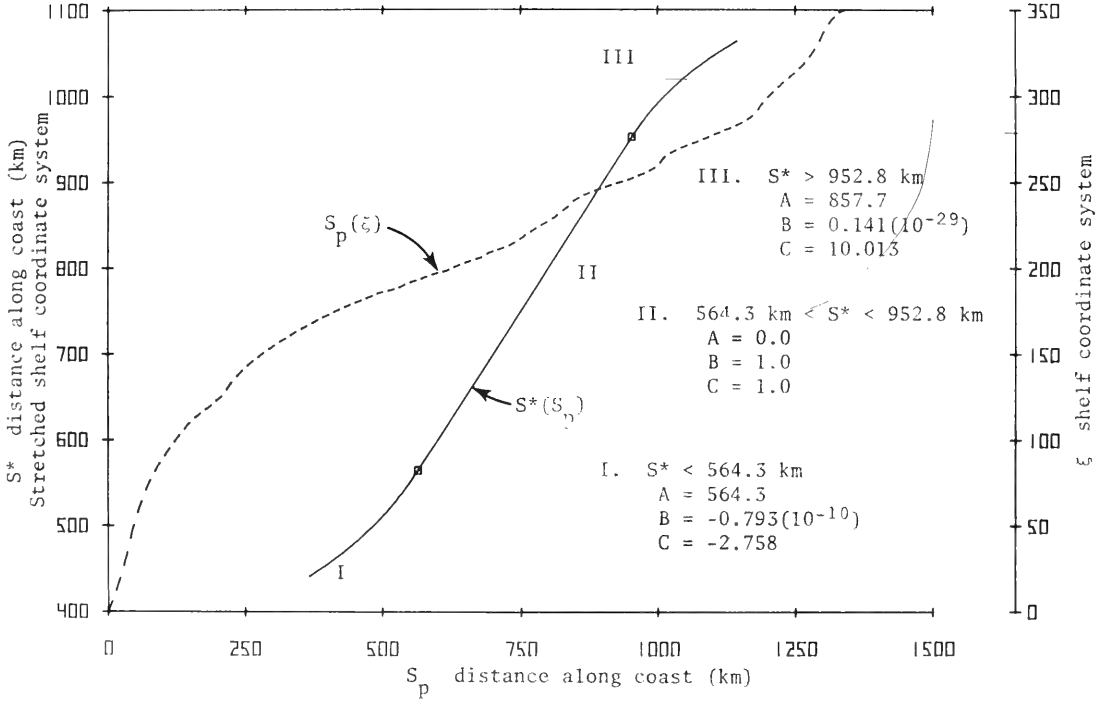

Figure 34. Functional relationships transforming S_p to S^* for Hurricane Gracie surge simulation.

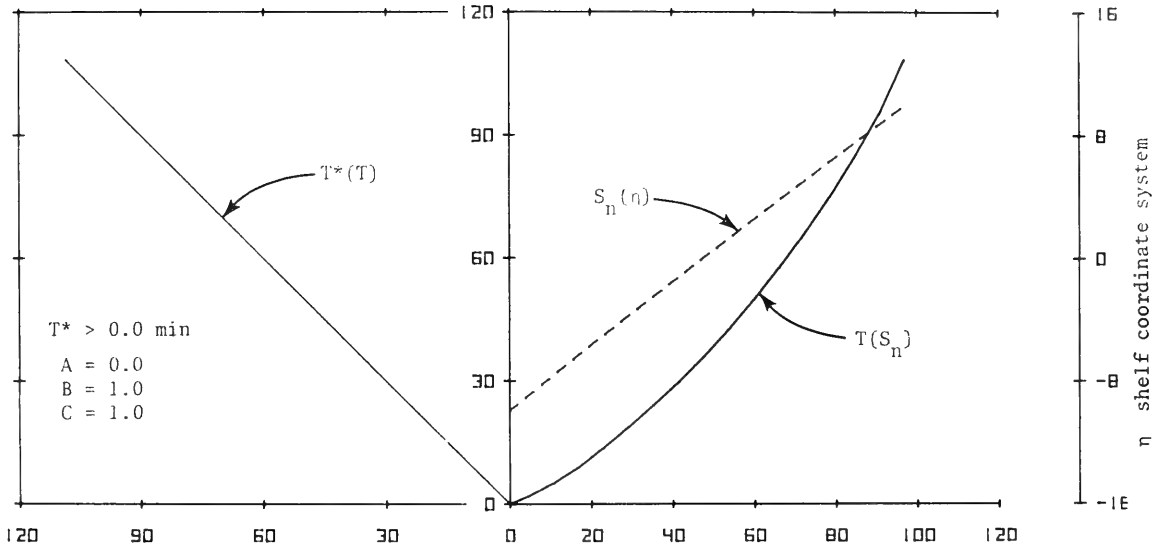

Figure 35. Functional relationships transforming η to T* for Hurricane Gracie surge simulation.

2. Storm Surge Equations.

The vertically integrated form of the quasi-linear long wave equations in a Cartesian system are well known (e.g., Welander, 1961). The appropriate forms for storm surge computation in the stretched shelf coordinate system are as follows:

$$\frac{\partial Q_{S^*}}{\partial t} - f\, Q_{T^*} + \frac{gD}{F\mu} \frac{\partial}{\partial S^*} (H - H_B) = \tau_{S^*} - \sigma_{S^*} , \qquad (40)$$

$$\frac{\partial Q_{T^*}}{\partial t} + f\, Q_{S^*} + \frac{gD}{F\nu} \frac{\partial}{\partial T^*} (H - H_B) = \tau_{T^*} - \sigma_{T^*} \qquad (41)$$

and

$$\frac{\partial H}{\partial t} + \frac{1}{F^2} \left[\frac{1}{\mu} \frac{\partial}{\partial S^*} (FQ_{S^*}) + \frac{1}{\nu} \frac{\partial}{\partial T^*} (FQ_{T^*}) \right] = 0 , \qquad (42)$$

where Q is the volume transport per unit width, τ is the wind stress divided by the water density, σ is the bottom resistance stress divided by water density, f is the Coriolis parameter, D is depth of water, H is the sea surface elevation relative to mean sea level, and H_B is the hydrostatic elevation of the sea surface corresponding to the atmospheric pressure anomaly. The term F is a variable scale factor associated with the conformal part of the orthogonal curvilinear coordinate system. Specifically,

$$F = \left[\left(\frac{\partial x}{\partial \xi} \right)^2 + \left(\frac{\partial y}{\partial \xi} \right)^2 \right]^{\frac{1}{2}} , \qquad (43)$$

where x and y are given by the transformation equations. The terms μ and ν, are additional scale factors that relate to the transformation of ξ to S^* and η to T^*, respectively, and are given by:

$$\mu = \frac{\partial \xi}{\partial S_p} \frac{\partial S_p}{\partial S^*} , \qquad (44)$$

and

$$\nu = \frac{\partial \eta}{\partial S_n} \frac{\partial S_n}{\partial T} \frac{\partial T}{\partial T^*} . \qquad (45)$$

Furthermore, $F^2\mu\nu$ corresponds to the Jacobian of the transformation in the sense that

$$A = \int_{R^*} \int F^2 \mu\nu \, dS^* \, dT^* , \qquad (46)$$

where A is the area of a closed region R in the x,y plane whose mapped image is R^*.

The kinematic wind-stress components τ_{S^*} and τ_{T^*} are related to their x,y component counterparts (τ_x, τ_y) at a given point by:

$$\tau_{S^*} = \tau_x \cos\theta + \tau_y \sin\theta \ , \tag{47}$$

and

$$\tau_{T^*} = -\tau_x \sin\theta + \tau_y \cos\theta \ , \tag{48}$$

where

$$\theta = \tan^{-1}\left(\frac{\partial y/\partial\xi}{\partial x/\partial\xi}\right) \ . \tag{49}$$

The relation between the wind stress and windspeed is:

$$\tau = K W_{10}^2 \ , \ K = \frac{\rho_A}{\rho_W} C_D \ , \tag{50}$$

where ρ_A is the air density, ρ_W is the water density, C_D is a nondimensional drag coefficient, and W_{10} is the windspeed at an elevation of 10 meters above the water surface. The value of K (Reid and Bodine, 1968) is taken as:

$$K = \begin{cases} K_1 & , \text{ if } W_{10} \leq 7.0 \text{ m}\cdot\text{s}^{-1} \\ K_1 + \left[1.0 - 7.0/W_{10}\right]^2 K_2 & , \text{ if } W_{10} \geq 7.0 \text{ m}\cdot\text{s}^{-1} \end{cases}$$

where K_1 is 1.1×10^{-6} and K_2 is 2.5×10^{-6}.

The values of K_1 and K_2 used by Whitaker, Reid, and Vastano (1973) for Lake Okeechobee were found to be too large for the shelf surge computations investigated in this study.

The form of the bed resistance terms are:

$$\sigma_{S^*} = \frac{K_o Q}{D^2} Q_{S^*} \ , \tag{52}$$

and

$$\sigma_{T^*} = \frac{K_o Q}{D^2} Q_{T^*} \ , \tag{53}$$

where

$$Q = [Q_{S*}^2 + Q_{T*}^2]^{\frac{1}{2}} , \qquad (54)$$

and K_o is a nondimensional drag coefficient taken as 2.5×10^{-3}.

3. Numerical Algorithm.

The numerical analogs of equations (40), (41), and (42) are based upon centered difference approximations of all terms (see App. F). The algorithm treats the time dependency explicitly and employs a computing lattice as shown in Figure 36 in which the transports, Q_{S*} and Q_{T*} are computed at the same location but are staggered in time and space with respect to the water level anomaly. This scheme facilitates a simple representation of the Coriolis and bottom stress terms in the difference equations. The surge model allows for variable bathymetry and arbitrary coastlines which are represented as a series of connecting straight line segments situated along lines of constant S* or T* . For the simulation of the Hurricane Camille storm surge, the arbitrary coastline feature of the algorithm is mandatory to delineate the delta. However, in the more usual application, the coast is a straight line in the computing grid.

The difference equations for Q_{S*}, Q_{T*}, and H at interior points of the computing grid are given by:

$$Q_{S*}(i,j,n+1) = (G_1 G_2 + f \Delta t G_3)/(G_1^2 + (f \Delta t)^2) , \qquad (55)$$

$$Q_{T*}(i,j,n+1) = (G_1 G_3 - f \Delta t G_2)/(G_1^2 + (f \Delta t)^2) , \qquad (56)$$

and

$$H(i,j,n+1) = H(i,j,n-1) - \frac{\Delta t}{F(i,j)^2} \left[\frac{F(i+1,j)\, Q_{S*}(i+1,j,n) - F(i-1,j)\, Q_{S*}(i-1,j,n)}{\mu(i)\, \Delta S^*} + \frac{F(i,j+1)\, Q_{T*}(i,j+1,n) - F(i,j-1)\, Q_{T*}(i,j-1,n)}{\nu(j)\, \Delta T^*} \right] \qquad (57)$$

where i , j , and n indices express the S* , T* , and time coordinates, respectively, and Δt is the numerical time step. The quantities G_1 , G_2 , and G_3 are given by:

$$G_1 = 1 + 2 K_o \Delta t\, Q(i,j,n-1)/\bar{D}^2 , \qquad (58)$$

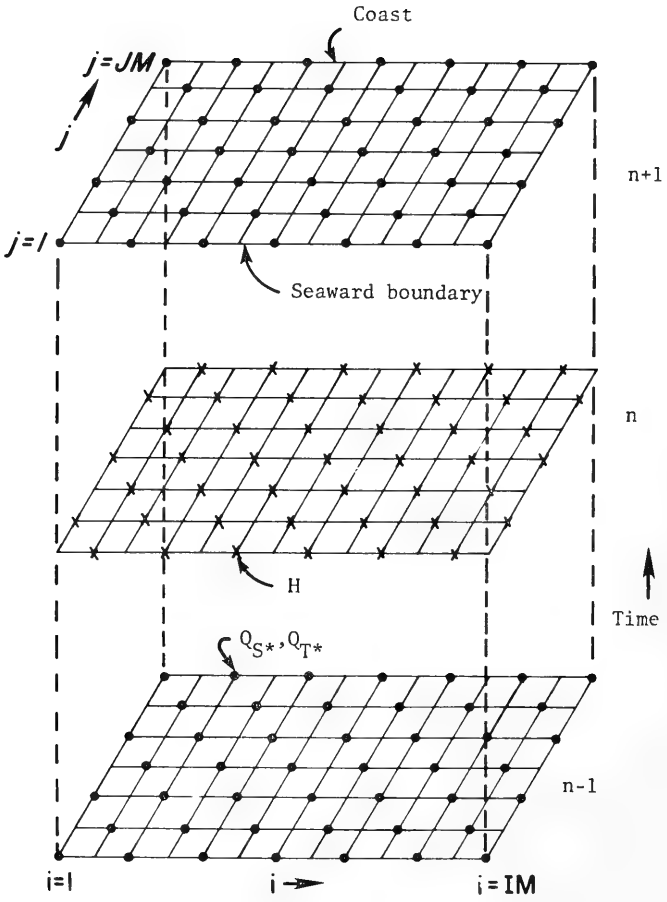

Figure 36. Scheme for computed variables.

$$G_2 = Q_{S*}(i,j,n-1) + f\,\Delta t\, Q_{T*}(i,j,n-1)$$

$$- \frac{g\,\Delta t\,\bar{D}}{\mu(i)\,F(i,j)\,\Delta S^*}\left[H(i+1,j,n) - H_B(i+1,j,n) - H(i-1,j,n) + H_B(i-1,j,n)\right] + 2\,\Delta t\,\tau_{S*}\ , \qquad (59)$$

$$G_3 = Q_{T*}(i,j,n-1) - f\,\Delta\, Q_{S*}(i,j,n-1)$$

$$- \frac{g\,\Delta t\,\bar{D}}{\nu(j)\,F(i,j)\,\Delta T^*}\left[H(i,j+1,n) - H_B(i,j+1,n) - H(i,j-1,n) + H_B(i,j-1,n)\right] + 2\,\Delta t\,\tau_{T*}\ , \qquad (60)$$

where

$$\bar{D} = \tfrac{1}{4}\left[D(i+1,j,n) + D(i-1,j,n) + D(i,j+1,n) + D(i,j-1,n)\right]\ . \qquad (61)$$

In order to maintain numerical stability, the time step must satisfy the condition:

$$\Delta t < \left\{\frac{F\mu\nu}{G_4}\,\frac{\Delta S^*\,\Delta T^*}{\sqrt{gD}}\right\}_{\min}\ , \qquad (62)$$

where

$$G_4 = \left[(\mu\,\Delta S^*)^2 + (\nu\,\Delta T^*)^2\right]^{\frac{1}{2}}\ , \qquad (63)$$

and the minimum value of the right-hand side of relation (26) is implied. Thus, a search of the grid is required for a proper selection of Δt. However, the conditions along the seaward boundary usually limit the time step because of the deeper water.

The values of μ, ν, F, and θ given by equations (44), (45), (46) and (49), are required at the appropriate computational grid points. A numerical spline under tension is employed to interpolate ξ given the IM values of $S_p(S^*)$. The scale factor, μ, is determined by:

$$\mu(i) = \frac{\xi(i+1) - \xi(i-1)}{2\Delta S^*} \qquad (64)$$

$$i = 1,2 \cdots IM\ ,$$

where $\xi(o)$ and $\xi(IM+1)$ are ascertained by expanding the computing grid one increment of ΔS^* to the left and right, respectively. In a similar fashion, the JM values of η may be determined and the scale factor ν given by:

$$\nu(j) = \frac{\eta(j+1) - \eta(j-1)}{2\ \Delta T^*} \quad , \tag{65}$$

$$j = 2,3 \cdots JM-1.$$

Since the computing grid may not be extended landward or toward deeper water, the approximation at $j = 1$ and $j = JM$ is made that:

$$\nu(1) = [\eta(2) - \eta(1)]/\Delta T^* \ , \tag{66}$$

and

$$\nu(JM) = [\eta(JM) - \eta(JM-1)]/\Delta T^* \ . \tag{67}$$

The area in the x,y plane of each grid block, including those from expanding the grid in the ξ direction, is determined by numerical procedure from the following relation:

$$A(i,j) = \int_{\eta_j}^{\eta_{j+1}} \int_{\xi_{i-1}}^{\xi_i} \left| \left(\frac{\partial x}{\partial \xi}\right)^2 + \left(\frac{\partial y}{\partial \xi}\right)^2 \right| d\xi\ d\eta \quad , \tag{68}$$

$$i = 1,2 \cdots IM+1 \ ,$$

$$j = 1,2 \cdots JM \ .$$

The scale factor associated with the conformal mapping is determined from equation (46) at intersectional points, excluding the coast and seaward boundary, by the expression:

$$F(i,j) = \left[\frac{A(i,j) + A(i,j+1) + A(i+1,j) + A(i+1,j+1)}{4\ \Delta S^*\ \Delta T^*\ \mu(i)\ \nu(j)}\right]^{\frac{1}{2}} \quad , \tag{69}$$

$$i = 1,2 \cdots IM \ ,$$

$$j = 2,3 \cdots JM-1 \ ,$$

and for grid points along $j = 1$ or JM by the approximation:

$$F(i,j) = \left| \frac{A(i,j) + A(i+1,j)}{2\ \Delta S^*\ \Delta T^*\ \mu(i)\ \nu(j)} \right|^{\frac{1}{2}} , \qquad (70)$$

$$i = 1,2 \cdots IM .$$

The angle, θ , relating the orientation of the stretched shelf coordinate system to the x,y plane is determined at grid points, excluding j = 1 and JM , by the following smoothing procedure:

$$\theta(i,j) = \frac{1}{8}\left[\theta^{\dagger}(i-1,j) + \theta^{\dagger}(i,j-1) + \theta^{\dagger}(i+1,j) + \theta^{\dagger}(i,j+1) + 4\theta^{\dagger}(i,j) \right] , \qquad (71)$$

$$i = 1,2 \cdots IM ,$$

$$j = 2,3 \cdots JM-1 ,$$

where $\theta^{\dagger}$ is given by equation (44). Along the sea and coastline boundaries we have

$$\theta(i,1) = \frac{1}{8}\left[\theta^{\dagger}(i-1,1) + 2\theta^{\dagger}(i,2) + \theta^{\dagger}(i+1,1) + 4\theta^{\dagger}(i,1) \right] , \qquad (72)$$

$$i = 1,2 \cdots IM ,$$

and

$$\theta(i,JM) = \frac{1}{8}\left[\theta^{\dagger}(i-1,JM) + 2\theta^{\dagger}(i,JM-1) + \theta^{\dagger}(i+1,JM) + 4\theta^{\dagger}(i,JM) \right] , \qquad (73)$$

$$i = 1,2 \cdots IM .$$

4. Boundary Conditions.

A wall condition is employed in the surge simulation along the coast while the surface elevation anomaly is placed in equilibrium with the atmospheric pressure along the seaward boundary. Vanishing normal derivatives of transport are specified on the lateral open boundaries. This condition is used by Jelesnianski (1965, 1966) and Forristall (1974), although it may not be the most desirable (Reid, 1975).

In the x,y plane the coast is curved making the wall (coast) and lateral boundary conditions difficult to apply in a rectilinear grid system. However, the stretched shelf coordinate system represents the coast as:

$$Q_{T^*} = 0 , \qquad (74)$$

or, the analog is simply,

$$Q_{T*}(i,JM,n+1) = 0 \ , \tag{75}$$

$$i = 1,3 \cdots IM \ .$$

Thus, total reflection is assured at the boundary. The flux, Q_{S*}, along the coastline is calculated from equation (55) with $\overline{D}$ taken as the two point average of the local fluid depths along the coast. The local depths ranged from 1.0 to 2.3 meters, depending on the seaward bottom slope and surrounding elevations. The water elevations along the coast are computed from the continuity relation as given by equation (57) with the following substitution:

$$F(i,JM+1)\ Q_{T*}(i,JM+1,n-1) = -F(i,JM-1)\ Q_{T*}(i,JM-1,n-1) \ , \tag{76}$$

$$i = 2,4 \cdots IM-2 \ .$$

This is an artifact consistent with total reflection.

For the simulation of the Hurricane Camille storm surge, the normal routine of the surge program was interrupted at those grid points representing the protruding Mississippi Delta. Along this part of the coast (the solid heavy line in Figures 28 and 29), the normal flux was set to zero and the tangential flux was determined from either equation (55) or equation (56) with the Coriolis term vanishing. The continuity relation is altered depending on the orientation of the boundary to be consistent with total reflection.

The open deep sea boundary condition is:

$$H(i,1,n+1) = H_B(i,1,n+1) \ , \tag{77}$$

$$i = 2,4 \cdots IM-1 \ ,$$

and

$$H(i,2,n+1) = [H(i-1,1,n+1) + H(i+1,1,n+1) + H(i-1,3,n+1) + H(i+1,3,n+1)]/4 \ , \tag{78}$$

$$i = 3,5 \cdots IM-2 \ .$$

Specifying the seaward boundary in this sawtooth form obviates the calculations of Q_{S*} and Q_{T*} along the boundary since they are not required for computations at interior points.

The lateral open boundary condition requires the normal gradient of the S*-directed transport to vanish,

$$\frac{\partial Q_{S^*}}{\partial S^*} = 0 \ . \tag{79}$$

This condition implies that along the left side of the grid,

$$Q_{S^*}(1,j,n+1) = Q_{S^*}(3,j,n+1) \ , \tag{80}$$

$$j = 3,5 \cdots JM$$

and along the right side,

$$Q_{S^*}(IM,j,n+1) = Q_{S^*}(IM-2,j,n+1) \ , \tag{81}$$

$$j = 3,5 \cdots JM \ .$$

The S*-directed transports for even j and $i=2$ or IM-1 are determined by the average of the two neighboring interior values. Additionally, the T*-directed transports are required along $i=2$ or IM-1 and are calculated from equation (56) where $\bar{D}$ is again the average of the local fluid depth along the boundary.

Special computations are required at seaward corner points (2,2) and (3,1). Simultaneous equations are solved for $Q_{T^*}(2,2,n+1)$ and $Q_{S^*}(3,1,n+1)$ with the approximation that $Q_{T^*}(3,1,n+1)$ is the average of the two neighboring interior values. Similar expressions are used at the right-hand seaward corner points.

Other conditions at the seaward and lateral boundaries were experimented with for the Hurricane Carla simulations. These included radiational conditions of the type discussed by Reid and Bodine (1968) and Reid (1975). The main differences, as anticipated, were close to the lateral boundaries where the "flow through" condition in equation (79) gave a more realistic rendition of the longshore flow.

The basic numerical model was used successfully by Alvarez (1973). Further testing of the algorithm, where in some cases an analytical solution was possible for comparison purposes, is presented in Appendix G.

5. Wind and Pressure Fields.

Of major importance in simulating the storm surge is the accurate portrayal of the hurricane wind field on the computing grid. Moreover, the representation of the wind must be time-dependent.

The Hydrometeorological Section of the National Weather Service (NWS) provided charts of the surface winds at 10 meters above mean

sea level and of the barometric pressure for Hurricanes Carla and Camille. One method for representing the wind field is to digitize the above charts for the hurricane in question. Usually the wind and pressure data depicting the storm are sampled in time at particular grid points and interpolated to provide the necessary input to the surge model. However, such input data are tedious and laborious to obtain and do not guarantee better quality of the input than can be obtained by analytical representations of the forcing fields. It is this latter approach which is used in this study.

For a given hurricane, the following parameters are sampled in time from the NWS charts: position, forward speed, central pressure, radius vector (relative to the storm movement) to maximum winds, and the maximum winds. With an analytical representation of the surface wind and pressure fields the above parameters need only to be interpolated in time.

The wind field representation prior to consideration of the land influence as given by Jelesnianski (1965) is employed in this study. The x,y-wind components for a stationary storm are:

$$\left.\begin{aligned} V_x &= \frac{V_R}{r_h}\left[- (x-x_h) \sin\phi - (y-y_h)\cos\phi \right] \\ \text{and} \\ V_y &= \frac{V_R}{r_h}\left[+ (x-x_h) \cos\phi - (y-y_h)\sin\phi \right] \end{aligned}\right\} F(r_h) \ , \qquad (82)$$

where

$$r_h = \left[(x-x_h)^2 + (y-y_h)^2\right]^{\frac{1}{2}} \ , \qquad (83)$$

V_R is the maximum wind, ϕ is the ingress angle, and $F(r_h)$ is $(r_h/R_h)^{3/2}$ if $r_h < R_h$ or $(R_h/r_h)^{1/2}$ if $r_h \geq R_h$. Distance from the storm center (x_h, y_h) to the region of maximum winds is R_h. The translation of the storm provides an alteration in the wind field which is carried out following the method of Jelesnianski (1965). This involves the vector addition to the above field of a supplemental velocity whose direction is parallel to that of the storm and whose magnitude depends only upon r_h. The resulting modified values of V_x and V_y are used to compute the wind-stress components:

$$\left.\begin{aligned} \tau_x &= K\,(V_x^2 + V_y^2)\,V_x\,, \\ \text{and} \qquad & \\ \tau_y &= K\,(V_x^2 + V_y^2)\,V_y\,. \end{aligned}\right\} \tag{84}$$

This constitutes the symmetric wind-stress field. The stress components in the stretched shelf coordinate system are determined by applying equation (84) in equations (47) and (48).

The surface atmospheric pressure field associated with the hurricane is given by:

$$P = P_o + (P_\infty - P_o)\, e^{-R_h/r_h}\,, \tag{85}$$

where P_o is the central pressure and P_∞ is the far field pressure. The term H_B in equations (40) and (41) is equivalent to $(P_\infty - P)/\rho_a g$.

The symmetric surface stress field does not reflect the influence of land. Without modeling this influence the analytically determined wind field near the coast would not be consistent with that from the NWS. A systematic procedure (App. H) is employed to alter the symmetric wind field such that it portrays the effect of land. These winds are referred to as deformed. Mr. Thomas Reid, Texas A&M University, Department of Oceanography, is responsible for the basic development of this wind model (unpublished manuscript). The pressure field was not altered in the nearshore region to conform with the wind field.

Figure 37(a) represents the symmetric Hurricane Carla wind field at 1600 Greenwich mean time (G.m.t.), 11 September 1961 (approximately 4 hours before the storm crossed the coast). Isovels are shown in meters per second. The analytically deformed wind field at this time is shown in Figure 37(b). The influence of land on the wind field is evidence even at a time when the storm is approximately 55 kilometers from the coast. Figures 38 and 39 show the symmetric (a) and deformed (b) winds at 2000 G.m.t., 11 September, and 0000 G.m.t., 12 September, respectively. The rotation and reduction of the wind vector in the nearshore region to reflect the land influence is illustrated in comparing Figure 40(a) for the symmetric case with Figure 40(b) for the deformed wind. These figures correspond to the contours shown in Figures 38(a) and 38(b), respectively. The arrows represent the wind vector placed such that the tail is at the computational point. The pressure fields, as determined from equation (85), for Hurricane Carla at the above times are shown in Figure 41(a,b,c) where the contours are in millibars. Although the pattern of isovels reflecting the land influence is in good agreement with

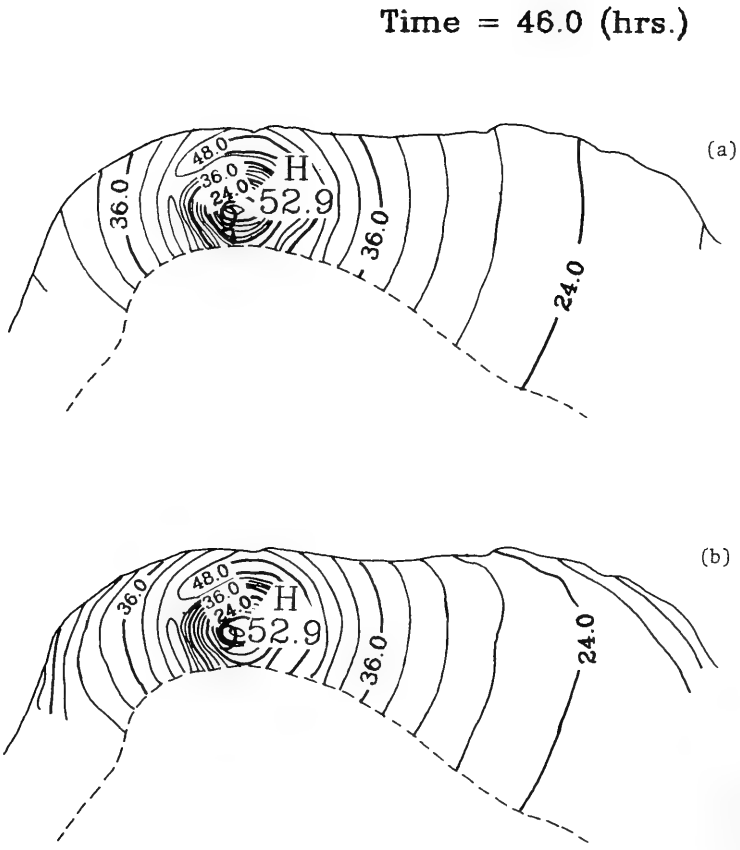

Figure 37. Hurricane Carla symmetric (a) and deformed (b) wind fields at 1600 G.m.t., 11 September 1961; isovels in meters per second.

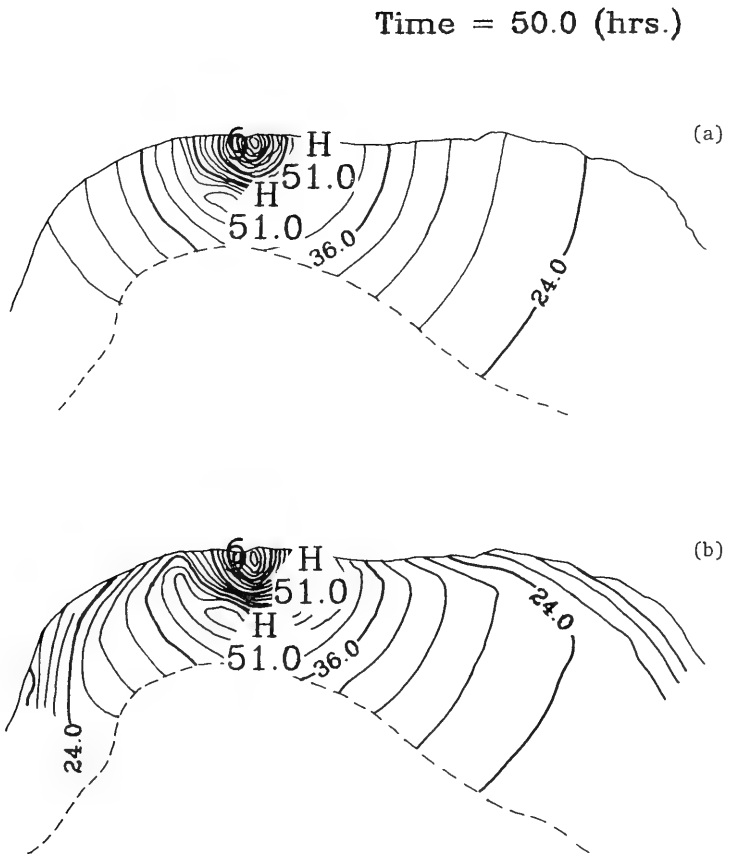

Figure 38. Hurricane Carla symmetric (a) and deformed (b) wind fields at 2000 G.m.t., 11 September 1961; isovels in meters per second.

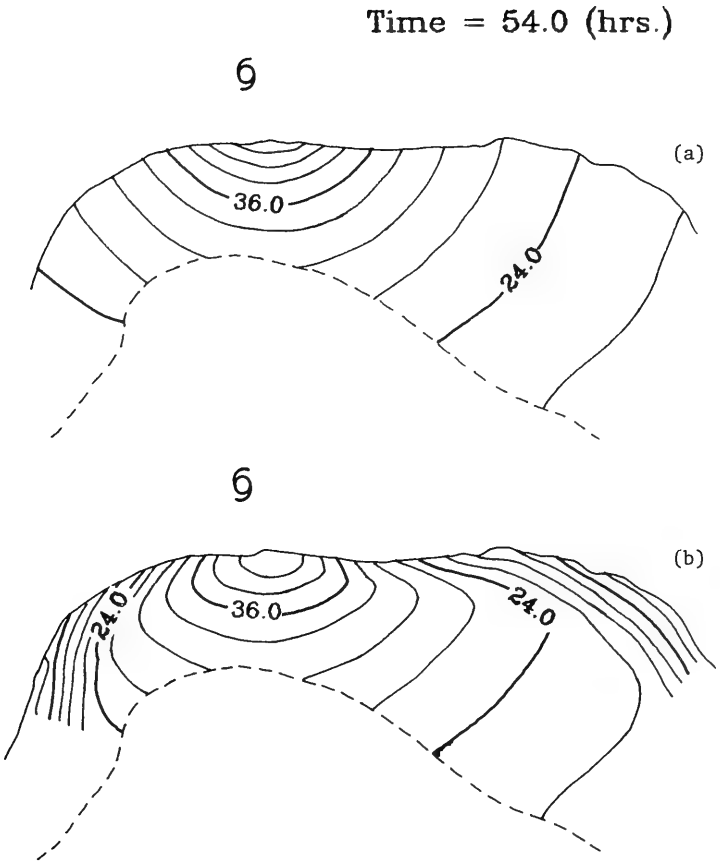

Figure 39. Hurricane Carla symmetric (a) and deformed (b) wind fields at 0000 G.m.t., 12 September 1961; isovels in meters per second.

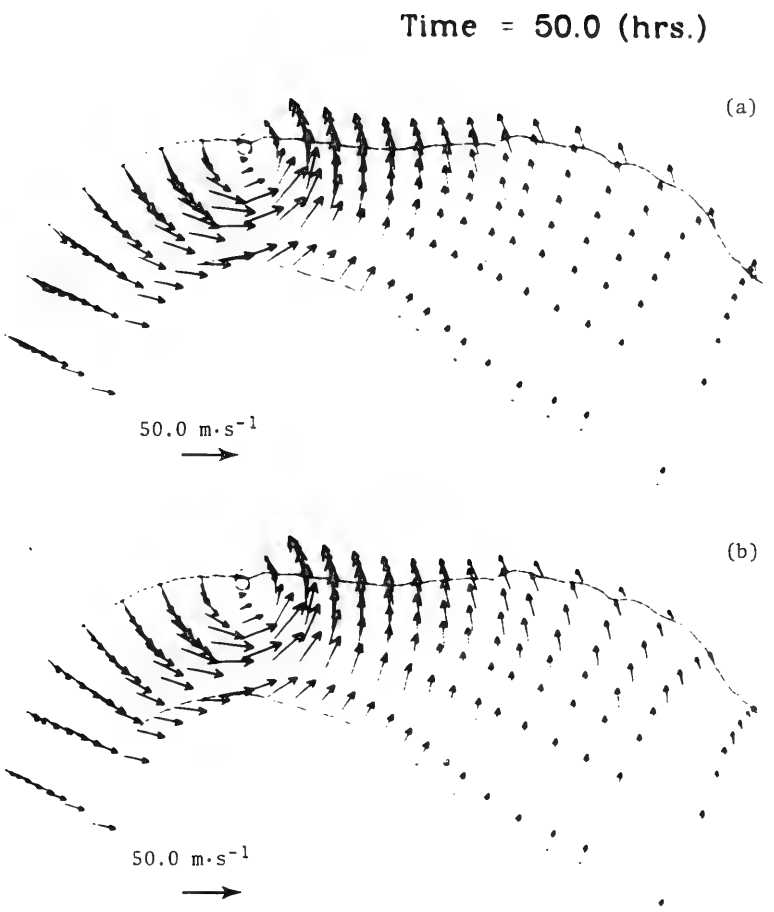

Figure 40. Hurricane Carla winds at selected points at 2000 G.m.t., 11 September 1961 for the symmetric (a) and deformed (b) representations.

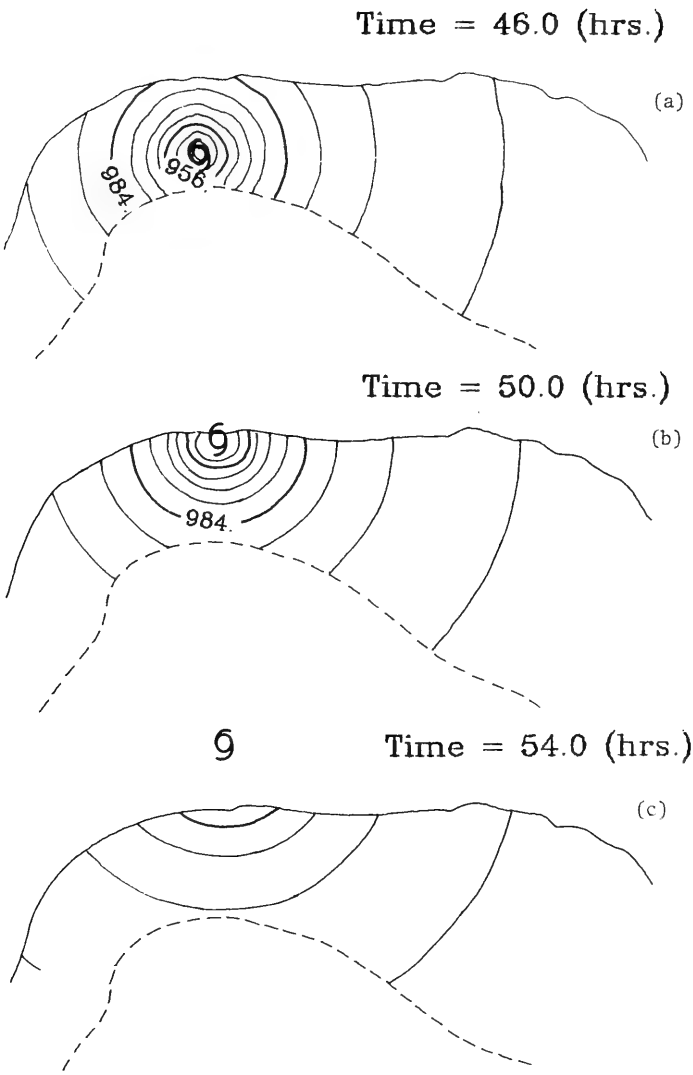

Figure 41. Hurricane Carla atmospheric pressure on 11 September 1961 at 1600 (a), at 2000 (b), and 0000 G.m.t., 12 September (c); contours in millibars.

those provided by NWS, the problem of specifying the proper deformation is not completely resolved.

The observed high winds which remain along the coast after the storm has proceeded inland are attained by setting R_h to be the distance the storm center is from that coastal area of persistent high winds. This procedure was also followed in modeling the winds from Hurricane Camille. However, R_h in the pressure expression was not allowed to increase in this manner.

The hydrographs at selected grid points along the coast are presented in Figure 42 illustrating the improved agreement with respect to the observed water levels in using a deformed wind forcing function rather than a symmetric one. The observed water levels, corrected for the astronomical tide, are indicated by squares. The computed water levels have been raised for comparison purposes to correspond to the local sea level at the start of the computations (1800 G.m.t., 9 September). The solid line represents the computed surge employing the deformed wind and the dashline shows the results with a symmetric wind. The surge computations were formed using identical boundary conditions.

The symmetric (a) and deformed (b) winds for Hurricane Camille at 0000 G.m.t. 18 August 1969 (approximately 4 hours before the storm crossed the coast), 0400 G.m.t. and 0800 G.m.t. on the same date are shown in Figures 43 through 45. The rotation and reduction of the wind stress for this storm are different from that of Hurricane Carla because of the differences in the coastal configuration. Figure 46 (a,b) shows the wind vectors for the symmetric and deformed representation of Hurricane Camille at the time the storm proceeded inland. The pressure fields at the above times are presented in Figure 47(a,b,c). The wind fields associated with Hurricane Gracie were not deformed because the documentation was not amenable to the deformation procedure. Also, R_h was not increased in the manner specified above after the storm crossed the coast. The symmetric winds at 1200 G.m.t., 29 September 1959, 1600 G.m.t. (the time the storm proceeded inland), and 2000 G.m.t. on the same date are shown in Figure 48. Figure 49 presents the pressure fields at the above times.

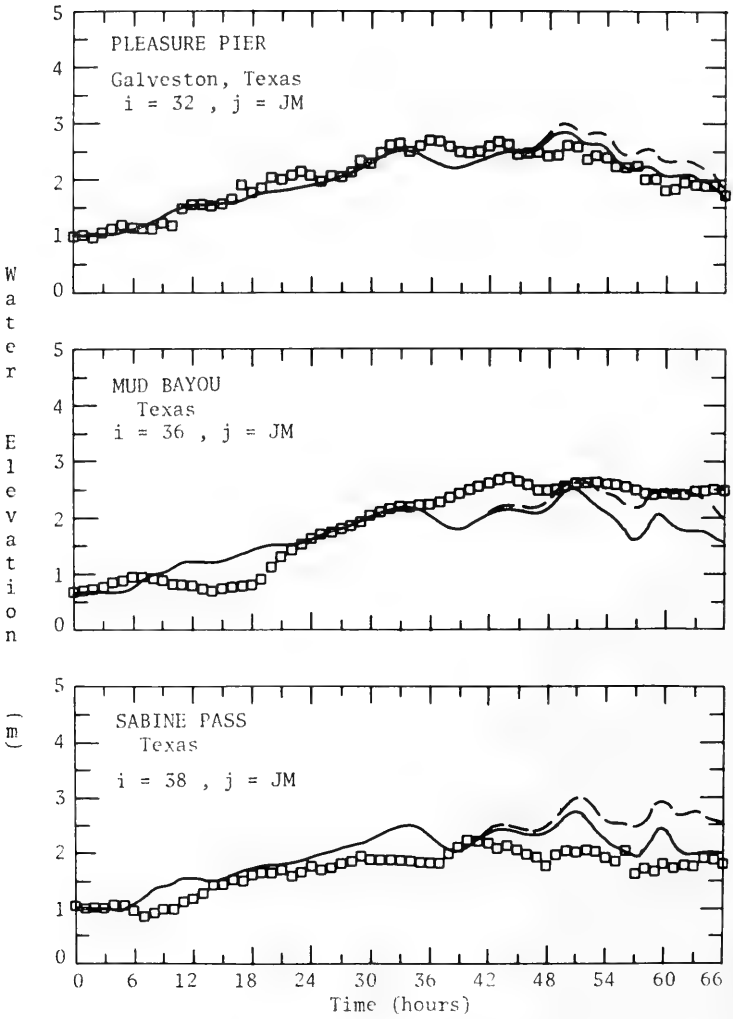

Figure 42. Observed (squares) and computed water levels using a deformed wind (solid) and a symmetric wind (dashed) for Hurricane Carla.

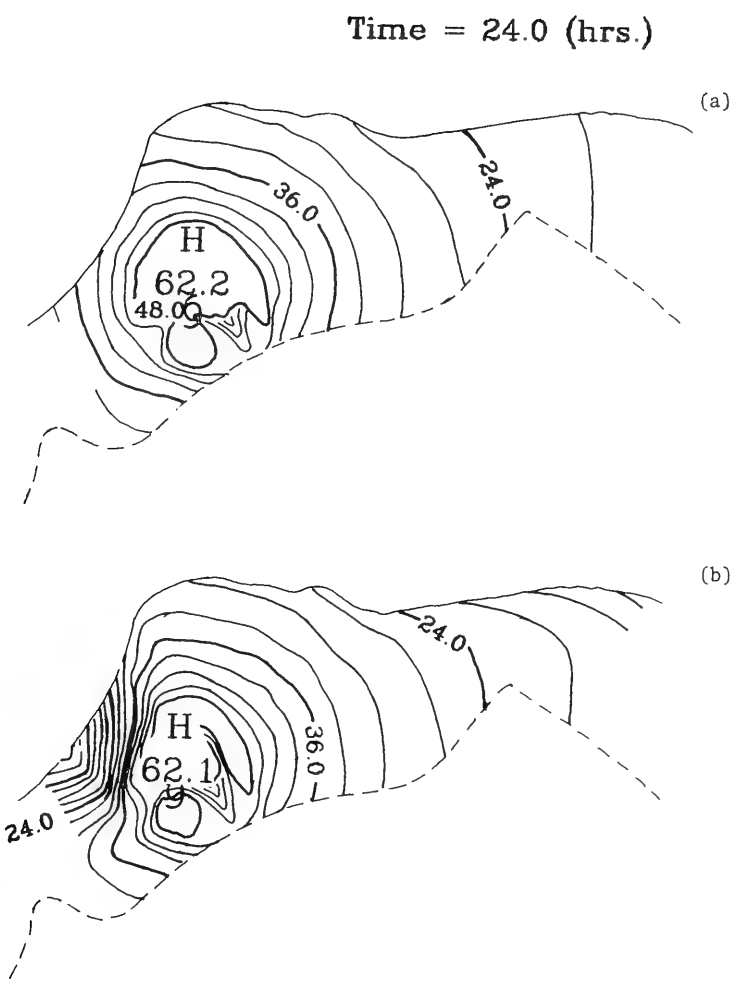

Figure 43. Hurricane Camille symmetric (a) and deformed (b) wind fields at 0000 G.m.t., 18 August 1969; isovels in meters per second.

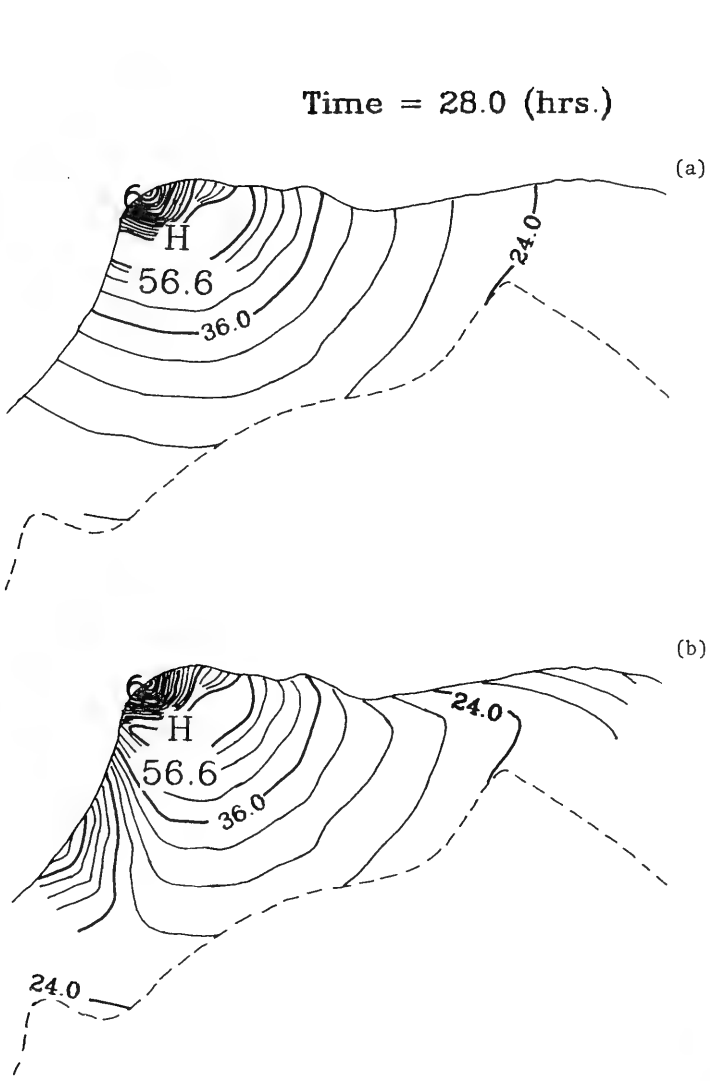

Figure 44. Hurricane Camille symmetric (a) and deformed (b) wind fields at 0400 G.m.t., 18 August 1969; isovels in meters per second.

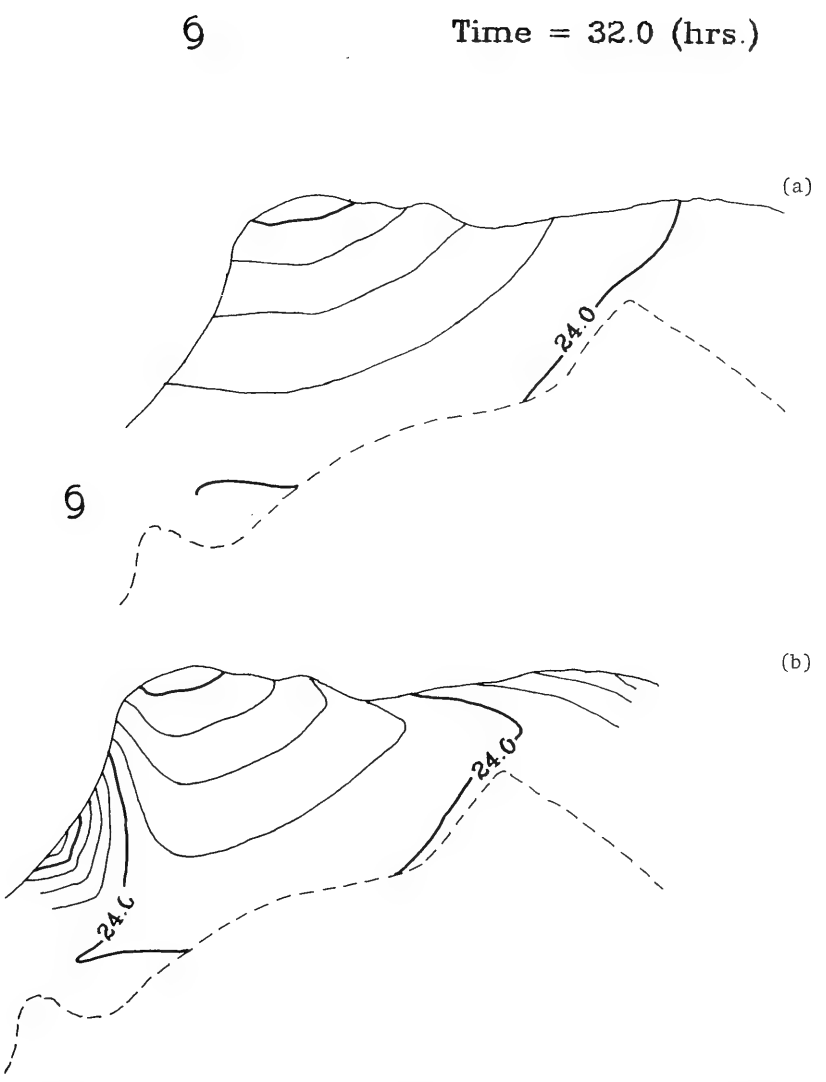

Figure 45. Hurricane Camille symmetric (a) and deformed (b) wind fields at 0800 G.m.t., 18 August 1969; isovels in meters per second.

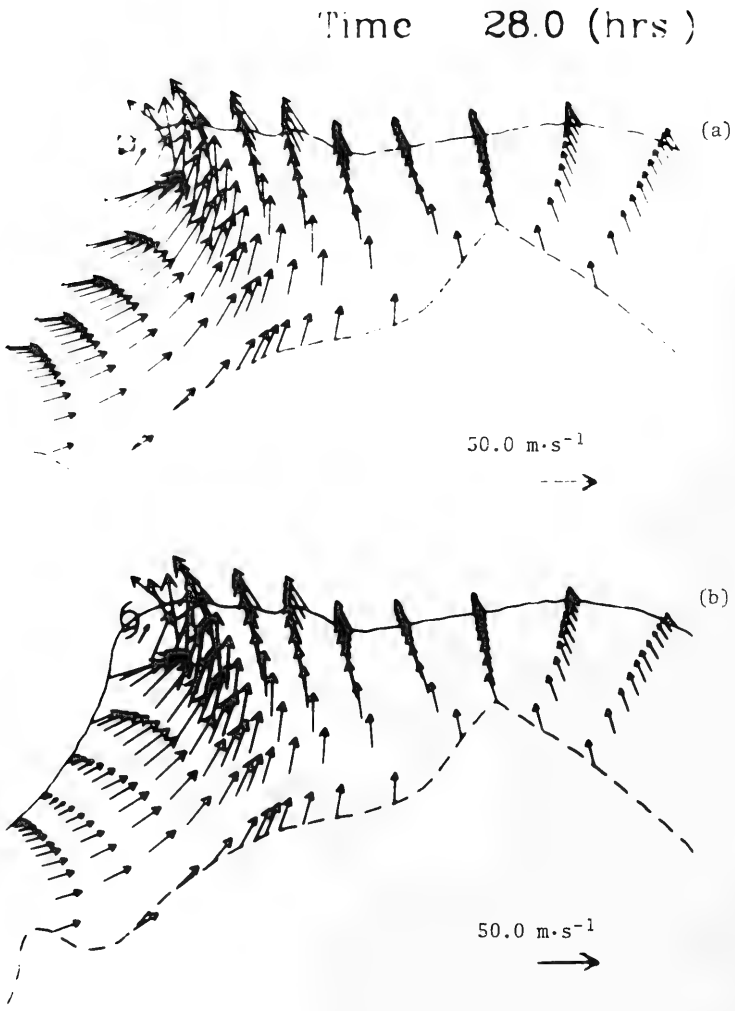

Figure 46. Hurricane Camille winds at selected points at 0400 G.m.t., 18 August 1969 for the symmetric (a) and deformed (b) representations.

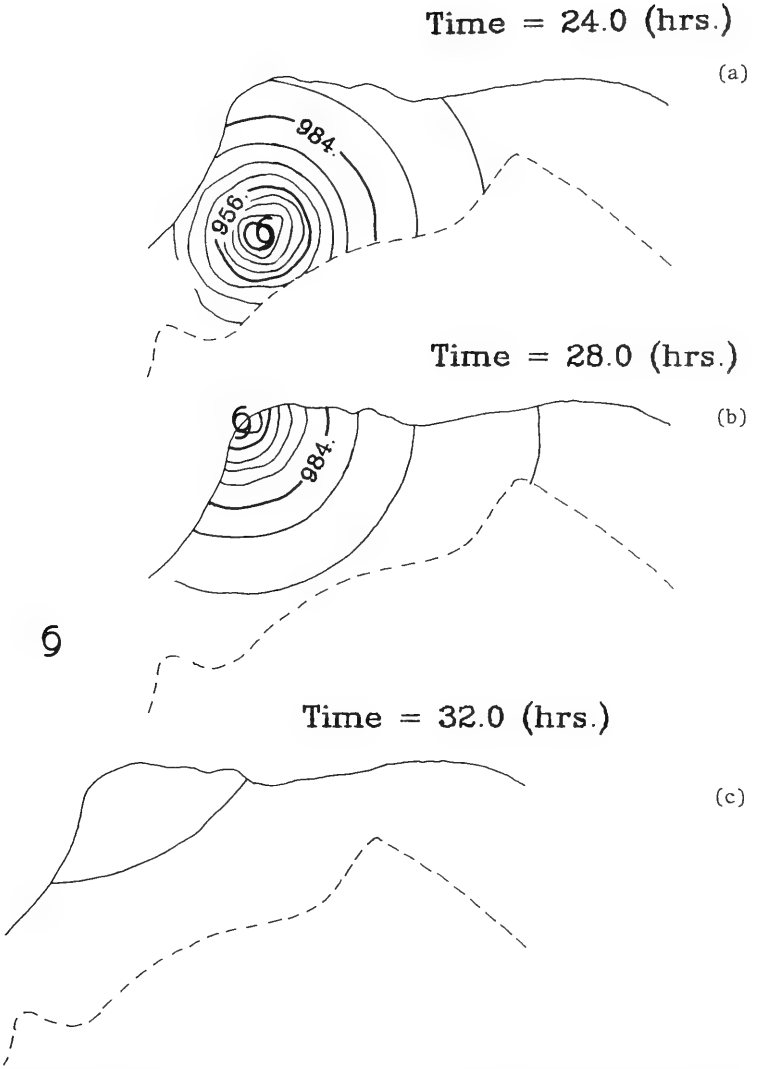

Figure 47. Hurricane Camille atmospheric pressure on 18 August 1969 at 0000 (a), at 0400 (b), and at 0800 G.m.t. (c); contours in millibars.

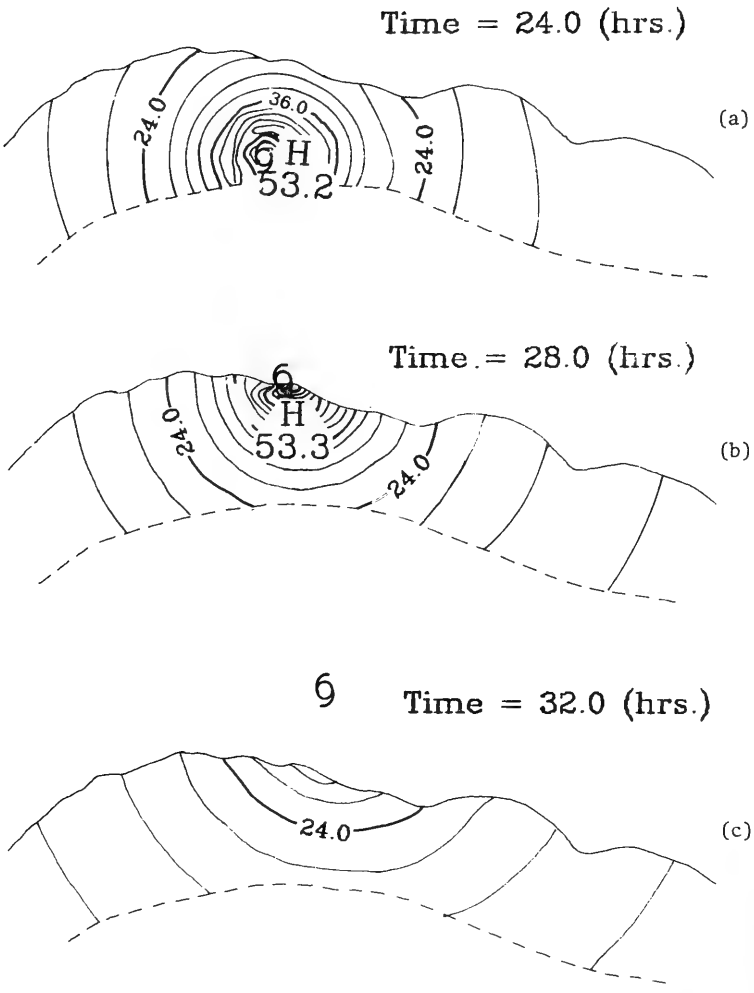

Figure 48. Hurricane Gracie symmetric winds on 29 September 1959 at 1200 (a), at 1600 (b), and at 2000 G.m.t. (c); isovels in meters per second.

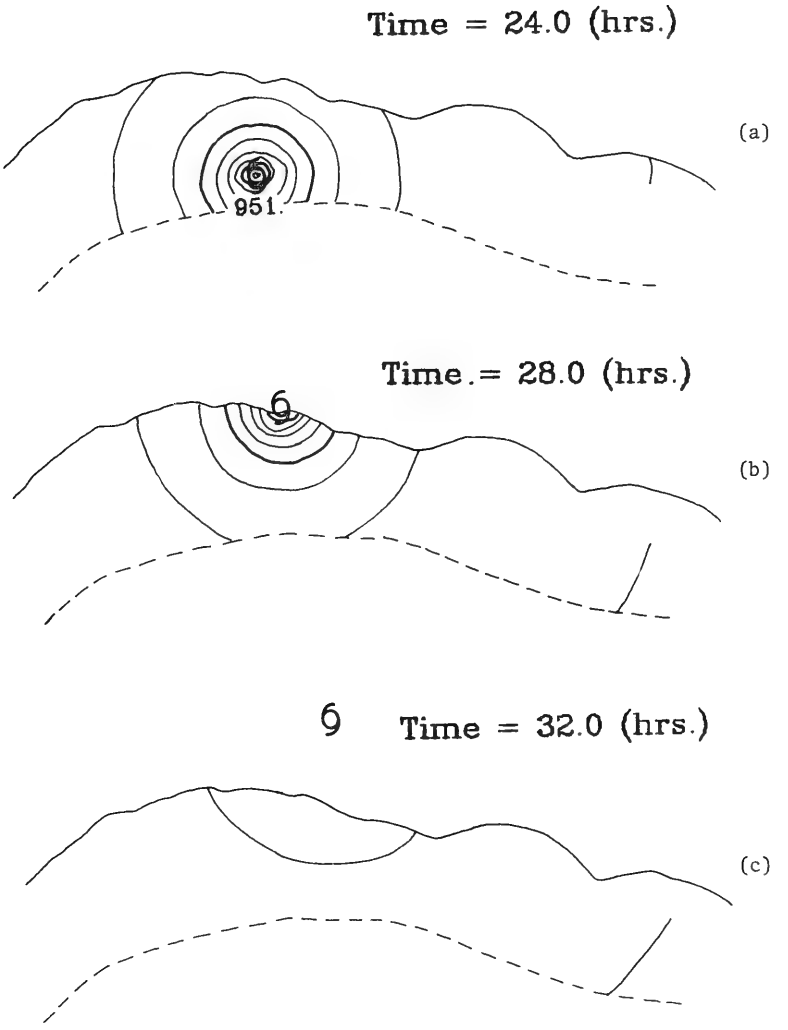

Figure 49. Hurricane Gracie atmospheric pressure on 29 September 1959 at 1200 (a), at 1600 (b), and at 2000 G.m.t. (c); contours in millibars.

IV. SIMULATION OF THE FREE WAVE IN AN ANNULUS

1. Problem Statement.

If the wind stress, bottom friction, atmospheric pressure, and the rotational effect of the earth are neglected, then the equations in Section III admit a simple analytic solution for free gravity waves of long wavelength. A study using curved boundaries will demonstrate the superiority of modeling the long gravity wave in orthogonal curvilinear coordinates over those models which employ rectilinear coordinates. Basically, the study involves comparing the numerical solution of a free-standing long wave in a 90° section of an annulus with an inner radius r_1 of 393 kilometers and an outer radius r_2 equal to $2r_1$ (Figure 50). The annulus is bounded on all sides by a vertical wall. The depth of the basin relative to the mean water level is assumed everywhere to be 40 meters.

The analytical solution for the free-wave oscillations in a section of an annulus may be obtained with some modifications from Lamb (art. 191, 1932). The boundary conditions require that:

$$\frac{\partial H}{\partial r} = 0 \ , \text{ at } r = r_1 \text{ and } r = r_2 \ , \tag{86}$$

and

$$\frac{\partial H}{\partial \theta} = 0 \ , \text{ at } \theta = 0° \text{ and } \theta = \pi/2 \ . \tag{87}$$

The analytical solution for the given initial conditions is:

$$H(r,\theta,t) = \sum_{m}^{\infty} \sum_{n}^{\infty} A_{m,n} \left[J_n(k_{m,n}r) - \frac{J_n'(k_{m,n}r_1)}{Y_n'(k_{m,n}r_1)} Y_n(k_{m,n}r) \right]$$

$$\cos n\theta \cos \sigma_{m,n} t \ , \tag{88}$$

$$m = 0,1 \cdots \ ,$$

$$n = 0,2 \cdots \ ,$$

where

$$\sigma_{m,n} = k_{m,n} \sqrt{g\,D} \ , \tag{89}$$

and for given n , $k_{m,n}$ is the m^{th} root of

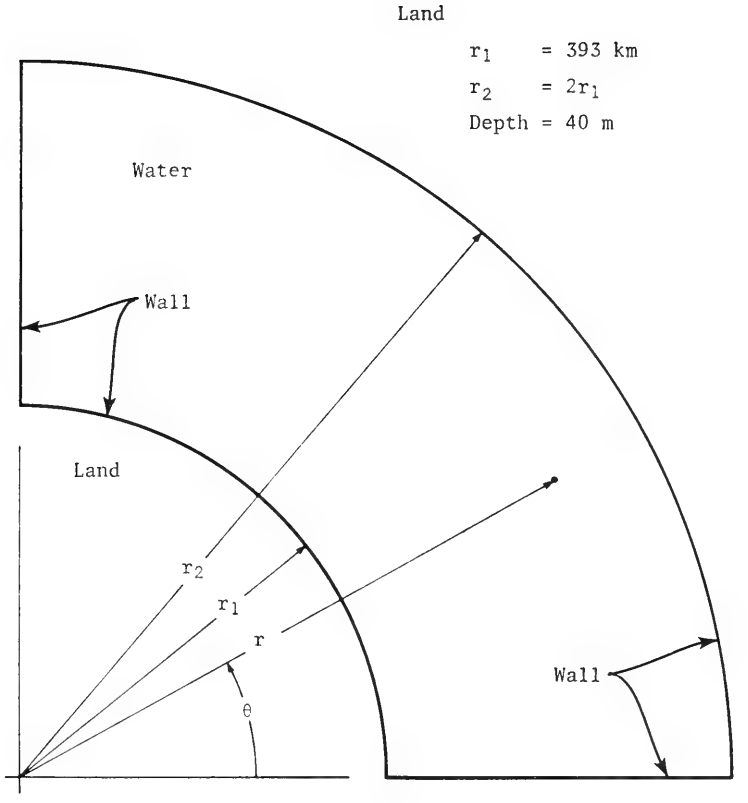

Figure 50. The annulus in polar coordinates (r,θ).

$$J_n'(kr_2)\ Y_n'(kr_1) - J_n'(kr_1)\ Y_n'(kr_2) = 0 \ . \qquad (90)$$

The terms J and Y are Bessel functions of the first and second kind, respectively. The order is given by the integer subscript and the superscript refers to differentiation with respect to the argument. The term A in equation (88) is an arbitrary constant representing the initial amplitude. The first azimuthal mode is for $n = 2$ and the lowest value of k that satisfies equation (90) is approximately $1.340/r_1$ meters^{-1}. The period of oscillation for this mode ($m = 0$, $n = 2$) is 25.85 hours.

The numerical solution of the free wave in the quarter annulus is sought by performing the integration in two different computing grids. In one case the grid is rectilinear (Figure 51), and in the other a polar system is used. In the rectilinear system the outer and inner radii of the annulus (the light line in Figure 51) is simulated in a stairstep fashion. Considering a limitation on computer time and storage, an acceptable rendition of the curved boundaries is present in the Cartesian grid. Proper representation of the quarter-annulus requires a transport point at corners *on the outer and inner boundaries*. Consequently, the rectilinear boundary is not symmetric about $\pi/4$. The locations of nine hydrograph positions are indicated by small boxes. Although the computing grid is 43 by 43, only 1,052 points are used to represent the annulus. In this grid system, ΔS^* and ΔT^* are just Δx and Δy , respectively, with $\Delta x = \Delta y = 19.65$ kilometers. The maximum allowable time step as determined from equation (62) is approximately 700 seconds where $F = \mu = \nu = 1$. Finally, the analog form of the long wave equations is obtained by setting those terms in equations (55) through (57) to zero which are neglected, and setting F , μ , and ν to one. The transports, Q_{S^*} , Q_{T^*} , are now aliases for Q_x and Q_y , respectively.

The numerical algorithm for the rectilinear grid system must be capable of determining if a computational point is interior, exterior, or on the boundary of the annulus. For exterior points, no calculations are performed. Grid points on the stairstep boundary require special attention subject to the condition of a wall. Furthermore, the numerical program must identify and apply the appropriate wall condition depending on whether the point in question is located at a boundary corner (an H computation) or on a segment of the boundary. Clearly, extensive programing and computer time is required to accomplish this task.

The other computing mesh which is used for obtaining the numerical solution of the free wave in the annulus is the polar (or stretched shelf coordinate) grid system (Figure 52). The transformation to the computing grid as shown in Figure 53 is accomplished

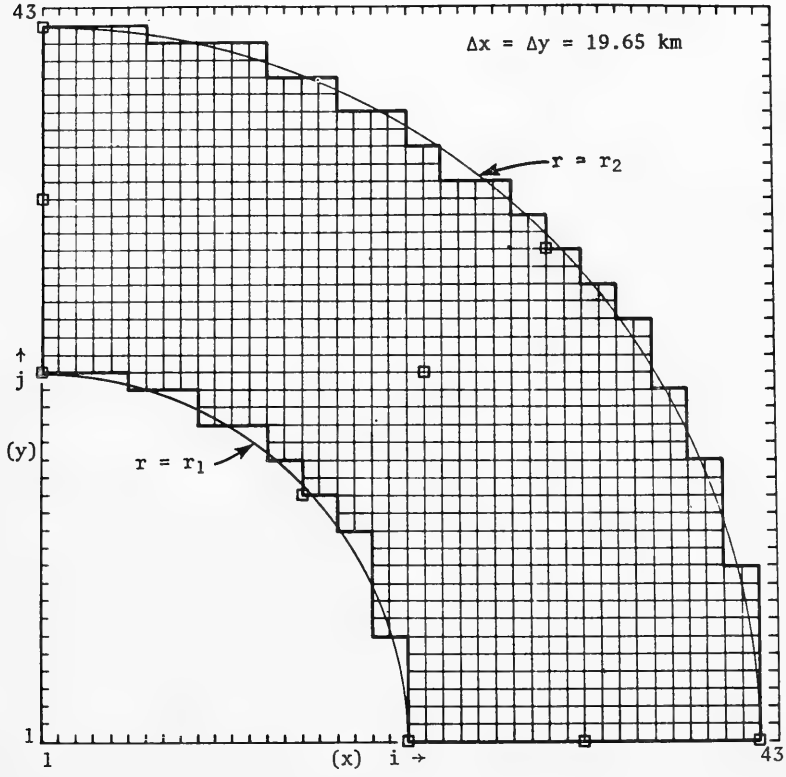

Figure 51. Rectilinear grid representing the annulus; location of hydrographs shown by (□).

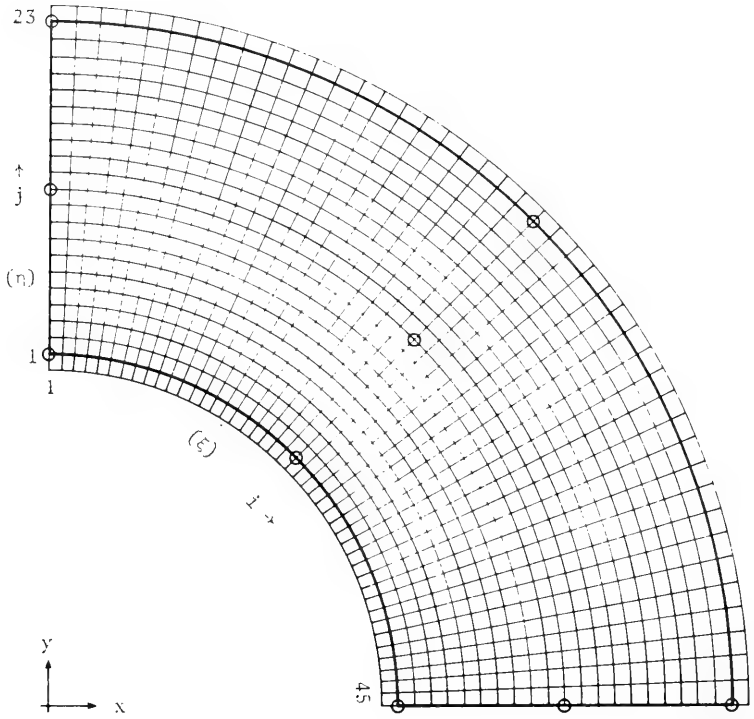

Figure 52. Polar grid representing the annulus; location of hydrographs shown by (o).

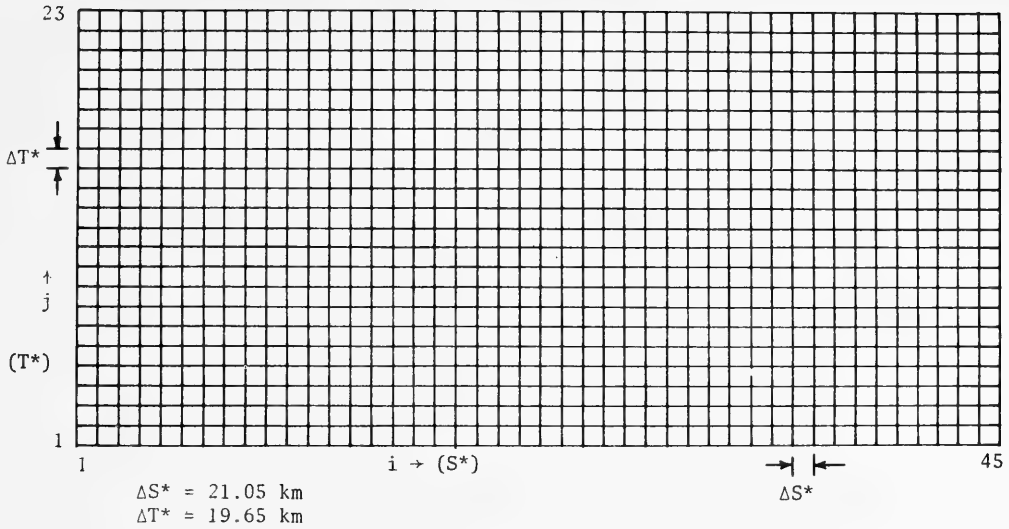

Figure 53. Computing grid for polar system representation of the annulus.

with $\mu = \nu = 1$, and

$$F(i,j) = \left[\frac{\pi}{88} \left(\frac{r_1 + (j - 2)^2 \, \Delta T^*}{\Delta S^*} \right) \right]^{\frac{1}{2}} , \qquad (91)$$

$$i - 1,2 \cdots 45 ,$$

$$j - 2,3 \cdots 22 ,$$

where $\Delta S^* = 21.05$ kilometers and $\Delta T^* = 19.65$ kilometers. Approximately the same number of computational points are employed in this system as that of Figure 51. The actual area of the annulus is well represented in both computing grids. Although the inner and outer boundaries are straight-line segments in the numerical grid sense, the portrayal of the annulus is certainly more representative than that shown in Figure 51. The positions of nine hydrographs in Figure 52 (denoted by large dots) correspond to the hydrograph positions in the rectilinear grid system. For the polar system, the maximum numerical time step is approximately 600 seconds. As a practical note, the stretched shelf coordinate system, although requiring less sophisticated programing and allowing better physical and mathematical portrayal of the boundaries, generally results in a smaller numerical time step than a rectilinear system of comparable scale.

2. Results.

For comparison purposes, a time step of 540 seconds is used in both grid systems for the numerical solution. As noted above, the polar grid program should compile and execute faster on the computer than the rectilinear grid program. On the IBM 360/65, the polar grid program required 0.47 minute to compile and 0.39 minute per 100 iterations. For the rectilinear system, the program consumed 0.59 minute to compile and 0.61 minute per 100 iterations.

The initial surface elevation condition which is imposed on both grid systems is that $\partial H/\partial \theta$ is a constant. For the rectilinear grid system,

$$H(i,j,0) = .1 - \frac{.4}{\pi} \tan^{-1} \left(\frac{j - 1}{i - 1} \right) , \qquad (92)$$

where only the i,j indices appropriate for the annulus are employed in the above relation. For the polar grid system, the same initial surface condition is determined as:

$$H(i,j,0) = .1 + .2\ (i - 1)\ , \qquad (93)$$

$$i = 1,2 \cdots 45\ ,$$

$$j = 2,3 \cdots 22\ .$$

The initial condition of constant azimuthal slope and no radial variation of H along a line of constant θ implies that there are several modes of seiching present; however, the dominate mode is for $m = 0$ and $n = 2$. This is indicated by Figures 54 and 55 which show the simulated surface topography at 27 hours in the rectilinear and polar grid systems, respectively. The solution in the polar grid is more representative of the analytical solution than that shown in the Cartesian system.

The hydrograph at $\theta = 0°$ and $r = r_1$ is shown in Figure 56 (a) where the water elevation as determined from the polar grid is the solid line and that from the rectilinear mesh is the dashline. Figure 56 (b,c) shows the hydrographs along $\theta = 0°$ for $r = r_m$ (the average radius of the annulus) and $r = r_2$, respectively. The three hydrographs along $\theta = \pi/2$ and the same r positions are shown in Figure 57 (a,b,c) and along the nodal line by Figure 58 (a,b,c). The average period of oscillation as determined from the hydrographs of Figures 56 and 57 is approximately 26 hours in the polar system and 28 hours in the rectilinear grid. The error in the period of oscillation (about 8 percent) for the rectilinear system is most evident in the figures by noting the lag of the dashline with respect to the solid line. The longer period of oscillation is directly related to the stairstep boundary. Effectively, the length of the basin is increased by the reflections introduced by these boundaries. This distortion is more than academic since many rectilinear grid models of enclosed irregular bays require adjustments to reproduce the fundamental seiching mode.

The analytical solution at any point is a smooth function of time. The solid lines in the various hydrographs portray this feature better than the dashlines which are contaminated by high-frequency spurious oscillations. The nodal line in the polar grid solution as evidenced by Figure 58 (a,b,c) remains fixed at $\theta = \pi/4$ which agrees with the theory. This is not observed in the rectilinear system. Although the hydrographs in the rectilinear grid are not positioned exactly on $\theta = \pi/4$ (actually, about 44°), the magnitude of the oscillation about $\pi/4$ is approximately 2 to 4 times larger than expected.

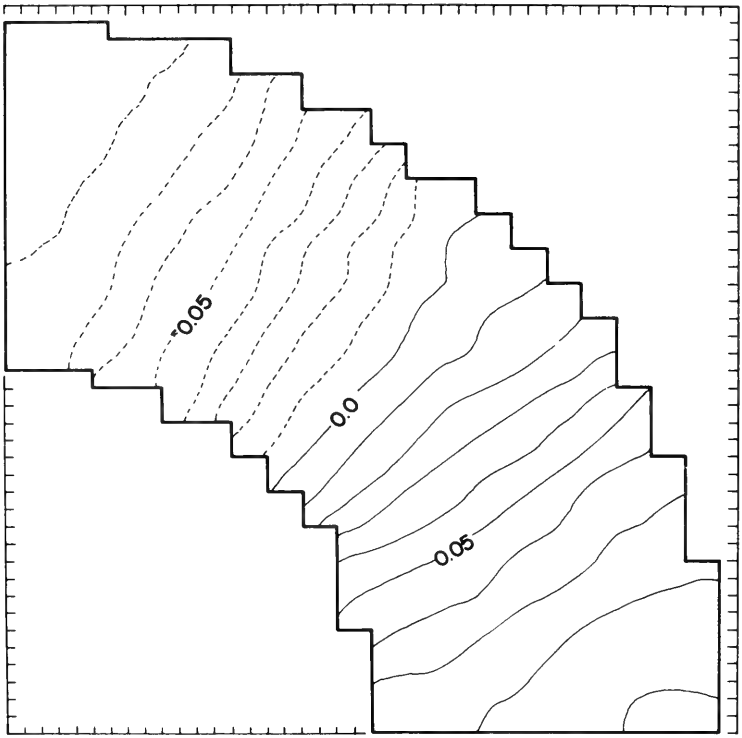

Figure 54. Computed water surface topography in 0.01-meter contour increments at 27 hours in the rectilinear grid system.

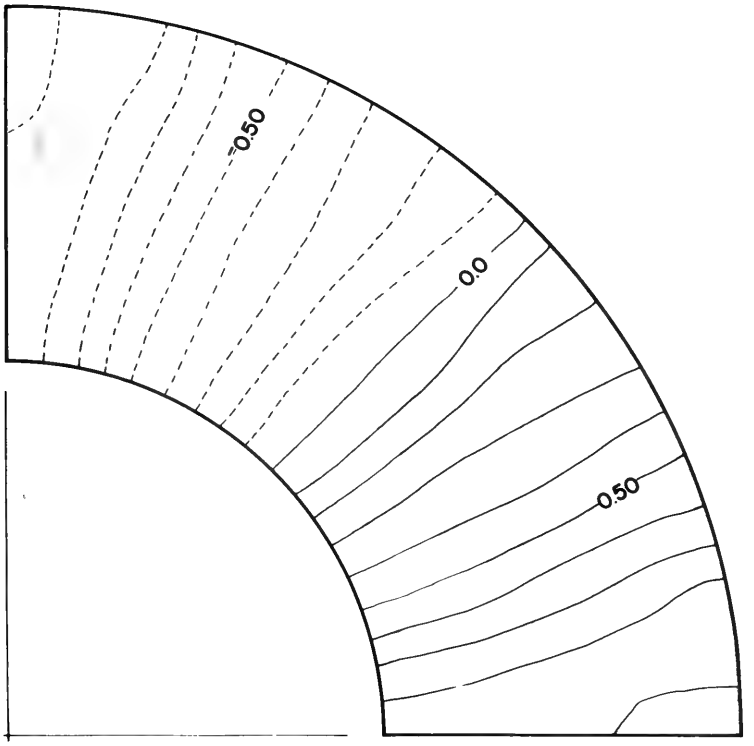

Figure 55. Computed water surface topography in 0.01-meter contour increments at 27 hours in the polar grid system.

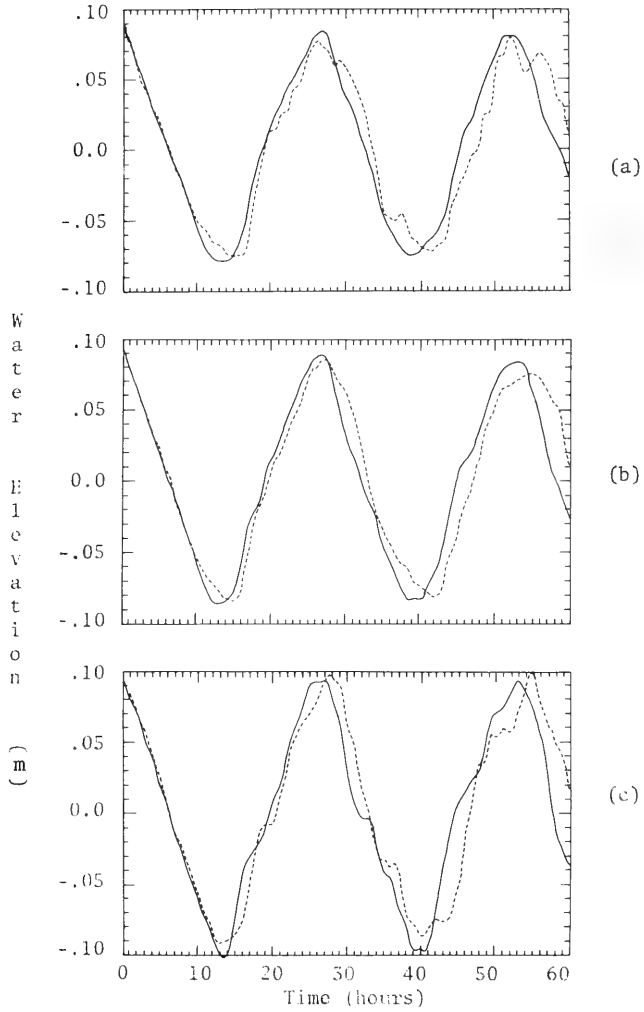

Figure 56. Hydrographs along $\theta = 0°$ and $r = r_1$ (a), r_m (b) and r_2 (c) for the polar grid (solid) and rectilinear grid (dashed).

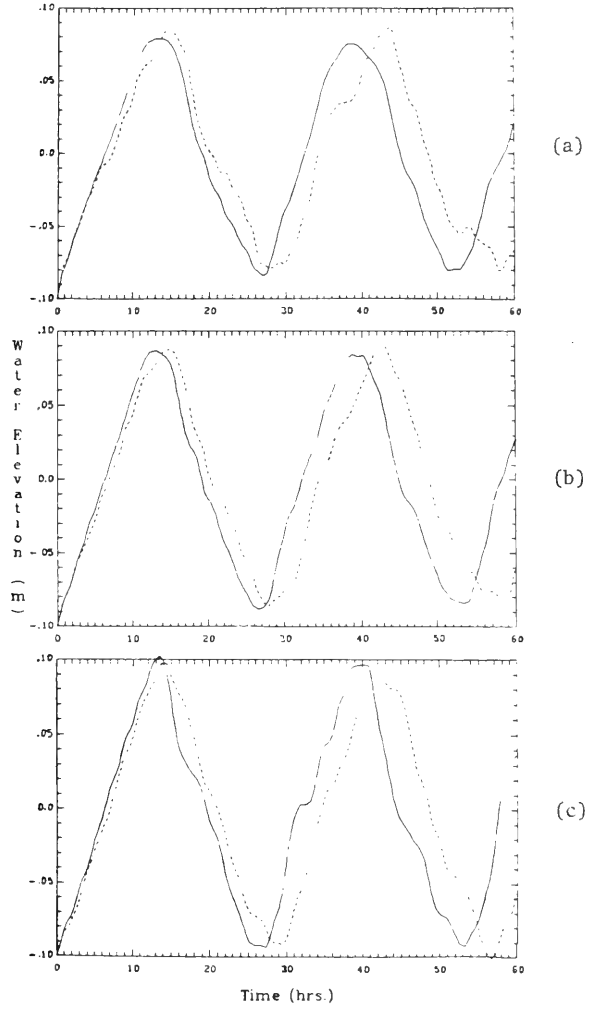

Figure 57. Hydrographs along $\theta = \pi/2$ and $r = r_1$ (a), r_m (b) and r_2 (c) for the polar grid (solid) and rectilinear grid (dashed).

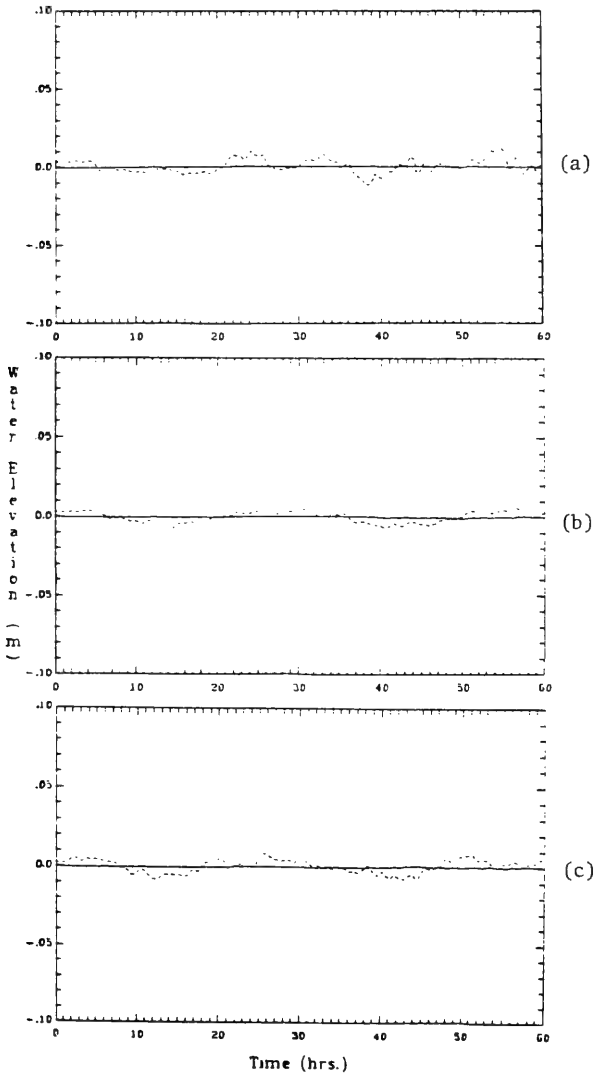

Figure 58. Hydrographs along $\theta = \pi/4$ and $r = r_1$ (a), r_m (b) and r_2 (c) for the polar grid (solid) and rectilinear grid (dashed).

V. STORM SURGE SIMULATION

1. Hurricane Carla.

Hurricane Carla was an immense, slow-moving, and meandering storm which struck the gulf coast south of Port Lavaca, Texas, at 2000 G.m.t. on 11 September 1961. The radius to maximum winds was 50 kilometers. The atmospheric pressure drop across the storm was 75 millibars. The maximum sustained winds were approximately 51 meters per second.

For numerical stability a time step of 180 seconds was used in the computations. The surge simulation was performed for a 66-hour period from 1800 G.m.t. on September to 1200 G.m.t on 12 September. The boundary conditions are those given in Section III. The wind fields are analytically deformed in a manner previously discussed. The observed (squares) and computed (solid line) water levels at selected grid points along the coast are shown in Figure 59. The observed water levels have been corrected for the astronomical tide. At the start of the computations, the water surface along the coast from Sabine Pass to the Matagorda Bay area was elevated by approximately 1 meter. Consequently, for comparison the computed water levels have been raised to correspond to the local sea level condition. The water surface topography in 0.5-meter contour increments at 46, 50, and 54 hours are shown in Figure 60. The computed maximum coastal surge profile corrected for the astronomical tide is presented in Figure 61. Indicated on the figure are the observed high-crest values from tide gages and water marks. The depression of the water surface to the left of the storm track (as viewed from the sea) and the low-peak surge in the Aransas Pass area results from the offshore wind and from simulating the coast as a wall. It should be emphasized that the surge model does not consider the coastal flooding from the shelf surge nor includes the influence of the increased communication between the semienclosed bays and the open sea. While the computations agree fairly well with those observed for the peak coastal surges, especially for the area to the right of storm landfall, and for the Galveston hydrography, there is some discrepancy for regions far from the storm track such as Sabine Pass. This might be attributed to the problem of proper deformation of the wind field (both speed and direction) to reflect the influence of land.

Considerable erosion of beaches and adjacent offshore areas along the Texas coast occurred during Hurricane Carla (U.S. Army Engineer District, Galveston 1962). Figure 62 shows the water velocity $\hat{V} = Q_{S*}\hat{i} + Q_{T*}\hat{j})/\overline{D}$ in centimeters per second at selected grid points for the same times as that in Figure 60. Of practical importance in assessing the erosion potential and transport of the material is the alongshore current, $Q_{S*}/\overline{D}$. In shallow water, the current is uniform from the surface to the sea bed. Values of the current in centimeters per second as a function of time at selected grid points are presented

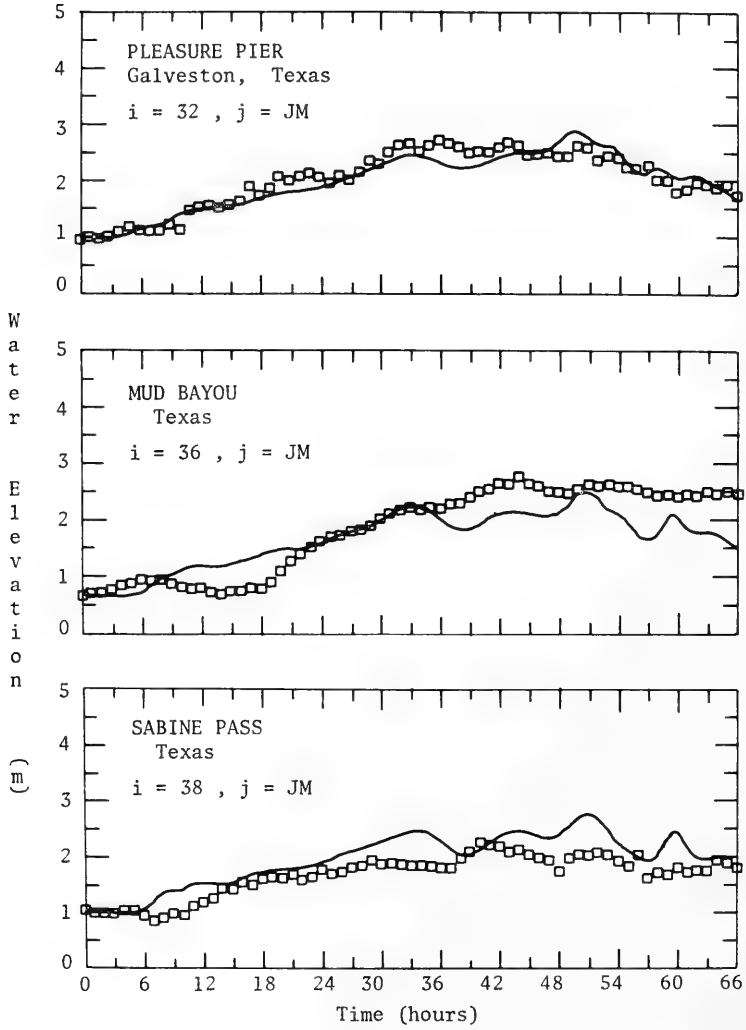

Figure 59. Observed (squares) and computed (solid) water levels for Hurricane Carla.

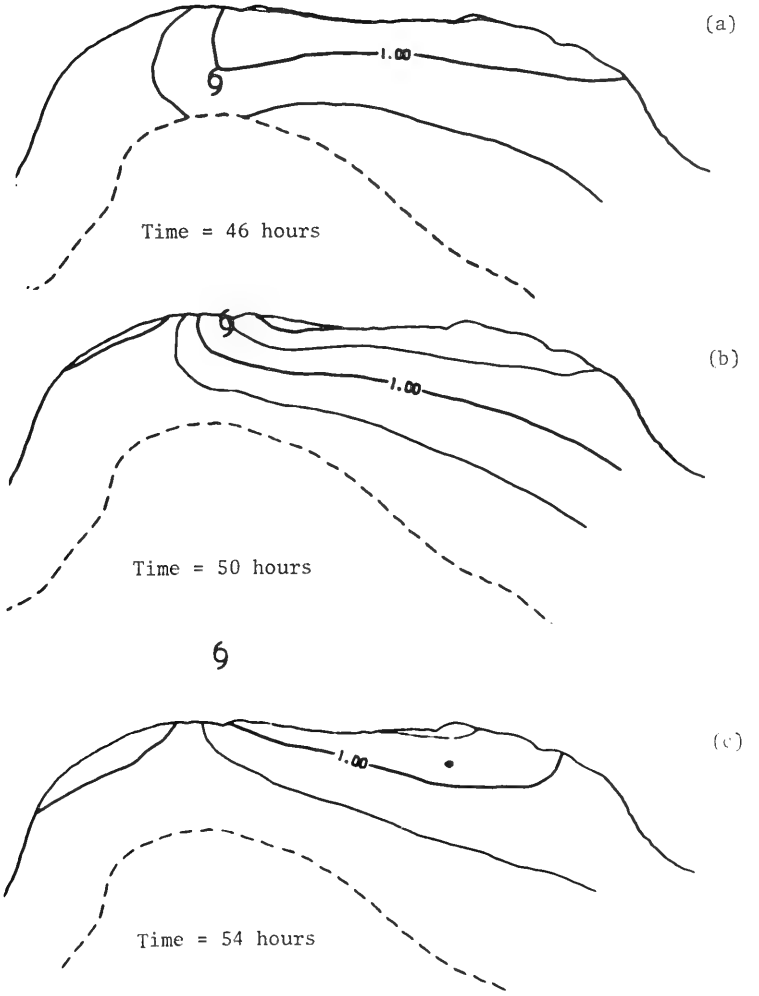

Figure 60. Computed water surface topography in 0.5-meter contour increments for Hurricane Carla at 46 (a), 50 (b), and 54 hours (c).

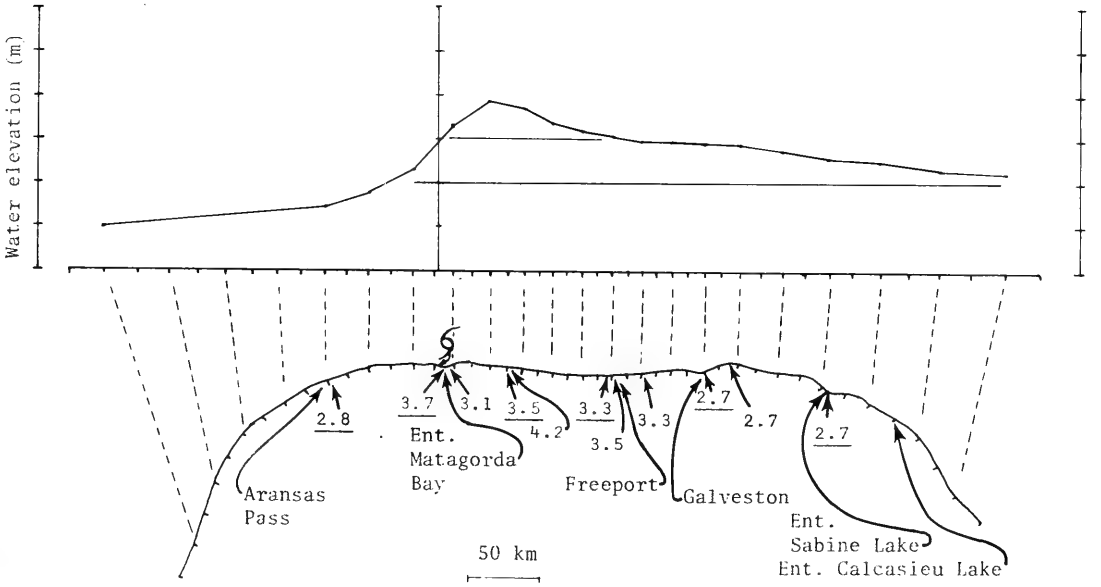

Figure 61. Computed high water of the coastal surges from Hurricane Carla corrected for the astronomical tide. The numbers distributed about the bottom curve representing the coastline are observed high water crests in meters from still high water marks and tide gages (underlined).

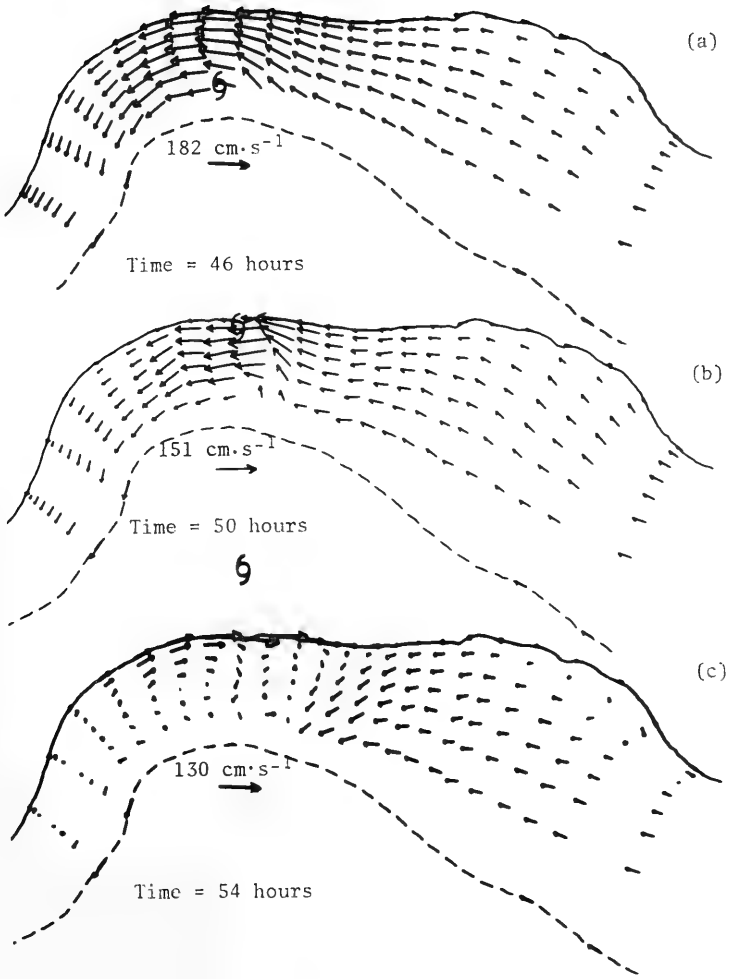

Figure 62. Computed water velocity in centimeters per second at selected grid points for Hurricane Carla at 46 (a), 50 (b), and 54 hours (c). Vector scale in centimeters per second.

in Figure 63. Also given is total transport in 10^6 cubic meters per second as a function of time across the transect lines indicated in the figure.

2. Hurricane Camille.

Hurricane Camille traversed the extensive low-lying marsh area of the Mississippi Delta, moving over the shallow waters of Breton and Chandeleur Sounds for 4 hours prior to landfall near Bay St. Louis, Mississippi, at approximately 0400 G.m.t., 18 August 1969. The radius to maximum winds was about 37 kilometers. The atmospheric pressure drop across the storm was 90 millibars. The maximum sustained winds were approximately 60 meters per second with the highest wind gusts estimated at 90 meters per second.

The surge simulation extended over a 48-hour period beginning at 0000 G.m.t. on 17 August. A time step of 60 seconds was selected for numerical stability. The boundary conditions are the same as those used in the Carla simulation. The Camille winds are analytically deformed as shown in Figures 43 through 45. The bottom drag coefficient was increased to 5×10^{-3} at computational grid points in the area bounded by $6 \leq i \leq 11$ and $14 \leq j \leq JM$ to simulate the larger resistance associated with the low flooded marsh lying northeast of the simulated Mississippi Delta (see Figures 28 and 65).

Figure 64 shows the observed and computed water levels at selected grid points along the coast. At Pascagoula, Mississippi, the water level increased from 2.2 to 4.5 meters in a 2-hour period indicating a strong convergence. In fact, the simulated hydrography at the approximate location of the maximum surge (Bay St. Louis) showed a similar convergence with the sea level rising from 2.9 to 7.0 meters in the same time period (figure not presented). The water surface topography in 1-meter contour increments at selected times from 24 to 36 hours illustrating the surge development is shown in Figures 65 through 73. The effect of the delta, modeled as a wall protruding from the coast, is visible in these figures by the presence of high water along the eastern side of the wall. The track of the storm with respect to the delta is such that the circulation is inhibited in this area resulting in the setup. The water velocity, $\hat{V}$, at the selected times and grid points as shown in Figure 74 are in accord with these observations. The computed maximum coastal surge envelope east of the delta presented in Figure 75 shows that the calculated peak surges are approximately that observed in the Gulfport to Pascagoula area (U.S. Army Engineer District, New Orleans, 1970). A test run employing a constant wind-stress coefficient, K, of 3×10^{-6} with the same boundary conditions produced a similar maximum surge envelope. There is qualitative agreement between the observed and predicted surge envelopes. This is shown by the relatively low water elevation of 2.7 meters near Hopedale, Louisiana,

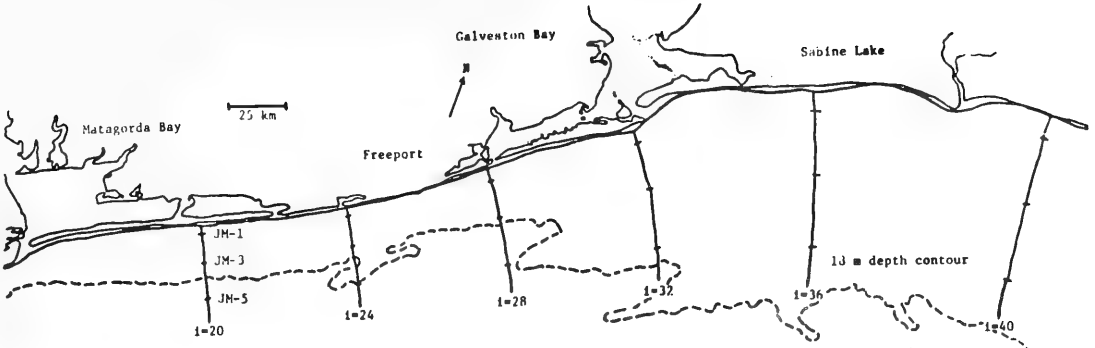

i=20

	TIME (hrs)			
	42	46	50	54
JM-1	-109	-119	- 99	-45
JM-3	-114	-117	- 99	11
JM-5	-115	-114	- 88	3
Σ	-.56	-.56	-.61	.06

i=28

	TIME (hrs)			
	42	46	50	54
JM-1	- 64	- 74	- 49	- 20
JM-3	- 70	- 80	- 58	- 44
JM-5	- 69	- 78	- 57	- 44
Σ	-.43	-.49	-.36	-.27

i=36

	TIME (hrs)			
	42	46	50	54
JM-1	- 44	- 50	- 27	- 18
JM-3	- 47	- 54	- 35	- 31
JM-5	- 47	- 55	- 37	- 37
Σ	-.35	-.41	-.27	-.23

i=24

	TIME (hrs)			
	42	46	50	54
JM-1	- 85	- 95	- 66	- 9
JM-3	- 85	- 91	- 62	- 13
JM-5	- 85	- 88	- 60	- 22
Σ	-.42	-.44	-.31	-.08

i=32

	TIME (hrs)			
	42	46	50	54
JM-1	- 52	- 63	- 37	- 28
JM-3	- 54	- 65	- 40	- 35
JM-5	- 52	- 62	- 40	- 33
Σ	-.38	-.45	-.29	-.24

i=40

	TIME (hrs)			
	42	46	50	54
JM-1	- 37	- 33	- 21	- 13
JM-3	- 44	- 42	- 35	- 13
JM-5	- 46	- 46	- 42	- 33
Σ	-.34	-.32	-.28	-.13

Figure 63. Values of alongshore current, $Q_{S*}/\overline{D}$, in centimeters per second as a function of time at selected grid points. Total alongshore transport in cubic meters per second is indicated by Σ.

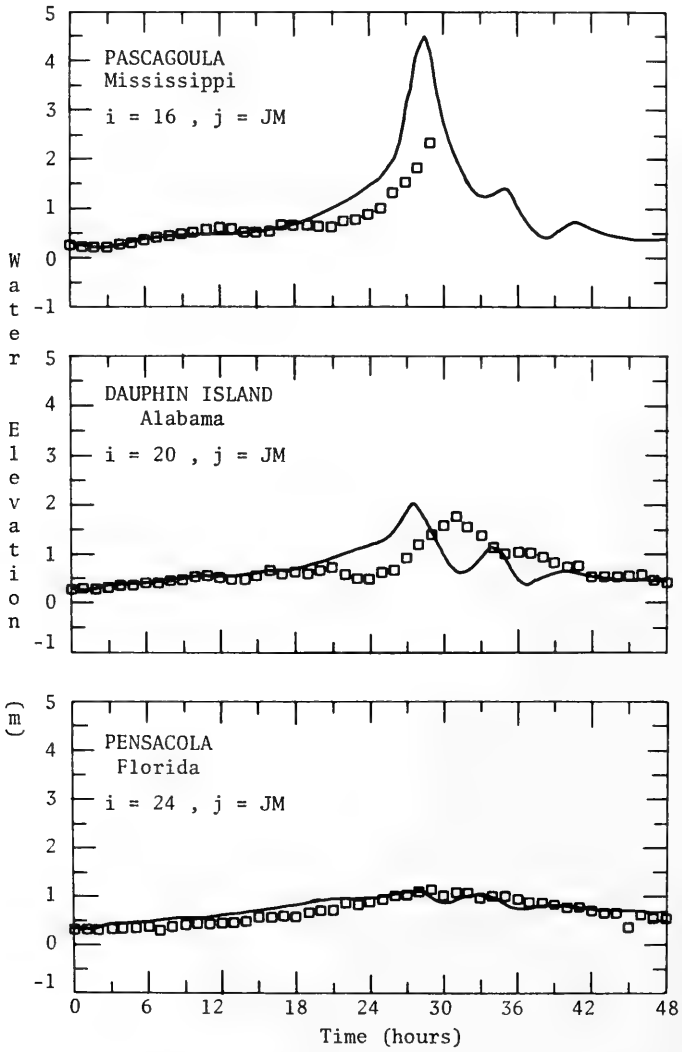

Figure 64. Observed (squares) and computed (solid) water levels for Hurricane Camille.

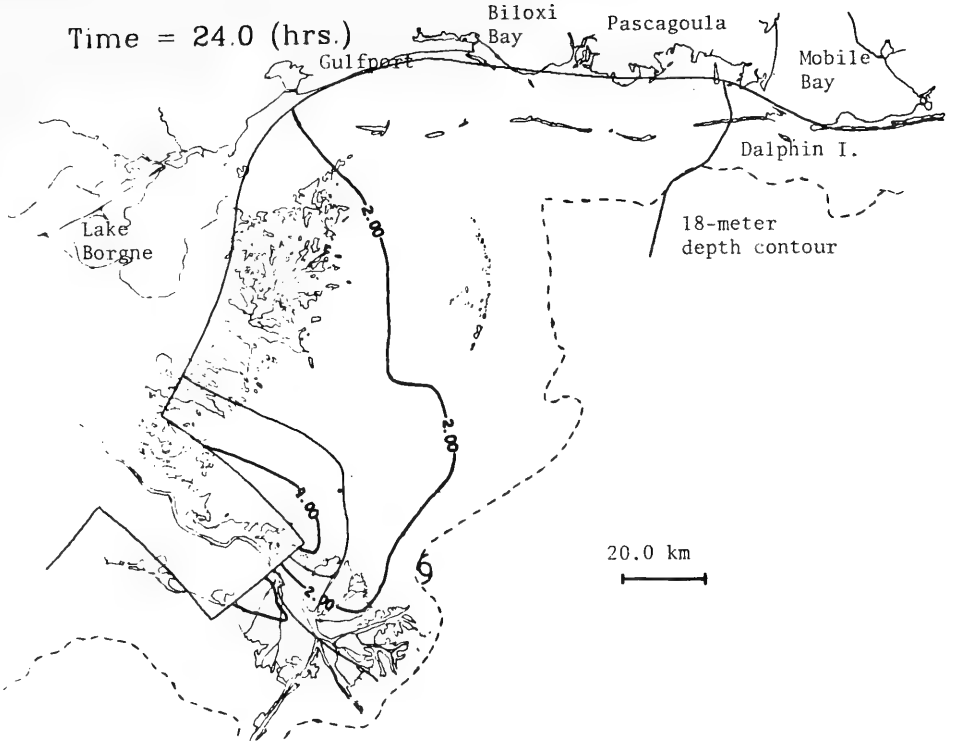

Figure 65. Computed water surface topography in 1.0-meter contour increments in the area of Breton, Chandeleur, and Mississippi Sounds for Hurricane Camille at 24 hours.

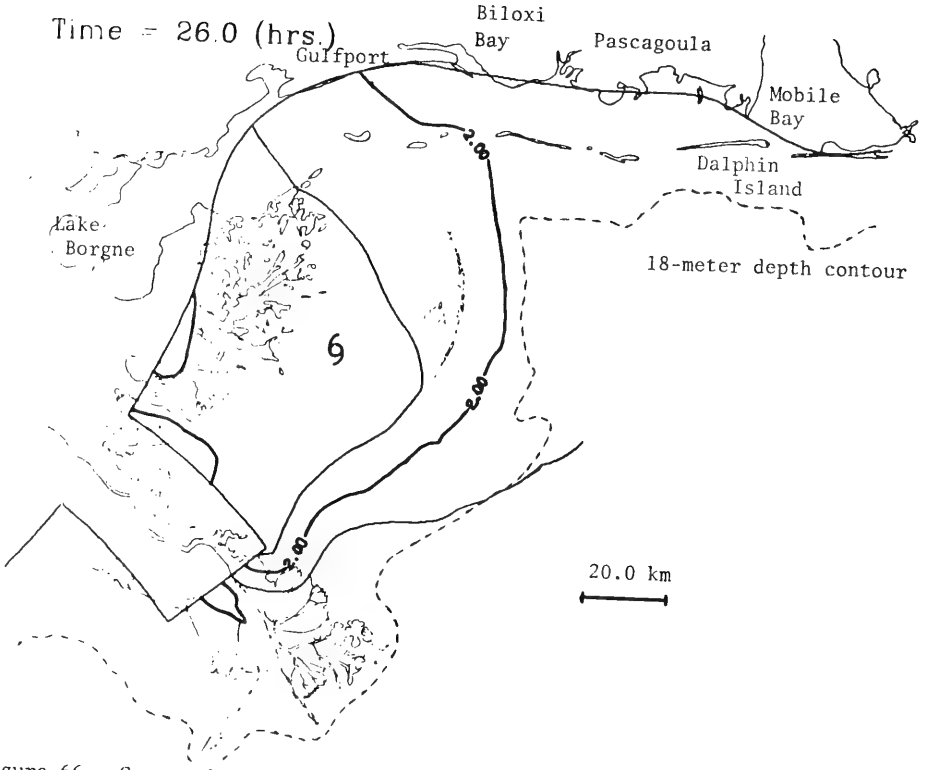

Figure 66. Computed water surface topography in 1.0-meter contour increments in the area of Breton, Chandeleur, and Mississippi Sounds for Hurricane Camille at 26 hours.

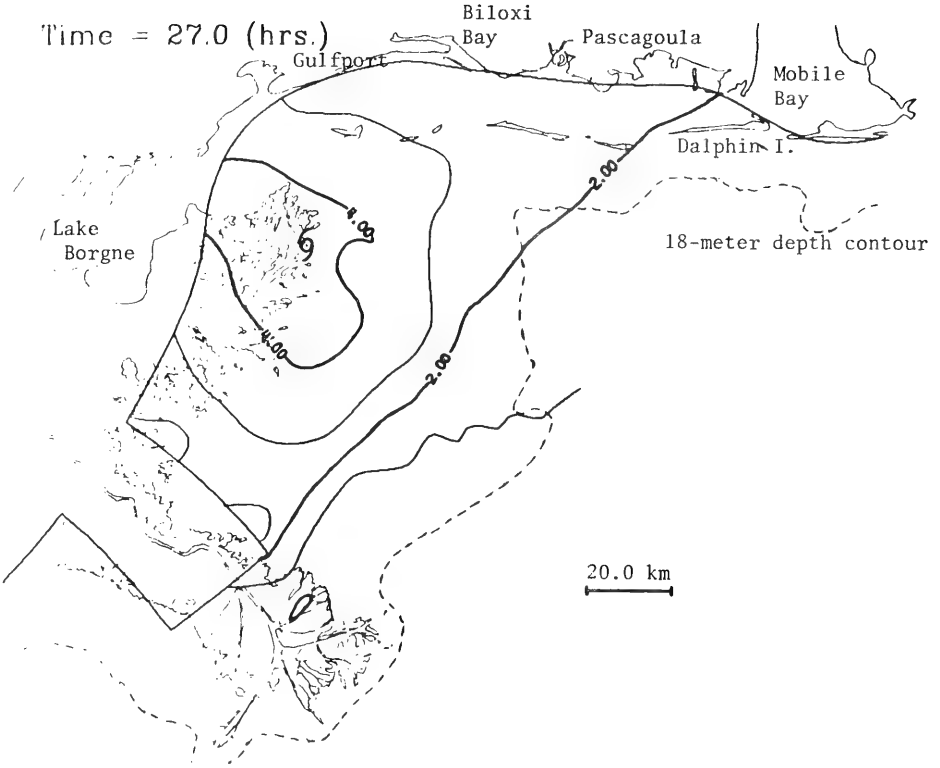

Figure 67. Computed water surface topography in 1.0-meter contour increments in the area of Breton, Chandeleur, and Mississippi Sounds for Hurricane Camille at 27 hours.

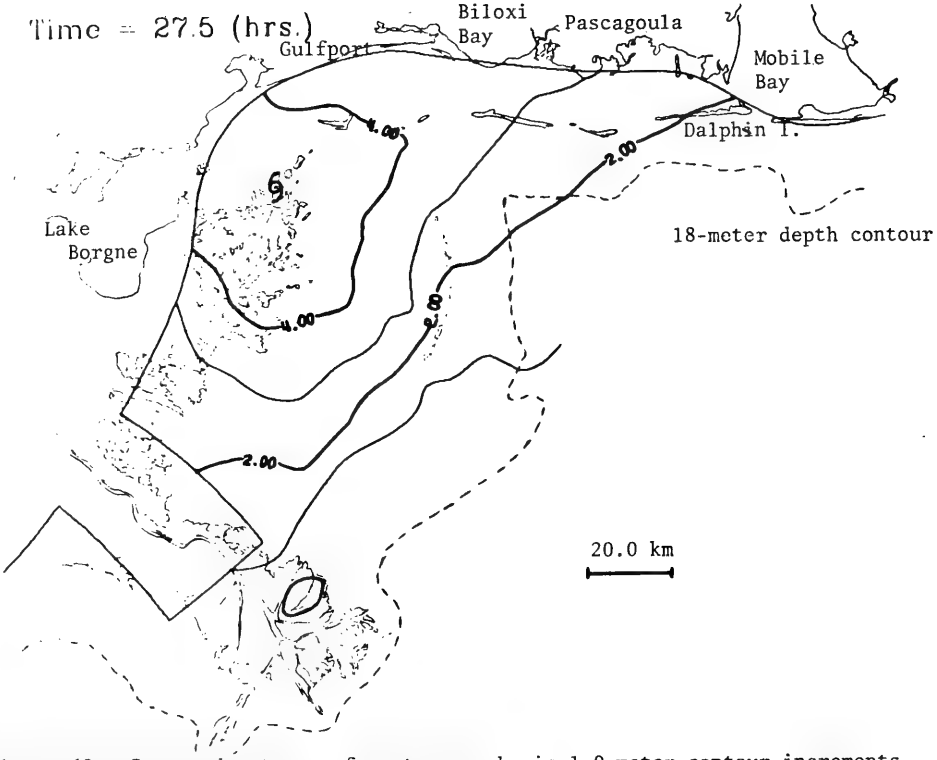

Figure 68. Computed water surface topography in 1.0-meter contour increments in the area of Breton, Chandeleur, and Mississippi Sounds for Hurricane Camille at 27.5 hours.

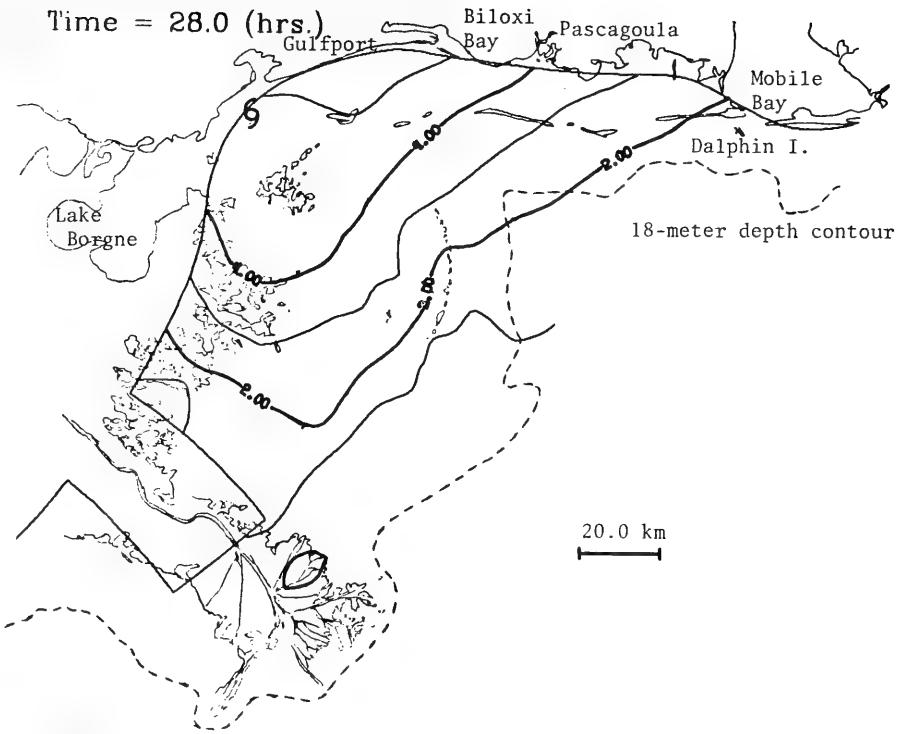

Figure 69. Computed water surface topography in 1.0-meter contour increments in the area Breton, Chandeleur, and Mississippi Sounds for Hurricane Camille at 28 hours.

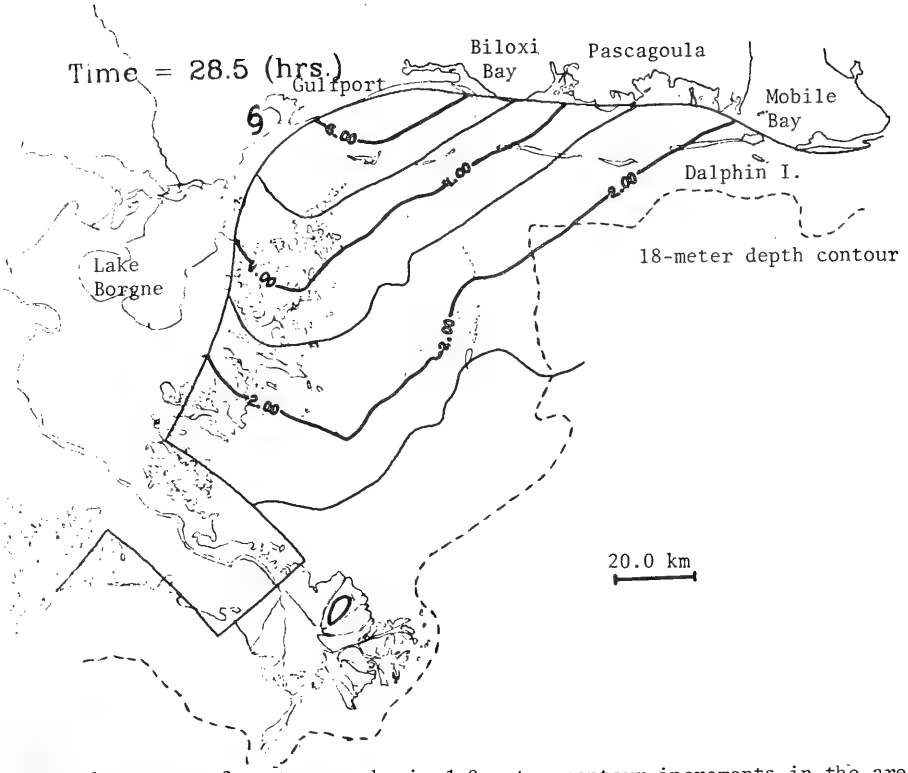

Figure 70. Computed water surface topography in 1.0-meter contour increments in the area of Breton, Chandeleur, and Mississippi Sounds for Hurricane Camille at 28.5 hours.

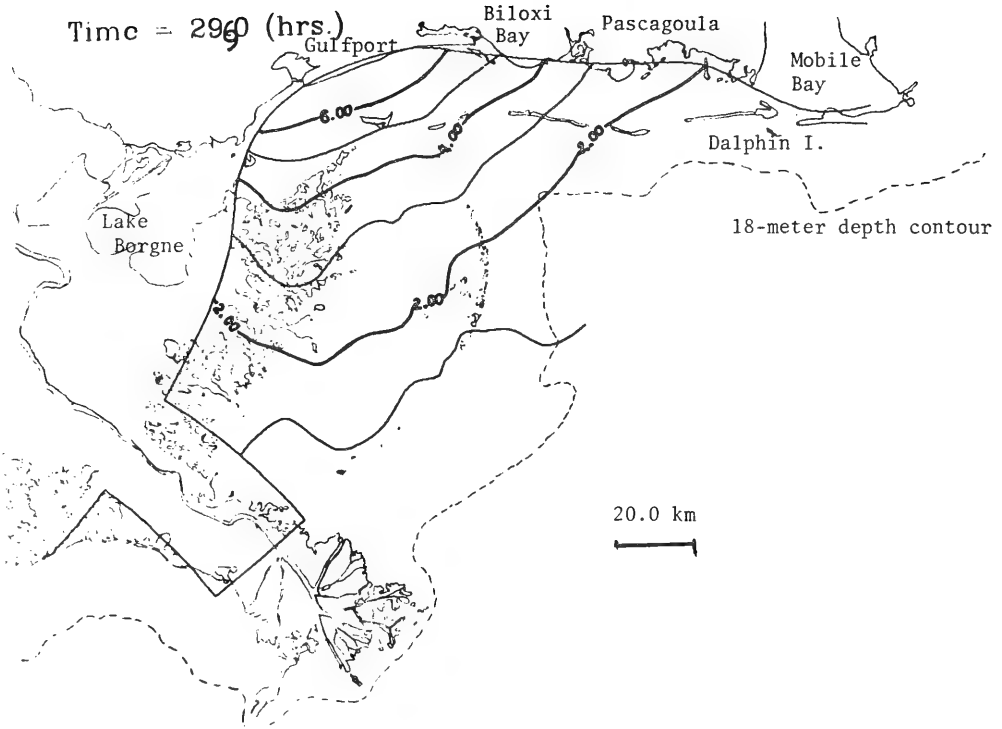

Figure 71. Computed water surface topography in 1.0-meter contour increments in the area of Breton, Chandeleur, and Mississippi Sounds for Hurricane Camille at 29 hours.

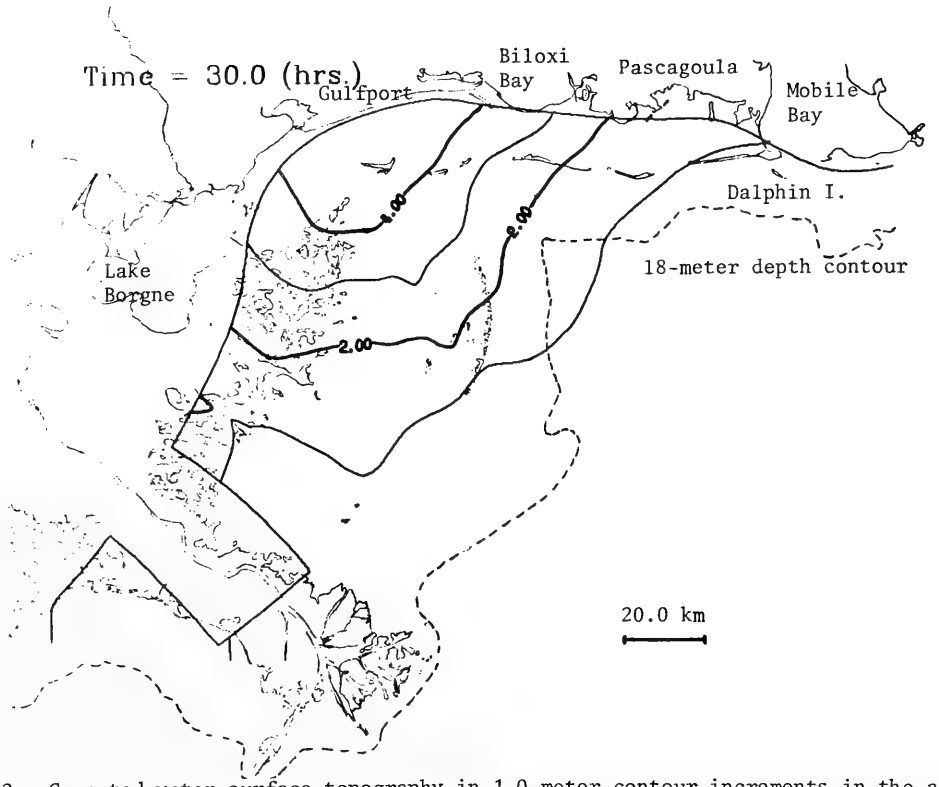

Figure 72. Computed water surface topography in 1.0-meter contour increments in the area of Breton, Chandeleur, and Mississippi Sounds for Hurricane Camille at 30 hours.

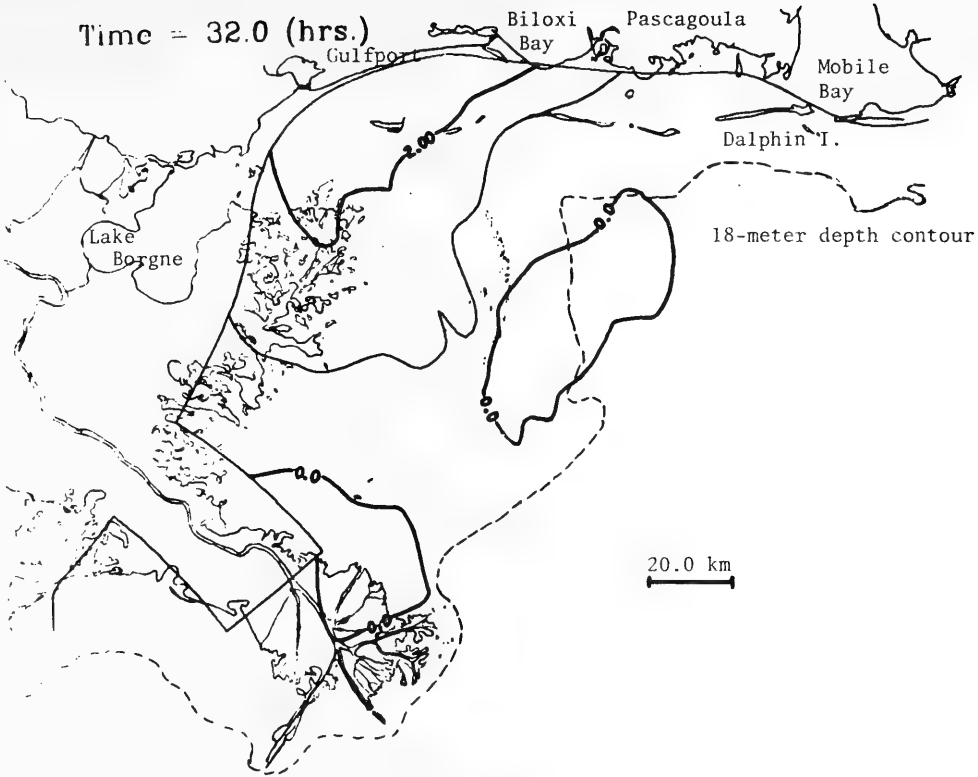

Figure 73. Computed water surface topography in 1.0-meter contour increments in the area of Breton, Chandeleur, and Mississippi Sounds for Hurricane Camille at 32 hours.

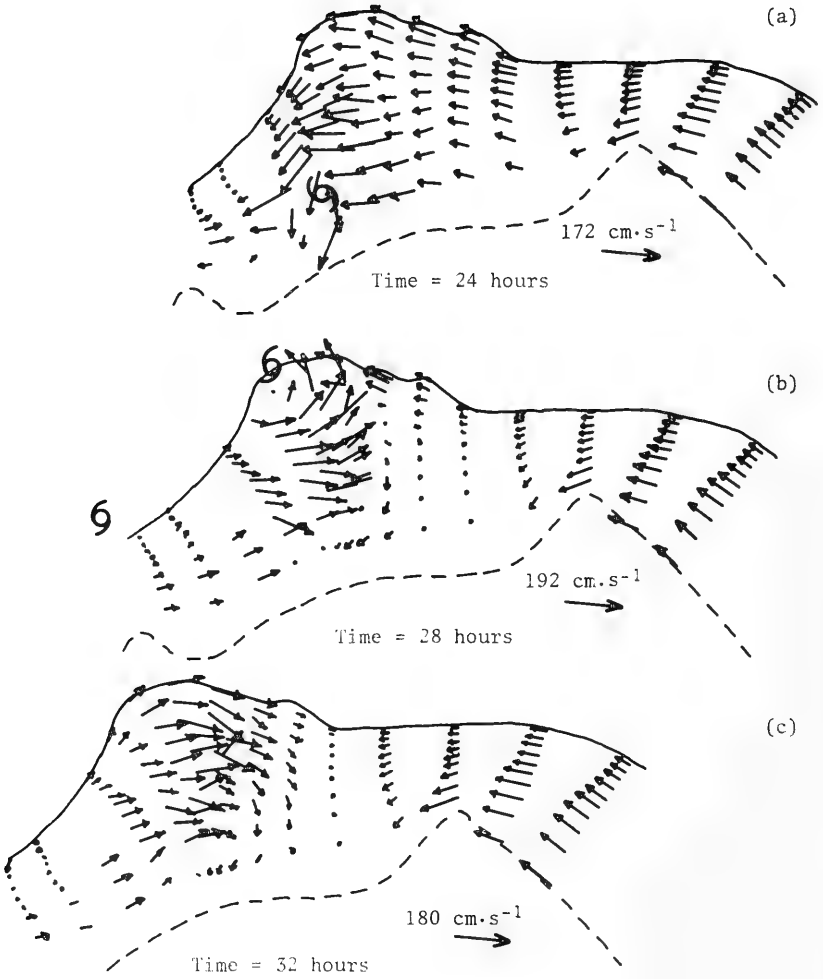

Figure 74. Computed water velocity in centimeters per second at selected grid points for Hurricane Camille at 24 (a), 28 (b), and 32 hours (c).

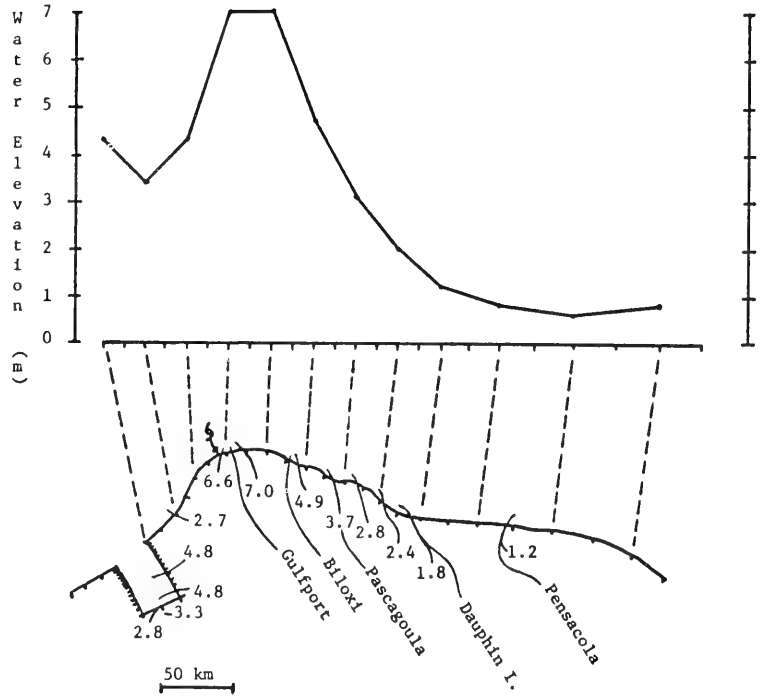

Figure 75. Computed high water of the coastal curves east of the delta from Hurricane Camille corrected for the astronomical tide. The numbers distributed about the bottom curve representing the coastline are observed still high water crests in meters.

in the marsh area south of Lake Borgne, and a high water mark of 4.8 meters along the eastern side of the Mississippi River levee. A part of the discrepancy between the observed and computed surges results from not considering the flooding of low coastal areas and the open communication of Mississippi Sound with Lake Borgne which is, in turn, connected with Lake Pontchartrain. The tide gage at Shell Beach located on the southern end of Lake Borgne crested at 3.4 meters. Another test simulation was conducted with the hurricane track moved 18 kilometers to the east. The results showed greater seaward circulation in Chandeleur Sound reducing the setup along the levee by approximately 1.5 meters. The location of the peak surge was shifted to the east but the surge magnitude was not reduced.

3. Hurricane Gracie.

Hurricane Gracie crossed the coast near Beaufort, South Carolina, at 1600 G.m.t. 29 September 1959. The radius to maximum winds was 25 kilometers. The atmospheric pressure in the eye was 950 millibars. The maximum sustained winds were approximately 50 meters per second.

A Cartesian grid for simulating the surge caused by Gracie is shown in Figure 76. The reach and grid spacing of this system are comparable to the curvilinear grid shown in Figure 32. The thin dashlines are a part of the transform-generated coast and seaward boundary curve (180-meter depth contour). The surge computations are performed with both grid systems using the same boundary conditions and forcing functions. The stairstep boundary representing the coast is the heavy solid line in Figure 76. Another difference between the models other than the coastline representation is that the Cartesian system's boundary, $j = 1$, extends farther seaward into deeper water than that of the curvilinear system.

For numerical stability a time step of 150 seconds was used in the computations with the curvilinear grid. The time step in the rectilinear system was taken as 75 seconds. The surge simulation was performed for a 48-hour period with zero hour corresponding to 1200 G.m.t. on 28 September.

The observed and computed water levels along the coast in the curvilinear (solid) and rectilinear (dashed) systems are shown in Figure 77. The inserts on Figure 76 show the simulated hydrograph locations. Figures 78 and 79 present the water surface topography in the curvilinear and rectilinear grids, respectively, at the same times and for the same contour increments. The depression of the water surface to the left of the storm track exhibited in both figures is similar to that from the Carla simulation. At the Savannah River entrance, the observed water level corrected for the astronomical tide is depressed after 27 hours reflecting the offshore-directed wind. The effect on the coastal surges and water surface topographies

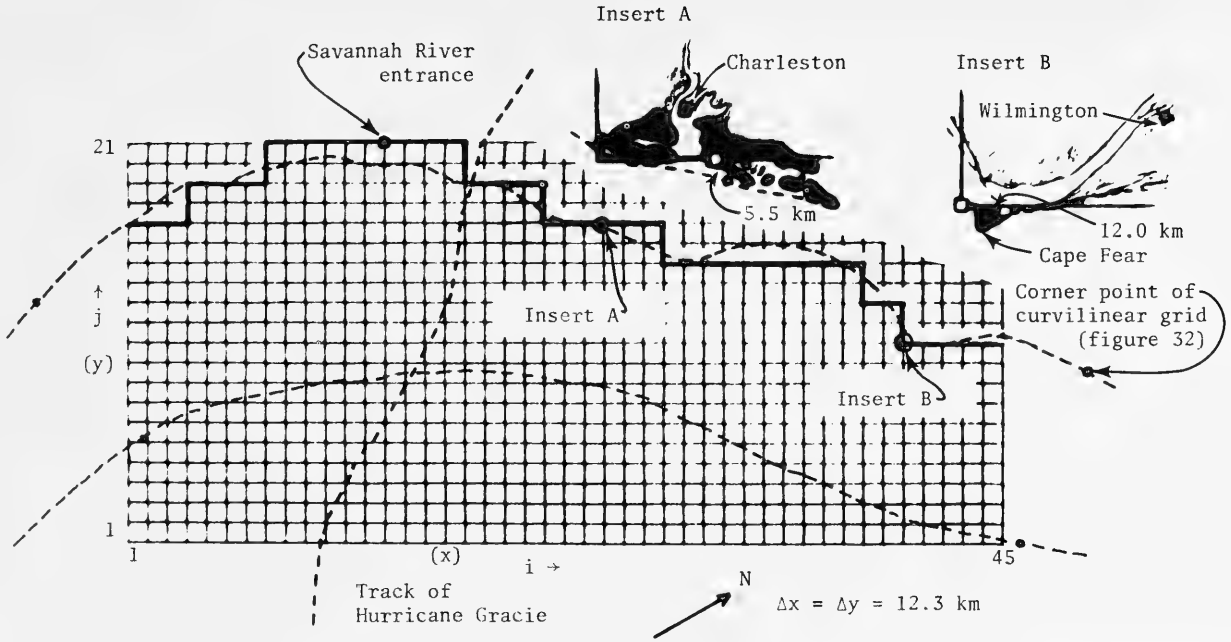

Figure 76. Cartesian grid for Hurricane Gracie storm surge simulation. The heavy solid line is the stairstep representation of the coast; dashlines are the transform-generated coastline and 180-meter depth contour. Inserts show simulated hydrograph locations along the coast in the rectilinear (□) and curvilinear (●) grids. Dots on the dashlines are corner points of the curvilinear grid given in Figure 32.

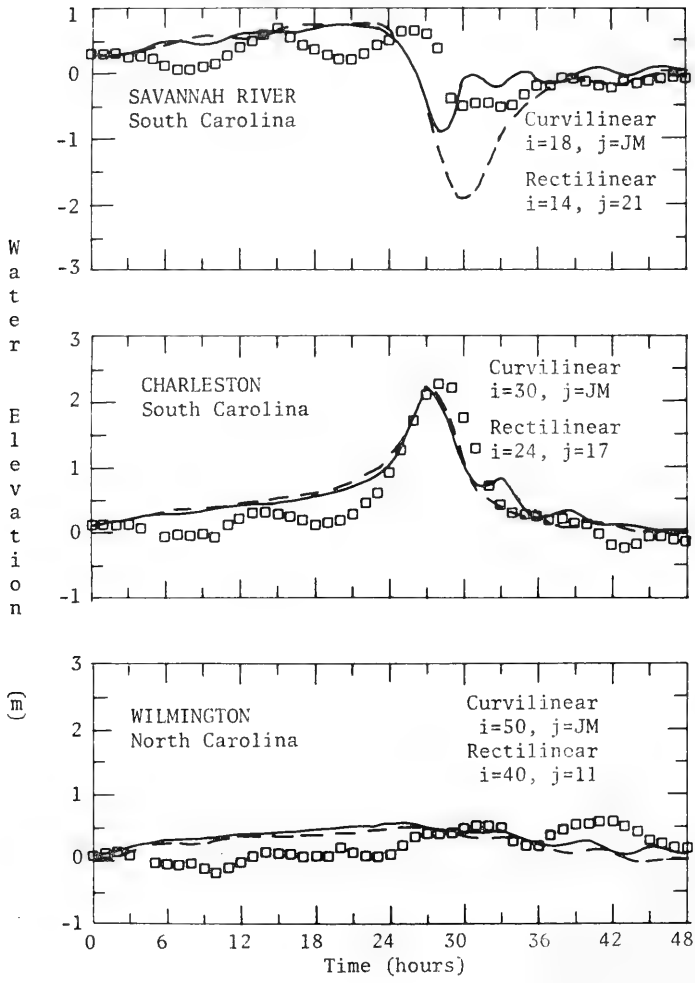

Figure 77. Observed (squares) and computed water levels for Hurricane Gracie in the curvilinear (solid) and rectilinear (dashline) grid systems.

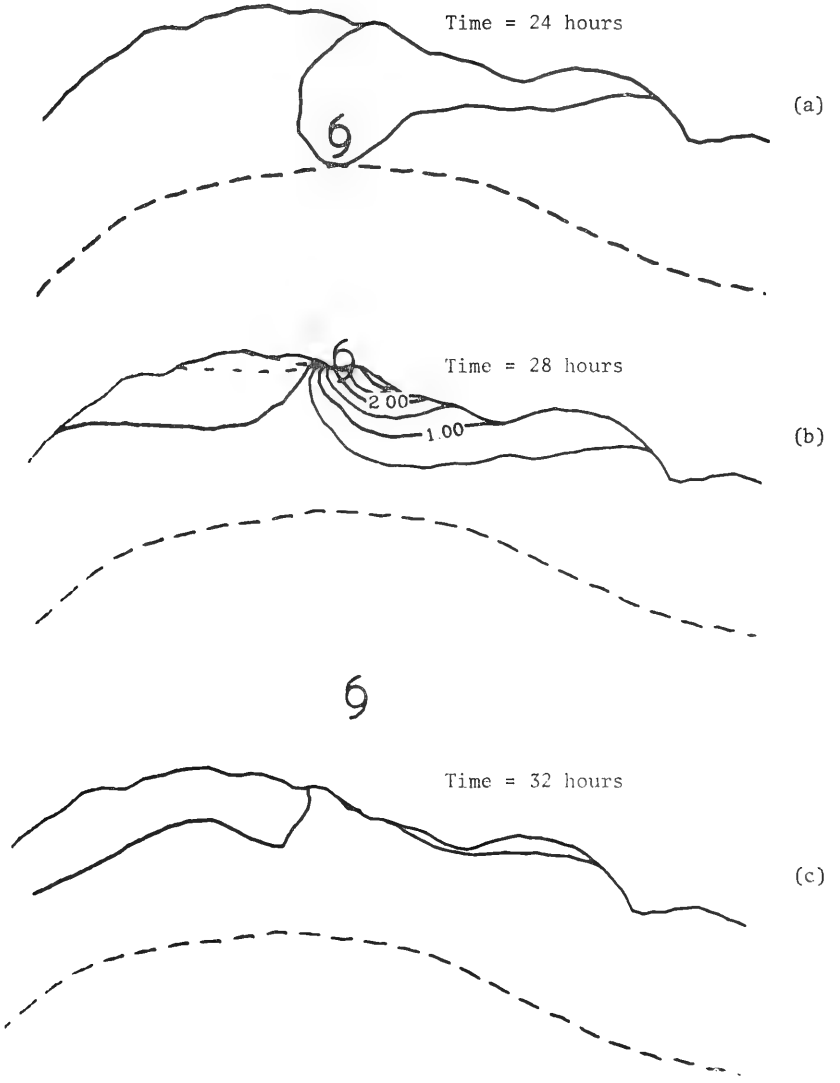

Figure 78. Computed water surface topography in 0.5-meter contour increments for Hurricane Gracie at 24 (a), 28(b), and 32 hours (c) in the curvilinear grid.

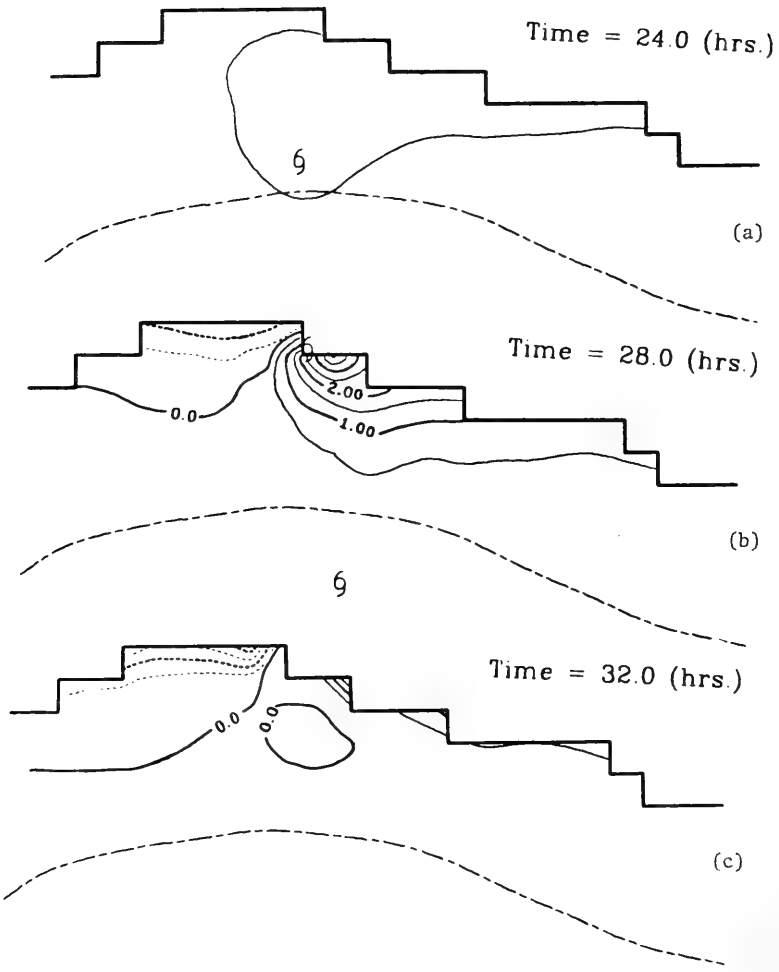

Figure 79. Computed water surface topography in 0.5-meter contour increments for Hurricane Gracie at 24 (a), 28 (b), and 32 hours (c) , in the rectilinear grid.

resulting from the stairstep portrayal of the coast boundary are shown through the comparison of Figures 78 and 79. The curvilinear model shows the maximum coastal water level at the time of landfall of approximately 3 meters while the Cartesian system predicts 4 meters. Furthermore, the peak surge of 4.5 meters in the Cartesian system occurred at the corner point (22, 19) over 2 hours after storm landfall.

The water velocity, $\hat{V}$, from the curvilinear system is presented in Figure 80. The figure also shows the development of a cyclonic current in the region from Cape Romain to Cape Fear resulting from the curved coastline and the extensive Frying Pan Shoals off Cape Fear. A similar current pattern is not observed in the rectilinear system.

The computed high water envelopes from both grids are shown in Figure 81. The stairstep rectilinear coastline is projected upon the curvilinear coastline providing a common basis for the comparison. Both systems predict a maximum surge comparable to that of the nearest observed high water mark. The effect of the rectilinear coastline on the surge envelope is seen in the figure by the relative water level maximums at the interior corner grid points. The primary contrast of the coastal envelope of computed surges in the two different grid systems is the greater variability of that from the rectangular grid. This leads to spurious results as can be seen particular for Savannah River.

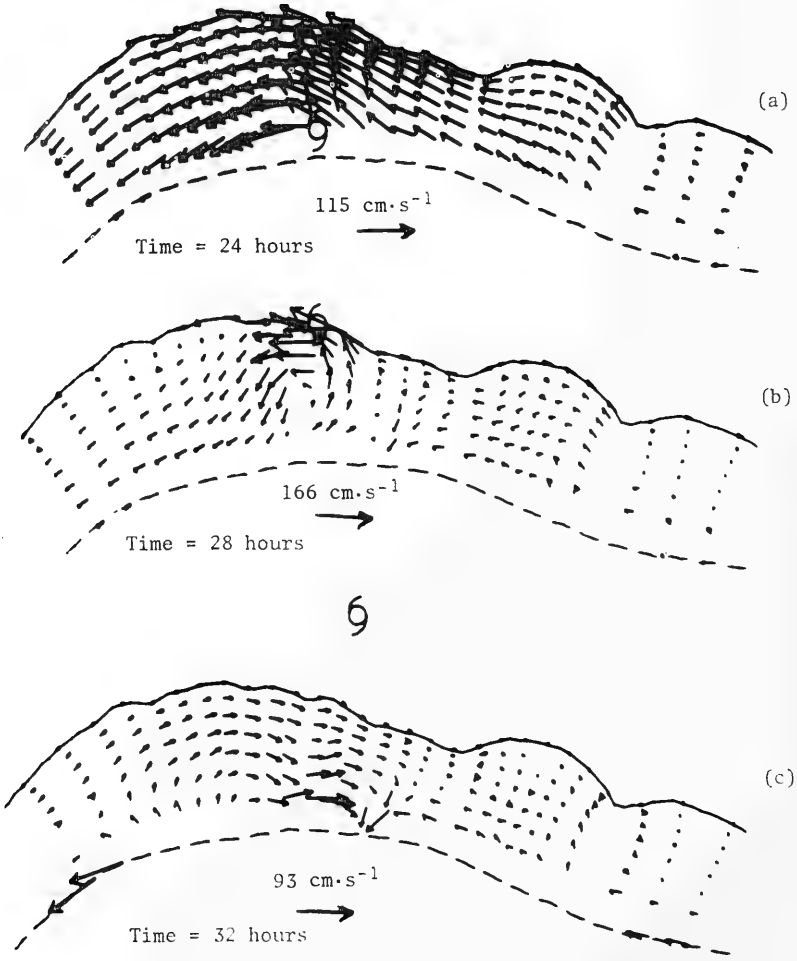

Figure 80. Computed water velocity in centimeters per second at selected grid points for Hurricane Gracie at 24 (a), 28 (b), and 32 hours (c) in the curvilinear grid. See Figure 5 for identification of capes referred to in the text.

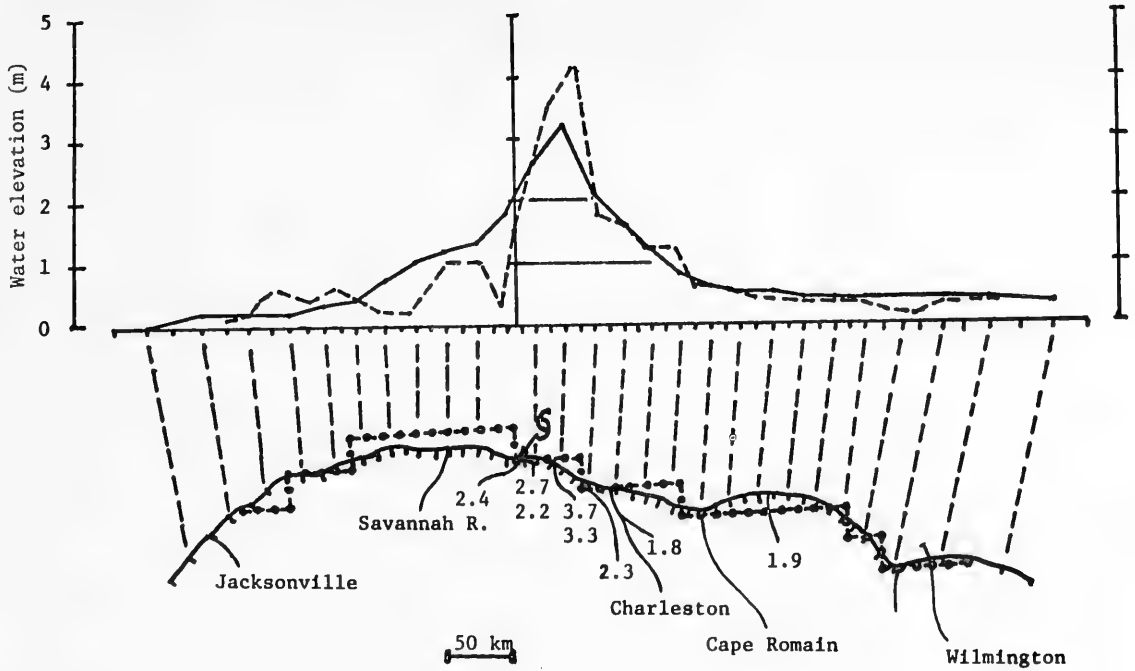

Figure 81. Computed high water of the coastal surges from Hurricane Gracie corrected for the astronomical tide in the curvilinear (top solid) and rectilinear (top dashline) grids. The numbers distributed about the bottom curve representing the coastline are observed still high water marks in meters.

VI. SUMMARY AND CONCLUSIONS

The development of the conformal mapping problem was completed for transforming the interior region bounded by two arbitrarily shaped curves and two parallel lateral boundaries into a rectangle in the image plane. Specifically, the coastline and seaward boundary curve taken as the 180-meter depth contour are transformed into the image plane as constant values of η. The bicurve fitting procedure was successively tested on five regions of the Continental Shelf in the Gulf of Mexico and east coast of the United States. The distinct advantages of the orthogonal curvilinear coordinate system over rectilinear representations of the coast are the accuracy and ease of specification of the boundary conditions. For long wave calculations, the numerical simulation of a free long wavelength gravity wave in a quarter annulus demonstrated the superiority of modeling the boundaries in curvilinear coordinates.

A two-dimensional time-dependent numerical storm surge model employing orthogonal curvilinear coordinates is presented. Since the transformation is conformal, the associated modification of the equations is minimized. The final coordinates allow for the greatest resolution near the coast over the area of principal storm surge development and modification. A second transformation is performed independently on each of the curvilinear coordinates to provide the desired spatial resolution in the shallower region near hurricane landfall.

Results of the numerical simulation in transformed coordinates of the storm surges along the gulf coast induced by Hurricanes Carla, Camille, and Gracie which crossed the east coast are presented. The surface wind fields are analytically represented. Additionally, a systematic procedure is employed to deform the symmetric wind fields of Carla and Camille in the nearshore region. The deformed Carla wind representation produces better agreement between the computed surges and that observed than a similar simulation with a symmetric wind. Although the pattern of windspeeds produced by the deformation procedure is in good agreement with those provided by NWS, the problem of specifying the proper orientation of the wind-stress vector in the nearshore region requires further study.

The surge simulations indicate that the model produces results in good agreement with the observed peak surges and hydrographs, especially in the area to the right of landfall. Moreover, the results from the simulation of the Hurricane Gracie surge indicate superior rendition in the curvilinear grid compared with that of the Cartesian grid. Certainly one contributor to any discrepancy between computed and observed water levels may result from the portrayal of the coast as a wall. Proper inclusion of attached bays, lakes, and flooding of low-lying areas should be pursued.

LITERATURE CITED

ALVAREZ, J.A., "Numerical Prediction of Storm Surges in the Rio de la Plata Area," Ph.D. Dissertation, University of Buenos Aires, Buenos Aires, Argentina, 1973.

DONN, W.L., "An Empirical Basis for Forecasting Storm Tides," *Bulletin of the American Meteorological Society*, Vol. 39, 1958, pp. 640-647.

FORRISTALL, G.Z., "Three-dimensional Structure of Storm-Generated Currents," *Journal of Geophysical Research*, Vol. 79, 1974, pp. 2721-2729.

GRAHAM, H.E., and NUNN, D.E., "Meteorological Considerations Pertinent to Standard Project Hurricane, Atlantic and Gulf Coasts of the United States," Report 33, National Hurricane Research Project, U.S. Department of Commerce, Washington, D.C., 1959.

JELESNIANSKI, C.P., "An Numerical Calculation of Storm Tides Induced by a Tropical Storm Impinging on a Continental Shelf," *Monthly Weather Review*, Vol. 93, 1965, pp. 343-358.

JELESNIANSKI, C.P., "Numerical Computations of Storm Surges Without Bottom Stress," *Monthly Weather Review*, Vol. 94, 1966, pp. 379-394.

JELESNIANSKI, C.P., "Numerical Computations of Storm Surges with Bottom Stress," *Monthly Weather Review*, Vol. 95, 1967, pp. 740-756.

JELESNIANSKI, C.P., "SPLASH I: Landfall Storms," TDL-46, National Oceanic and Atmospheric Administration, National Weather Service, Silver Spring, Md., 1972.

LAMB, H., *Hydrodynamics*, Dover, New York, 1932.

MIYAZAKI, M., "A Numerical Computation of the Storm Surge of Hurricane Carla 1961 in the Gulf of Mexico," Technical Report No. 10, University of Chicago, Chicago, Ill., 1963.

PLATZMAN, G.W., "The Dynamical Prediction of Wind Tides on Lake Erie," *Meteorological Monographs*, Vol. 4, 1963.

PLATZMAN, G.W., "Two-dimensional Free Oscillations in Natural Basins," *Journal of Physical Oceanography*, Vol. 2, 1972, pp. 117-138.

RAO, D.B., "Free Gravitational Oscillations in Rotating Rectangular Basins," *Journal of Fluid Mechanics*, Vol. 25, 1966, pp. 523-555.

REID, R.O., "Comment on 'Three-dimensional Structure of Storm-generated Currents' by G.Z. Forristal," *Journal of Geophysical Research*, Vol. 80, 1975, pp. 1184-1185.

REID, R.O., and VASTANO, A.C., "Orthogonal Coordinates for Analysis of Long Gravity Waves Near Islands," *Proceedings, American Society of Civil Engineers, Santa Barbara Specialty Conference in Coastal Engineering*, 1966, pp. 1-20.

REID, R.O., and BODINE, B.R., "Numerical Model for Storm Surges in Galveston Bay," *Proceedings, American Society of Civil Engineers, Journal of Waterway and Harbours Division*, Paper 5805, Vol. 94, No. WW1, 1968, pp. 33-57.

SCHWEIKERT, D.G., "An Interpolation Curve Using a Spline under Tension," *Journal of Mathematics and Physics*, Vol. 45, 1966, pp. 312-317.

U.S. ARMY ENGINEER DISTRICT, GALVESTON, "Report on Hurricane Carla 9-12 September 1961," Galveston, Tex., 1962.

U.S. ARMY ENGINEER DISTRICT, NEW ORLEANS, "Report on Hurricane Camille 14-22 August 1969," New Orleans, La., 1970.

WELANDER, P., "Numerical Prediction of Storm Surges," *Advances in Geophysics*, Vol. 8, Academic Press, New York, 1961.

WHITAKER, R.E., REID, R.O., and VASTANO, A.C., "Drag Coefficient at Hurricane Wind Speeds as Deduced from Numerical Simulation of Dynamic Water Level Changes in Lake Okeechobee," Ref. 73-13-T, Department of Oceanography, Texas A&M University, College Station, Tex., 1973.

APPENDIX A

CONFORMAL MAPPING COEFFICIENTS

FOR THE

GULF COAST REGION FROM ATCHAFALAYA BAY TO APALACHEE BAY

β = 0.1991531E 02

B_o = 0.1129102E 03

λ = 317.5

n	B_n	C_n
1	-0.1861917E 02	-0.2013675E 01
2	-0.2804652E 02	0.6239547E 01
3	0.6403131E 01	-0.5958148E 01
4	-0.2530149E 01	0.5130100E 01
5	0.1531121E 01	0.2273190E 01
6	0.1498879E-01	0.3512568E 01
7	-0.4953118E 00	-0.1606539E 01
8	-0.1035305E 01	0.1131842E 01
9	-0.2334446E 00	-0.6252772E-01
10	0.5907305E-01	0.6906291E 00
11	0.4296697E 00	-0.1417943E 00
12	-0.2997332E-01	0.1326714E-01
13	0.4310032E-01	-0.2609431E 00
14	-0.6075356E-02	0.1616244E-01
15	0.1117075E 00	-0.4899038E-01
16	0.5209380E-01	0.7586825E-01
17	0.7516444E-02	-0.2902573E-01
18	-0.1997321E-01	0.3440024E-01
19	-0.5793062E-03	-0.3394415E-01
20	0.1344183E-01	0.2085055E-01
21	0.1558170E-01	-0.5309362E-02
22	0.3357759E-02	0.1572620E-01

Note: all quantities are in x,y units.

n	B_n	C_n
23	0.4536543E-02	-0.4705735E-02
24	-0.6767012E-02	0.4449189E-02
25	0.5650939E-03	0.1541801E-02
26	-0.3992960E-02	0.6915852E-02
27	0.2905252E-02	0.2670427E-02
28	-0.5924194E-03	0.3155482E-02
29	0.3964610E-03	-0.1662592E-02
30	-0.8709535E-03	0.5550052E-03
31	0.4148923E-03	-0.1224325E-02
32	0.4497680E-03	0.1261886E-02
33	0.5558960E-03	-0.2653040E-03
34	-0.4054087E-03	0.4554733E-03
35	-0.2529798E-03	-0.5726672E-03
36	-0.2813288E-03	0.5050778E-04
37	0.3256833E-03	-0.1838352E-03
38	0.1094875E-03	0.1940636E-03
39	0.1343705E-03	-0.1790418E-03
40	-0.8795955E-04	-0.2377543E-04
41	-0.8443834E-05	-0.1661804E-03
42	-0.1611809E-04	0.9141980E-04
43	0.4455329E-04	0.5842209E-05
44	-0.2129783E-04	0.6875678E-04
45	-0.1393920E-05	-0.3022245E-04
46	-0.3849607E-04	0.5177958E-05
47	0.1427432E-04	-0.1272952E-04
48	-0.3892541E-05	0.1886662E-04
49	0.1366723E-04	-0.1514819E-05
50	-0.9772998E-05	0.1114408E-04
51	-0.3762842E-05	-0.7410708E-05
52	-0.7610149E-05	0.6834680E-05
53	0.8511489E-06	-0.3682432E-05
54	-0.8219286E-06	0.5019881E-05
55	0.2588446E-05	-0.2587597E-05
56	-0.1645242E-05	0.7941880E-06
57	0.9023091E-06	-0.2933107E-05
58	-0.1668636E-05	-0.7180398E-07
59	0.8869575E-06	-0.9114828E-06
60	-0.4799319E-06	0.1067656E-05
61	0.6261487E-06	-0.4895755E-06
62	-0.5237882E-06	0.2304607E-06
63	-0.4759656E-07	-0.8925043E-06
64	-0.2598815E-06	0.1912503E-06
65	0.3273941E-06	-0.2104335E-06
66	0.2930804E-07	0.3730255E-06
67	0.1020638E-06	-0.1417030E-06
68	-0.2422100E-06	0.5916811E-07

n	B_n	C_n
69	-0.5880160E-08	-0.1276744E-06
70	-0.4626684E-07	0.1424694E-06
71	0.1153690E-06	0.1719058E-07
72	-0.1692220E-07	0.8880539E-07
73	0.6679772E-09	-0.6668830E-07
74	-0.4858599E-07	0.1698348E-07
75	0.2245889E-07	-0.2062551E-07
76	0.4829538E-08	0.5085036E-07
77	0.2210185E-07	-0.2895261E-08
78	-0.1637371E-07	0.1013160E-07
79	0.5777583E-09	-0.1960430E-07
80	-0.6394433E-08	0.8530744E-08
81	0.1182490E-07	-0.2038007E-08
82	0.6501393E-09	0.9465726E-08
83	0.2608579E-08	-0.6092815E-08
84	-0.4322956E-08	0.1981510E-08
85	0.1574734E-08	-0.3446277E-08
86	-0.4726193E-10	0.4146546E-08
87	0.2415840E-08	-0.9092067E-09
88	-0.1000588E-08	0.1491153E-08
89	0.6742753E-09	-0.1408612E-08
90	-0.6728380E-09	0.1087402E-08
91	0.1012167E-08	-0.1879313E-09
92	-0.3016696E-09	0.9163199E-09
93	0.3236860E-09	-0.3496718E-09
94	-0.3145593E-09	0.4997083E-09
95	0.3353653E-09	-0.1249788E-09
96	-0.3262997E-10	0.4405611E-09
97	0.1631445E-09	-0.1501641E-09
98	-0.1375170E-09	0.1637698E-09
99	0.1072999E-09	-0.9262971E-10
100	-0.1384905E-11	0.1895707E-09
101	0.1086742E-09	-0.1663476E-10
102	-0.5080765E-10	0.6890670E-10
103	0.1376387E-10	-0.7510520E-10
104	-0.2277743E-10	0.4346501E-10
105	0.5459146E-10	-0.7598091E-11
106	0.5370517E-11	0.4664877E-10
107	0.1355941E-10	-0.2425636E-10
108	-0.2422210E-10	0.4706750E-11
109	0.7556705E-11	-0.1434774E-10
110	0.3368470E-12	0.2010955E-10
111	0.1447254E-10	0.1050866E-11
112	-0.5194694E-11	0.7150311E-11
113	-0.4364368E-13	-0.9073677E-11
114	-0.4752083E-11	0.3138752E-11

n	B_n	C_n
115	0.4553522E-11	-0.6452875E-12
116	0.7602034E-12	0.6237037E-11
117	0.1944547E-11	-0.1114412E-11
118	-0.2436083E-11	0.1234543E-11
119	0.1917147E-12	-0.1740079E-11
120	-0.4928470E-12	0.1649892E-11
121	0.1484346E-11	0.5327387E-13
122	-0.1348819E-12	0.1120676E-11
123	0.3641300E-12	-0.5990049E-12
124	-0.5487838E-12	0.2460370E-12
125	0.2406558E-12	-0.3448143E-12
126	-0.7911185E-13	0.4439149E-12
127	0.3179581E-12	-0.5831951E-13
128	-0.8611943E-13	0.2390251E-12
129	0.7238470E-13	-0.1814728E-12
130	-0.1361322E-12	0.5573903E-13
131	0.6817892E-13	-0.9745736E-13
132	-0.1436969E-13	0.1152394E-12
133	0.8566666E-13	-0.1163015E-13
134	-0.3499625E-13	0.5682837E-13
135	-0.7835616E-15	-0.5510710E-13
136	-0.4394792E-13	0.1780100E-13
137	0.2349419E-13	-0.1272599E-13
138	0.4395810E-14	0.4233778E-13
139	0.1976828E-13	-0.3816127E-14
140	-0.1687651E-13	0.7731344E-14
141	-0.1897316E-14	-0.1672038E-13
142	-0.6781451E-14	0.9221180E-14
143	0.1174166E-13	0.2324292E-14
144	0.6883079E-15	0.1088460E-13
145	0.2116535E-14	-0.4276968E-14
146	-0.5574005E-14	0.4950588E-15
147	0.1321551E-14	-0.3220331E-14
148	0.5106463E-15	0.4241152E-14
149	0.3148336E-14	0.2514837E-15
150	-0.8159113E-15	0.1642851E-14
151	0.4507668E-16	-0.1803004E-14
152	-0.1082406E-14	0.5420030E-15
153	0.9193219E-15	-0.2248083E-15
154	0.2152137E-16	0.1072704E-14
155	0.5440539E-15	-0.2019489E-15
156	-0.4207780E-15	0.2787050E-15
157	0.1240553E-15	-0.3249225E-15
158	-0.1809934E-15	0.2896084E-15
159	0.2134241E-15	-0.6586600E-16
160	-0.6414966E-16	0.2533124E-15

n	B_n	C_n
115	0.4553522E-11	-0.6452875E-12
116	0.7602034E-12	0.6237037E-11
117	0.1944547E-11	-0.1114412E-11
118	-0.2436083E-11	0.1234543E-11
119	0.1917147E-12	-0.1740079E-11
120	-0.4928470E-12	0.1649892E-11
121	0.1484346E-11	0.5327387E-13
122	-0.1348819E-12	0.1120676E-11
123	0.3641300E-12	-0.5990049E-12
124	-0.5487838E-12	0.2460370E-12
125	0.2406558E-12	-0.3448143E-12
126	-0.7911185E-13	0.4439149E-12
127	0.3179581E-12	-0.5831951E-13
128	-0.8611943E-13	0.2390251E-12
129	0.7238470E-13	-0.1814728E-12
130	-0.1361322E-12	0.5573903E-13
131	0.6817892E-13	-0.9745736E-13
132	-0.1436969E-13	0.1152394E-12
133	0.8566666E-13	-0.1163015E-13
134	-0.3499625E-13	0.5682837E-13
135	-0.7835616E-15	-0.5510710E-13
136	-0.4394792E-13	0.1780100E-13
137	0.2349419E-13	-0.1272599E-13
138	0.4395810E-14	0.4233778E-13
139	0.1976828E-13	-0.3816127E-14
140	-0.1687651E-13	0.7731344E-14
141	-0.1897316E-14	-0.1672038E-13
142	-0.6781451E-14	0.9221180E-14
143	0.1174166E-13	0.2324292E-14
144	0.6883079E-15	0.1088460E-13
145	0.2116535E-14	-0.4276968E-14
146	-0.5574005E-14	0.4950588E-15
147	0.1321551E-14	-0.3220331E-14
148	0.5106463E-15	0.4241152E-14
149	0.3148336E-14	0.2514837E-15
150	-0.8159113E-15	0.1642851E-14
151	0.4507668E-16	-0.1803004E-14
152	-0.1082406E-14	0.5420030E-15
153	0.9193219E-15	-0.2248083E-15
154	0.2152137E-16	0.1072704E-14
155	0.5440539E-15	-0.2019489E-15
156	-0.4207780E-15	0.2787050E-15
157	0.1240553E-15	-0.3249225E-15
158	-0.1809934E-15	0.2896084E-15
159	0.2134241E-15	-0.6586600E-16
160	-0.6414966E-16	0.2533124E-15

APPENDIX B

CONFORMAL MAPPING COEFFICIENTS

FOR THE

EAST COAST REGION FROM CAPE KENNEDY TO PAMLICO SOUND

$$\beta = 0.9917248E\ 01$$

$$B_o = 0.7052965E\ 02$$

$$\lambda = 350.0$$

n	B_n	C_n
1	-0.4282722E 02	-0.6295406E 02
2	-0.2821791E 02	-0.2364755E 02
3	0.1238905E 02	0.1391628E 02
4	0.4424074E 01	-0.7596874E 00
5	-0.4208601E 01	-0.2879633E 00
6	-0.2069723E 00	-0.7998557E 00
7	0.8464327E 00	0.2104794E 01
8	0.3291799E 00	0.1254503E 01
9	-0.9578854E 00	-0.1678884E 01
10	-0.2837964E 00	0.1566365E 00
11	0.4488817E 00	0.8259152E 00
12	-0.6342903E-02	-0.1633873E 00
13	-0.2921963E 00	-0.6565279E-01
14	0.5386317E-01	0.1499777E 00
15	-0.3311124E-01	0.2785084E-01
16	-0.1305802E 00	-0.1012938E 00
17	0.5479731E-01	0.5412336E-01
18	0.1251435E 00	0.1918038E 00
19	-0.2086312E 00	-0.1557431E 00
20	0.1179140E 00	0.1029936E 00
21	-0.1145189E 00	-0.9353477E-01
22	0.2414525E-03	0.3330456E-01

Note: All quantities are in x,y units.

n	B_n	C_n
23	0.8573616E-01	0.9928739E-01
24	-0.7312429E-01	-0.8458531E-01
25	0.2609131E-01	0.4790343E-01
26	-0.1153731E-01	0.7979628E-02
27	-0.4611936E-01	-0.5418998E-01
28	0.4978760E-01	0.5558310E-01
29	-0.2400338E-01	-0.1138851E-01
30	0.1476795E-04	-0.3498875E-02
31	0.1241791E-01	0.2114711E-01
32	-0.2015296E-01	-0.1866217E-01
33	-0.3106954E-02	-0.3141602E-02
34	0.1246096E-01	0.1712414E-01
35	-0.8497261E-02	-0.7135786E-02
36	0.1999057E-02	0.3350719E-02
37	0.7288672E-03	0.1991504E-02
38	-0.4637495E-02	-0.4495025E-02
39	-0.1242511E-02	0.2243265E-02
40	0.3494871E-02	0.2640330E-02
41	-0.2765389E-02	-0.2747552E-02
42	0.1414528E-02	0.3619528E-02
43	-0.1092573E-02	-0.9984830E-03
44	-0.9259579E-03	-0.9879367E-03
45	-0.5194661E-03	0.2608439E-03
46	0.1018548E-02	0.1251844E-02
47	-0.1744783E-03	0.4048508E-03
48	-0.7579974E-03	-0.9583365E-03
49	-0.7027556E-04	0.3260849E-03
50	0.4199664E-03	0.8679996E-03
51	-0.7979686E-03	-0.9469851E-03
52	0.3107551E-03	0.4645595E-03
53	-0.8603580E-04	0.2324108E-03
54	0.2109174E-03	0.1610583E-03
55	-0.7456832E-03	-0.6130417E-03
56	0.4462914E-03	0.5053631E-03
57	0.1591920E-03	0.2789015E-03
58	-0.4656487E-03	-0.4364236E-03
59	-0.1767847E-04	-0.3461981E-05
60	0.3108399E-03	0.3941085E-03
61	-0.2931331E-03	-0.2285753E-03
62	0.9328238E-04	0.6377204E-04
63	-0.1720886E-04	0.3975330E-04
64	-0.2056900E-05	0.3830773E-04
65	-0.1169271E-03	-0.1068096E-03
66	0.4905240E-04	0.4872639E-04
67	0.1576664E-04	0.5831511E-04
68	0.3167627E-04	0.4053138E-04

n	B_n	C_n
69	-0.6564516E-04	-0.6221421E-04
70	-0.1748351E-04	-0.6976138E-05
71	-0.3665496E-04	-0.1472825E-04
72	0.1004876E-03	0.9884777E-04
73	-0.6544378E-04	-0.5987761E-04
74	-0.9563962E-05	0.5112865E-06
75	0.2498129E-04	0.3470853E-04
76	-0.4729294E-05	-0.9627895E-05
77	-0.5541350E-04	-0.4661179E-04
78	0.3305452E-04	0.3855478E-04
79	0.3570346E-04	0.3692045E-04
80	-0.1589919E-04	-0.1510879E-04
81	-0.6349276E-04	-0.5784341E-04
82	0.5024117E-04	0.5088720E-04
83	0.8936679E-05	0.1105513E-04
84	-0.2985104E-04	-0.2949389E-04
85	0.1793947E-05	0.5432613E-05
86	0.2884307E-04	0.2892528E-04
87	-0.2289115E-04	-0.2226605E-04
88	-0.1679210E-04	-0.1523216E-04
89	0.1770000E-04	0.1914123E-04
90	0.1685304E-04	0.1635740E-04
91	-0.2674495E-04	-0.2516768E-04
92	0.4792071E-05	0.5086707E-05
93	0.7401914E-05	0.8127184E-05
94	-0.5577534E-05	-0.5464997E-05
95	-0.2972263E-05	-0.2235201E-05
96	0.7447946E-05	0.7659644E-05
97	-0.3168895E-05	-0.2746120E-05
98	-0.1356275E-05	-0.1211409E-05
99	-0.2609007E-05	-0.2086289E-05
100	0.3675452E-05	0.3609181E-05
101	-0.1076716E-05	-0.6883366E-06
102	0.5550138E-06	0.6827090E-06
103	-0.4192928E-06	-0.1706489E-06
104	-0.1196023E-05	-0.1206698E-05
105	-0.8345894E-06	-0.5846961E-06
106	0.3115964E-05	0.3220246E-05
107	-0.2167556E-05	-0.2048756E-05
108	-0.1715321E-06	-0.1886759E-06
109	0.9170421E-06	0.1148447E-05
110	0.1282769E-06	0.1347521E-06
111	-0.2130699E-05	-0.2057237E-05
112	0.1366156E-05	0.1406525E-05
113	0.1128959E-05	0.1234005E-05
114	-0.1028800E-05	-0.1018851E-05

n	B_n	C_n
115	-0.1313448E-05	-0.1246324E-05
116	0.1556963E-05	0.1568967E-05
117	-0.8436349E-08	0.6716857E-07
118	-0.7523938E-06	-0.7546471E-06
119	-0.1622793E-06	-0.1113204E-06
120	0.1139069E-05	0.1150875E-05
121	-0.6527602E-06	-0.6168775E-06
122	-0.7496735E-06	-0.7392705E-06
123	0.7258587E-06	0.7580750E-06
124	0.5221784E-06	0.5233002E-06
125	-0.9612895E-06	-0.9294666E-06
126	0.2009010E-06	0.2025572E-06
127	0.3099258E-06	0.3316641E-06
128	-0.1067625E-06	-0.1017822E-06
129	-0.2802620E-06	-0.2645621E-06
130	0.2269661E-06	0.2307490E-06
131	0.9356683E-07	0.1065546E-06
132	-0.1395750E-06	-0.1389416E-06
133	-0.1529258E-06	-0.1394174E-06
134	0.2155629E-06	0.2168193E-06
135	-0.3408843E-07	-0.2498253E-07
136	-0.2487944E-07	-0.2277810E-07
137	-0.7241448E-07	-0.6482588E-07
138	0.6702049E-07	0.6857988E-07
139	0.1388121E-07	0.2008024E-07
140	-0.4186880E-07	-0.4101790E-07
141	-0.3901641E-07	-0.3311435E-07
142	0.1001300E-06	0.1005498E-06
143	-0.4257138E-07	-0.3833354E-07
144	-0.4805924E-07	-0.4716878E-07
145	0.7135057E-08	0.1083863E-07
146	0.7447608E-07	0.7493753E-07
147	-0.5374578E-07	-0.5108661E-07
148	-0.2760153E-07	-0.2660881E-07
149	0.3739260E-07	0.3958593E-07
150	0.1614653E-07	0.1627980E-07
151	-0.5449028E-07	-0.5204399E-07
152	0.2701048E-07	0.2722371E-07
153	0.1567296E-07	0.1715007E-07
154	-0.1215744E-07	-0.1168664E-07
155	-0.2149563E-07	-0.2018866E-07
156	0.1988487E-07	0.2019971E-07
157	0.3930207E-08	0.4938983E-08
158	-0.7725944E-08	-0.7394348E-08
159	-0.9216542E-08	-0.8195819E-08
160	0.1577168E-07	0.1577933E-07

APPENDIX C

CONFORMAL MAPPING COEFFICIENTS

FOR THE

EAST COAST REGION FROM PAMLICO SOUND TO PENOBSCOT BAY

β = 0.2185243E 02

B_o = 0.1045535E 03

λ = 374.0

n	B_n	C_n
1	0.8453177E 01	-0.7390710E 02
2	-0.2573375E 02	0.1146656E 02
3	0.2456377E 01	-0.1316729E 02
4	-0.4028893E 01	0.8089012E 01
5	-0.1294892E 01	-0.5803839E 01
6	0.7517704E 00	0.2271722E 01
7	-0.6833593E 00	-0.6068285E 00
8	0.8799276E 00	0.8849853E 00
9	-0.5689548E 00	-0.1988623E 00
10	0.4709852E 00	0.3153988E 00
11	-0.3505102E 00	-0.1405933E 00
12	-0.5908696E-01	-0.1611297E 00
13	0.1106679E 00	0.2047055E 00
14	-0.3838463E-01	-0.7570612E-01
15	-0.2045463E-01	0.3443124E-02
16	-0.2993307E-01	-0.4593338E-01
17	0.5519173E-01	0.9201282E-01
18	-0.3588944E-01	-0.6882453E-01
19	0.2528971E-01	0.5296847E-01
20	-0.2555390E-01	-0.4396246E-01
21	0.2158327E-01	0.3201135E-01
22	-0.2883616E-01	-0.3150356E-01

Note: All quantities are in x,y units.

n	B_n	C_n
23	0.1704723E-01	0.1959118E-01
24	-0.8218482E-02	-0.7724181E-02
25	0.5179290E-02	0.3032119E-02
26	-0.3015715E-02	0.1962418E-03
27	0.7938925E-02	0.4886530E-02
28	-0.7356405E-02	-0.4150771E-02
29	0.2120303E-02	0.1651054E-03
30	-0.2383103E-02	-0.1145616E-02
31	0.1206459E-02	0.4586522E-03
32	-0.4140623E-03	0.1666064E-03
33	0.3749528E-03	0.1318797E-03
34	0.4151922E-03	0.5995615E-03
35	-0.6242518E-03	-0.6716528E-03
36	0.4518004E-03	0.4600859E-03
37	-0.1179293E-03	-0.8762798E-04
38	-0.1105091E-03	-0.1055562E-03
39	-0.2618267E-03	-0.2268526E-03
40	0.3328708E-03	0.2950658E-03
41	-0.2192205E-03	-0.1689196E-03
42	0.1223145E-03	0.8370787E-04
43	-0.8201750E-04	-0.3827059E-04
44	0.1276652E-03	0.9639813E-04
45	-0.7408037E-04	-0.4502090E-04
46	0.4022771E-04	0.2078711E-04
47	-0.6535150E-04	-0.5105330E-04
48	0.6436008E-05	0.1149840E-05
49	-0.7533055E-05	-0.4203695E-05
50	0.3087624E-04	0.3067982E-04
51	-0.8448817E-05	-0.8395030E-05
52	-0.3737144E-05	-0.2279463E-05
53	0.1095498E-04	0.9629463E-05
54	-0.6501159E-05	-0.4204831E-05
55	-0.5406307E-05	-0.7233290E-05
56	-0.2243007E-05	-0.3883919E-06
57	0.4238569E-05	0.2996593E-05
58	-0.1688697E-05	-0.5217331E-06
59	0.3522237E-05	0.2865336E-05
60	-0.2636244E-05	-0.2091638E-05
61	0.1468087E-05	0.1271618E-05
62	-0.1664401E-05	-0.1547839E-05
63	0.1622032E-05	0.1669010E-05
64	-0.1230003E-05	-0.1246244E-05
65	-0.2369571E-06	-0.1536769E-06
66	0.8677358E-07	0.4681078E-07
67	0.7202404E-06	0.7948224E-06
68	-0.6796483E-06	-0.7270842E-06

n	B_n	C_n
69	0.4362259E-06	0.4967463E-06
70	-0.1076482E-06	-0.1408421E-06
71	0.2459019E-07	0.6843044E-07
72	-0.8354027E-07	-0.1090609E-06
73	-0.6969583E-07	-0.4082953E-07
74	0.8715353E-09	-0.1360970E-07
75	-0.1097112E-07	0.3200026E-08
76	0.7904828E-07	0.7580621E-07
77	0.2604376E-07	0.3055979E-07
78	-0.4817723E-07	-0.4740579E-07
79	-0.1023679E-07	-0.9549385E-08
80	0.3521189E-07	0.3772427E-07
81	-0.5271849E-07	-0.5426599E-07
82	0.2211178E-07	0.2568847E-07
83	-0.7624720E-08	-0.9943246E-08
84	0.1252196E-07	0.1546092E-07
85	-0.4998075E-08	-0.6723383E-08
86	0.6099036E-08	0.8111858E-08
87	-0.6119723E-08	-0.7255402E-08
88	0.6175922E-09	0.1844900E-08
89	-0.3125592E-08	-0.3619169E-08
90	0.5604718E-08	0.6055163E-08
91	-0.6158700E-08	-0.6123951E-08
92	0.1393683E-08	0.1397110E-08
93	0.2143876E-08	0.2388478E-08
94	-0.3371285E-09	-0.4858387E-09
95	-0.3013834E-09	-0.3522048E-10
96	0.1219308E-09	-0.5434760E-10
97	-0.4478535E-09	-0.2261494E-09
98	-0.2622187E-09	-0.3687815E-09
99	0.1349961E-09	0.2747322E-09
100	-0.8012752E-10	-0.1470834E-09
101	0.1434538E-09	0.2115796E-09
102	-0.7944631E-10	-0.9777419E-10
103	0.4699801E-09	0.4927398E-09
104	-0.3936562E-09	-0.3841869E-09
105	-0.6882636E-10	-0.7195172E-10
106	0.2980914E-10	0.4737523E-10
107	0.6826086E-10	0.5899223E-10
108	-0.1151273E-09	-0.9696301E-10
109	0.1011029E-09	0.9092571E-10
110	-0.3327474E-10	-0.1965071E-10
111	0.2431345E-10	0.1711629E-10
112	-0.8947284E-11	-0.8525016E-12
113	-0.9061761E-12	-0.3881352E-11
114	-0.1896980E-10	-0.1490955E-10

n	B_n	C_n
115	-0.7091571E-11	-0.7886334E-11
116	0.1821453E-10	0.1942668E-10
117	-0.3987485E-11	-0.3115765E-11
118	-0.9260623E-11	-0.9532116E-11
119	0.7307409E-11	0.8761047E-11
120	0.9487284E-11	0.8745027E-11
121	-0.1281272E-10	-0.1153168E-10
122	0.5417571E-11	0.4703519E-11
123	-0.4854271E-11	-0.3870245E-11
124	0.1272995E-11	0.8034556E-12
125	-0.8162463E-12	-0.2376758E-12
126	0.2438756E-11	0.2222751E-11
127	-0.1364847E-11	-0.1078558E-11
128	0.7146806E-12	0.6671415E-12
129	-0.4318938E-12	-0.3278873E-12
130	0.1000946E-11	0.1055302E-11
131	-0.2052629E-11	-0.2062567E-11
132	0.6150933E-12	0.7127636E-12
133	0.4740078E-12	0.4288399E-12
134	-0.3935754E-12	-0.3039050E-12
135	0.1734885E-12	0.1294625E-12
136	0.1226613E-12	0.1895801E-12
137	-0.1624964E-12	-0.1929000E-12
138	0.2376018E-13	0.6448195E-13
139	0.1584382E-13	0.3484010E-14
140	-0.7575429E-13	-0.5707148E-13
141	-0.1601686E-13	-0.1698161E-13
142	-0.2932933E-13	-0.2245293E-13
143	0.1456978E-12	0.1498009E-12
144	-0.1147427E-12	-0.1142878E-12
145	0.2950459E-13	0.3582161E-13
146	0.2668761E-13	0.2435500E-13
147	-0.2074897E-13	-0.1477572E-13
148	-0.2806369E-13	-0.3055096E-13
149	0.2675362E-13	0.3108986E-13
150	-0.2478613E-13	-0.2643752E-13
151	0.1650332E-13	0.1933177E-13
152	-0.1226408E-14	-0.2120201E-14
153	0.7071394E-14	0.8649775E-14
154	-0.9688173E-14	-0.9941355E-14
155	-0.3497994E-15	0.3751107E-15
156	0.4112430E-14	0.4258614E-14
157	-0.3376250E-14	-0.3143469E-14
158	-0.3620927E-14	-0.3306923E-14
159	0.5159257E-14	0.5141815E-14
160	-0.6439003E-15	-0.3103656E-15

n	B_n	C_n
161	-0.1550099E-14	-0.1644377E-14
162	0.1889396E-14	0.2176993E-14
163	-0.1462261E-14	-0.1562678E-14
164	0.9551015E-16	0.3085169E-15
165	-0.1863618E-15	-0.2563539E-15
166	0.4924783E-15	0.6232375E-15
167	-0.6975117E-15	-0.7213222E-15
168	0.2073116E-15	0.2703232E-15
169	0.2038455E-15	0.2139917E-15
170	0.2677031E-15	0.2874004E-15
171	-0.6432034E-15	-0.6162772E-15
172	0.4125446E-15	0.4083402E-15
173	-0.1303287E-15	-0.9925271E-16
174	-0.1122934E-15	-0.1216983E-15
175	0.4706550E-16	0.7034376E-16
176	0.5562112E-16	0.4932992E-16
177	-0.7287517E-16	-0.5844015E-16
178	0.6455897E-16	0.6172391E-16
179	-0.1810812E-17	0.7176773E-17
180	-0.2519457E-16	-0.2643164E-16
181	-0.2583353E-16	-0.2060503E-16
182	0.9397427E-17	0.9356655E-17
183	0.2849965E-16	0.3153878E-16
184	-0.4353317E-16	-0.4277073E-16
185	0.2342945E-16	0.2463311E-16
186	0.6163340E-17	0.7743982E-17
187	-0.1038789E-16	-0.1057159E-16
188	-0.2545895E-17	-0.5732719E-18
189	0.8582216E-17	0.8081919E-17
190	-0.1292874E-16	-0.1126496E-16

APPENDIX D

CONFORMAL MAPPING COEFFICIENTS

FOR THE

GULF COAST REGION FROM LAGUNA MADRE TO MARSH ISLAND

$$\beta = 0.2110953E\ 02$$

$$B_o = 0.9507864E\ 02$$

$$\lambda = 360.0$$

n	B_n	C_n
1	-0.4349387E 02	-0.6817682E 02
2	-0.3166200E 02	0.1942726E 02
3	0.1242251E 02	-0.1173821E 01
4	-0.5063650E 01	-0.1447072E-01
5	0.1671185E 01	-0.1921633E 01
6	-0.3597688E 01	-0.6733062E 00
7	0.1419286E 01	0.1366718E 01
8	-0.1179494E 01	-0.3091359E 00
9	0.4119087E 00	0.1335779E 00
10	-0.3775935E 00	0.4832629E-02
11	0.7971597E-01	0.5321220E-01
12	-0.1080030E 00	0.1605034E 00
13	-0.1290084E-01	-0.1559888E 00
14	-0.5963697E-01	0.1403255E 00
15	-0.1379531E-01	-0.6387305E-01
16	-0.3508482E-01	0.9618145E-01
17	0.6604981E-02	-0.4127430E-01
18	-0.1430117E-01	0.2133995E-01
19	0.9392757E-02	-0.2286828E-01
20	-0.1132046E-01	0.2392460E-01
21	-0.1077687E-02	-0.2269067E-02
22	-0.1274931E-01	0.6320797E-02

Note: All quantities are in x,y units.

n	B_n	C_n
23	0.4066765E-02	0.1411975E-02
24	-0.1667407E-02	0.4639465E-03
25	0.3995597E-03	-0.2636588E-03
26	-0.1886219E-02	0.5682681E-03
27	0.9077224E-03	0.7603890E-03
28	-0.1559198E-02	-0.4942792E-03
29	0.9190331E-03	0.3348908E-03
30	-0.1143825E-02	-0.1035753E-03
31	0.3795230E-03	0.1781575E-03
32	-0.6712531E-03	0.9487823E-04
33	0.4371286E-03	-0.5756764E-05
34	-0.5835288E-03	0.1470665E-03
35	0.1835159E-03	-0.3212969E-04
36	-0.2512983E-03	0.3041208E-03
37	-0.1043564E-04	-0.2444959E-03
38	0.1022287E-04	0.2326994E-03
39	-0.8843900E-05	-0.1970086E-03
40	-0.1278813E-04	0.1541862E-03
41	-0.2613426E-04	-0.9325938E-04
42	-0.1440295E-04	0.1033448E-03
43	-0.5079823E-05	-0.5277937E-04
44	-0.2383447E-04	0.3246609E-04
45	0.2685109E-04	-0.2672389E-05
46	-0.4311551E-04	-0.2036345E-05
47	0.2635192E-04	0.1142295E-04
48	-0.2369922E-04	0.2308075E-05
49	0.1060475E-04	-0.2816660E-05
50	-0.1190996E-04	0.5396716E-05
51	0.7969119E-05	-0.7342735E-06
52	-0.9435032E-05	0.3056901E-05
53	0.3592144E-05	-0.2802860E-05
54	-0.3163786E-05	0.5202766E-05
55	0.8069733E-06	-0.3204935E-05
56	-0.3156197E-05	0.2976863E-05
57	0.2082134E-05	-0.3100245E-06
58	-0.2780215E-05	0.7375353E-06
59	0.1130891E-05	-0.7168670E-06
60	-0.6122396E-06	0.1450043E-05
61	-0.1845171E-06	-0.1119710E-05
62	-0.3365420E-06	0.1101896E-05
63	0.8938491E-07	-0.4542400E-06
64	-0.3012036E-06	0.5235447E-06
65	-0.3673406E-08	-0.3582571E-06
66	-0.1414085E-06	0.4244058E-06
67	0.7388365E-07	-0.1289455E-06
68	-0.3226247E-06	0.5886075E-07

n	B_n	C_n
69	0.2731474E-06	0.1002326E-06
70	-0.2802570E-06	-0.3232754E-07
71	0.1234109E-06	0.1089280E-07
72	-0.9498712E-07	0.8281825E-07
73	0.1907564E-07	-0.6229692E-07
74	-0.3855900E-07	0.7623788E-07
75	0.1227572E-07	-0.4725345E-07
76	-0.2280785E-07	0.5952231E-07
77	-0.4772584E-08	-0.3917647E-07
78	-0.1305931E-07	0.4041384E-07
79	0.1346654E-07	-0.1214022E-07
80	-0.3178457E-07	-0.4018400E-10
81	0.2829028E-07	0.1231370E-07
82	-0.2833683E-07	-0.5542695E-08
83	0.1390158E-07	0.4292090E-08
84	-0.1041305E-07	0.3628934E-08
85	0.2942560E-08	-0.3900482E-08
86	-0.2494349E-08	0.7090147E-08
87	-0.2140656E-08	-0.6023740E-08
88	0.1858878E-08	0.8399496E-08
89	-0.3792454E-08	-0.6924818E-08
90	0.1902798E-08	0.6096819E-08
91	-0.9630992E-09	-0.2973249E-08
92	-0.1545032E-08	0.1536916E-08
93	0.1794988E-08	0.3730956E-09
94	-0.2454563E-08	-0.5550416E-09
95	0.1989445E-08	0.9392092E-09
96	-0.2018450E-08	-0.6327296E-09
97	0.1354043E-08	0.7495602E-09
98	-0.1189770E-08	-0.2610046E-09
99	0.5607077E-09	0.9228998E-10
100	-0.2872680E-09	0.3045806E-09
101	-0.9899369E-10	-0.3766485E-09
102	0.9587729E-10	0.5183951E-09
103	-0.1920187E-09	-0.3851055E-09
104	0.8736652E-10	0.3454421E-09
105	-0.8521299E-10	-0.2178382E-09
106	-0.3684938E-11	0.1826045E-09
107	-0.3185317E-11	-0.8295703E-10
108	-0.5854169E-10	0.6188589E-10
109	0.5440021E-10	-0.7061680E-11
110	-0.7843175E-10	0.3384400E-11
111	0.5485389E-10	0.1760203E-10
112	-0.5931984E-10	-0.1176308E-11
113	0.3508252E-10	0.7755597E-11
114	-0.3359514E-10	0.3438477E-11

n	B_n	C_n
115	0.1969359E-10	0.3890720E-12
116	-0.2062679E-10	0.5851155E-11
117	0.1077043E-10	-0.1611202E-11
118	-0.1097489E-10	0.6770954E-11
119	0.3749065E-11	-0.5035324E-11
120	-0.3668546E-11	0.8181160E-11
121	-0.4585235E-12	-0.5946987E-11
122	-0.7479945E-12	0.7430294E-11
123	-0.1297924E-11	-0.5151255E-11
124	0.9331983E-13	0.5351474E-11
125	-0.8512745E-12	-0.3465696E-11
126	-0.4626511E-12	0.3223064E-11
127	0.2742915E-12	-0.1365864E-11
128	-0.1541422E-11	0.8782235E-12
129	0.1520291E-11	0.2639725E-12
130	-0.1946227E-11	-0.2869286E-12
131	0.1428788E-11	0.6296024E-12
132	-0.1423591E-11	-0.1924273E-12
133	0.8095198E-12	0.2416221E-12
134	-0.6745650E-12	0.1149748E-12
135	0.2695209E-12	-0.1547703E-12
136	-0.1687758E-12	0.4097250E-12
137	-0.9926446E-13	-0.3738514E-12
138	0.6907761E-13	0.4700165E-12
139	-0.1294383E-12	-0.3406081E-12
140	0.1702639E-13	0.2911647E-12
141	0.1289878E-14	-0.1232917E-12
142	-0.1019788E-12	0.9033253E-13
143	0.9003627E-13	-0.6354048E-14
144	-0.1253069E-12	-0.1082376E-14
145	0.1061812E-12	0.4432039E-13
146	-0.1132419E-12	-0.1362410E-13
147	0.7077363E-13	0.2450861E-13
148	-0.6203187E-13	0.3025605E-14
149	0.3443273E-13	-0.1103780E-13
150	-0.1978280E-13	0.3760087E-13

APPENDIX E

CONFORMAL MAPPING COEFFICIENTS

FOR THE

GULF COAST REGION FROM MATAGORDA BAY TO TIMBALIER BAY

$$\beta = 0.3266563E\ 02$$

$$B_o = C.6402541E\ 02$$

$$\lambda = 273.5$$

n	B_n	C_n
1	-0.1345455E 02	-0.1288847E 02
2	-0.9308576E 01	-0.1253234E 02
3	0.3063064E-01	0.3363035E 01
4	0.1601213E 00	0.1091622E 01
5	-0.5839307E 00	0.3596888E-01
6	-0.1973795E 00	-0.2109445E 00
7	-0.8462828E-01	0.7170513E-02
8	0.5467411E-02	0.1255086E 00
9	-0.5171223E-01	-0.7066019E-02
10	-0.1875502E-01	-0.1100479E-01
11	-0.9801641E-02	0.2472862E-01
12	-0.6387778E-02	0.8628163E-02
13	-0.7022325E-02	-0.2627833E-02
14	0.1439277E-02	0.4072074E-02
15	-0.1912029E-02	0.1500307E-02
16	-0.1524055E-02	-0.1732375E-03
17	0.1180221E-03	0.1046393E-02
18	-0.1692594E-03	0.3270761E-03
19	-0.2428762E-03	0.1903720E-03
20	-0.3506050E-03	-0.1241541E-04
21	0.1094825E-03	0.2524455E-03
22	-0.5571678E-04	0.2129799E-04

Note: All quantities are in x,y units.

n	B_n	C_n
23	-0.3508286E-04	0.4048488E-04
24	-0.3781496E-04	0.1144816E-04
25	-0.1100774E-04	0.7667904E-05
26	0.1147495E-05	0.1734318E-04
27	-0.1094296E-04	0.1076357E-05
28	-0.4207996E-05	0.3205748E-05
29	0.5165113E-06	0.4804680E-05
30	-0.4495374E-05	-0.1510631E-05
31	0.1638793E-06	0.2080999E-05
32	-0.3129110E-06	0.1036824E-05
33	-0.6398391E-06	0.1503427E-06
34	-0.4498215E-06	0.2416694E-07
35	-0.1756886E-07	0.3424218E-06
36	-0.1769853E-06	0.5768333E-07
37	0.7405710E-08	0.1475192E-06
38	-0.7561528E-07	0.1673027E-07
39	-0.7744518E-07	-0.1173998E-07
40	0.6988301E-08	0.4872761E-07
41	-0.4358078E-08	0.2379178E-07
42	-0.1503878E-07	0.2633515E-08
43	-0.1138452E-07	0.4058880E-09
44	-0.2927226E-08	0.5011941E-08
45	-0.1103974E-08	0.4151303E-08
46	0.2882630E-09	0.3492370E-08
47	-0.2926841E-08	-0.6412142E-09
48	-0.1887702E-08	-0.3581659E-09
49	0.9733139E-09	0.1969457E-08
50	-0.3007952E-09	0.3454068E-09
51	-0.7999266E-09	-0.3613920E-09
52	0.1161606E-09	0.4086191E-09
53	-0.7690208E-10	0.1136903E-09
54	-0.1189104E-09	0.4280468E-11
55	-0.2874996E-10	0.5436114E-10
56	-0.2802484E-11	0.5472514E-10
57	-0.3628853E-10	0.1553833E-12
58	-0.1222868E-10	0.1212419E-10
59	-0.1351430E-10	0.3202698E-11
60	0.3004845E-11	0.1421820E-10
61	-0.8372742E-12	0.6312961E-11
62	-0.1001310E-10	-0.5179364E-11
63	-0.1548850E-11	0.1694957E-11
64	0.2762174E-11	0.4953277E-11
65	-0.1505011E-11	-0.6499526E-13
66	-0.1677040E-11	-0.7356988E-12
67	-0.5156210E-13	0.6046279E-12
68	0.5781286E-13	0.4984966E-12

n	B_n	C_n
69	-0.1041335E-12	0.1796432E-12
70	-0.1568783E-12	0.3310604E-13
71	-0.1837509E-12	-0.5014898E-13
72	0.1567779E-13	0.1026365E-12
73	0.2315409E-13	0.8053887E-13
74	-0.5380629E-13	-0.1513999E-13
75	-0.2038725E-13	0.5883847E-14
76	-0.3208841E-14	0.1435158E-13
77	-0.3887471E-14	0.7881177E-14
78	-0.3711868E-14	0.4015387E-14
79	-0.2710063E-14	0.2644683E-14
80	-0.3346254E-14	0.2852854E-15
81	-0.2722021E-15	0.2089868E-14
82	-0.9054219E-15	0.6752858E-15
83	-0.6686436E-15	0.4262505E-15
84	0.4528349E-16	0.7726821E-15
85	-0.4635597E-15	0.1653144E-16
86	-0.4206397E-15	-0.9398101E-16
87	0.1195950E-15	0.3406087E-15
88	0.3487004E-17	0.1529711E-15
89	-0.1428360E-15	-0.4310367E-16
90	-0.7437915E-16	-0.7557572E-17
91	0.9476944E-17	0.5468383E-16
92	0.9402026E-17	0.4018428E-16
93	-0.1877212E-16	0.1510602E-17
94	-0.2430040E-16	-0.1058724E-16
95	0.9067852E-18	0.1027978E-16
96	0.4315170E-17	0.1060953E-16
97	-0.5278773E-17	-0.1059649E-17
98	-0.3236399E-17	-0.3837736E-18
99	-0.1450895E-18	0.1789194E-17
100	-0.4036873E-18	0.8961303E-18
101	-0.4485805E-18	0.4323934E-18
102	-0.2379904E-18	0.3522038E-18
103	-0.3704013E-18	0.3119870E-19
104	-0.1238881E-18	0.1467032E-18
105	-0.4614470E-19	0.1364687E-18
106	-0.5354953E-19	0.6953575E-19
107	-0.3109555E-19	0.5270040E-19
108	-0.5224460E-19	0.4158915E-20
109	-0.3378779E-19	0.4444477E-20
110	0.1095373E-19	0.3675055E-19
111	-0.6428718E-20	0.1105266E-19
112	-0.1517489E-19	-0.3314663E-20
113	-0.4393596E-20	0.3585689E-20
114	-0.7806073E-21	0.4601044E-20

n	B_n	C_n
115	-0.1171447E-20	0.2500088E-20
116	-0.7940360E-21	0.1693249E-20
117	-0.1933520E-20	-0.2610540E-21
118	-0.8870977E-21	0.2520655E-21
119	0.2674643E-21	0.1042381E-20
120	-0.1754523E-21	0.3496690E-21
121	-0.3950036E-21	-0.4001404E-22
122	-0.1662322E-21	0.7399500E-22
123	-0.5284034E-22	0.1107630E-21
124	-0.9163815E-23	0.1029530E-21
125	-0.2624163E-22	0.4904399E-22
126	-0.6267675E-22	-0.1173602E-22
127	-0.2173399E-22	0.1347398E-22
128	0.3621932E-23	0.2753237E-22
129	-0.7417667E-23	0.8646540E-23
130	-0.8227958E-23	0.2775776E-23
131	-0.4502831E-23	0.3098042E-23
132	-0.4149869E-23	0.1014040E-23
133	0.5361735E-25	0.3567867E-23
134	-0.2502105E-24	0.2145265E-23
135	-0.1881883E-23	-0.2450173E-24
136	-0.9528138E-24	0.1759776E-24
137	0.2784993E-25	0.7901839E-24
138	-0.1268508E-24	0.3927325E-24
139	-0.2404606E-24	0.1230278E-24
140	-0.2257453E-24	0.3025528E-25
141	-0.9371613E-25	0.7837279E-25
142	-0.6119151E-26	0.1128174E-24
143	-0.3691736E-25	0.4537704E-25
144	-0.4870207E-25	0.7270641E-26
145	-0.1853093E-25	0.1869381E-25
146	-0.1358211E-25	0.1267911E-25
147	-0.9092645E-26	0.9077216E-26
148	-0.1953950E-26	0.1107780E-25
149	-0.5698583E-26	0.3105713E-26
150	-0.7086726E-26	-0.1015449E-26

APPENDIX F

NUMERICAL ANALOGS OF SURGE EQUATIONS

Admissible finite difference analogs of equations (40) and (41) which are nominally centered at i , j , n (bearing in mind the storage of variables in Figure 36), are as follows:

$$
\begin{aligned}
&\left[Q_{S*}(i,j,n+1) - Q_{S*}(i,j,n-1)\right]/2\Delta t \\
&- f\left[Q_{T*}(i,j,n+1) + Q_{T*}(i,j,n-1)\right]/2 \\
&+ (g\overline{D}/F(i,j)\mu(i))\left[H(i+1,j,n) - H_B(i+1,j,n)\right. \\
&\left. - H(i-1,j,n) + H_B(i-1,j,n)\right]/2\Delta S* \\
&= \tau_{S*}(i,j,n) - (K_o Q(i,j,n-1)/\overline{D}^2)Q_{S*}(i,j,n+1) \qquad \text{(F-1)}
\end{aligned}
$$

and

$$
\begin{aligned}
&\left[Q_{T*}(i,j,n+1) - Q_{T*}(i,j,n-1)\right]/2\Delta t \\
&+ f\left[Q_{S*}(i,j,n+1) + Q_{S*}(i,j,n-1)\right]/2 \\
&+ (g\overline{D}/F(i,j)\nu(j))\left[H(i,j+1,n) - H_B(i,j+1,n)\right. \\
&\left. - H(i,j-1,n) + H_B(i,j-1,n)\right]/2\Delta T* \\
&= \tau_{T*}(i,j,n) - (K_o Q(i,j,n-1)/\overline{D}^2)Q_{T*}(i,j,n+1) \ , \qquad \text{(F-2)}
\end{aligned}
$$

where Q is as defined by equation (54) and $\overline{D}$ as defined by equation (61) is the arithmetic average of the four values of D about the point i,j at which the flow is evaluated. All terms are spatially centered at i,j and all but the bottom friction terms are exactly centered at time level n . The latter involve flow components at the new level n+1 and at the old level n-1 within the flow magnitude term Q . This form is known to lead to a stable algorithm (Reid and Bodine, 1968). The Coriolis terms are exactly centered at n as well as i,j . Equations (F-1) and (F-2) represent two equations in the two new Q components $Q_{S*}(i,j,n+1)$ and $Q_{T*}(i,j,n+1)$ in terms of quantities at previous times and are readily solved for each component individually. The resulting explicit relations for these components are given by equation (55) where G_1 , G_2 , G_3 are defined in equations (58) to (60).

The centered finite difference analog of the continuity equation (42) leads directly to the explicit relation for H at the new time level given by equation (57).

APPENDIX G

MODEL VERIFICATION

Prior to the surge computations the conservative properties of the numerical model were examined. The model was applied first to seiches in an enclosed square basin 12 kilometers on a side and 5 meters deep. The number of grid increments along each side was 20. To invoke the most severe seiching mode, the water surface was initially assigned a linear slope downward from one end of the basin (j=JM) to the opposite end (j=1). The initial setup for the nonrotating basin computations was 50 centimeters, but this was reduced to 10 centimeters when rotation was allowed to suppress unnecessary fluctuations. The time step taken for all test runs was 50 seconds.

The simulation of a uninodal seiche in a nonrotating basin was considered first. With the specified time step, the period of the severest mode is theoretically 68.57 Δt.

Figure G-1 shows that the computed fundamental period is within one-time increment of the theoretical period.

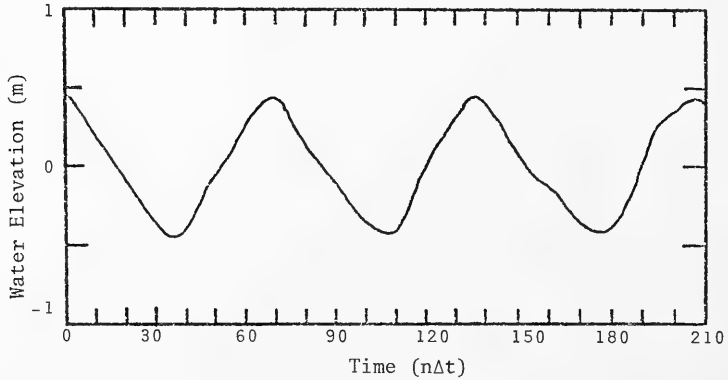

Figure G-1. Computed water level at grid point (21,20) for uninodal seiche test case.

The time variation of the volume, potential, kinetic, and total energies are given in Figure G-2. Each of these quantities are area-weighted sums. This evaluation scheme should exhibit small perturbations more readily than unweighted sums of the variables over the grid. The variation of the volume, potential, kinetic, and total energies is small, with the potential energy showing the largest deviation.

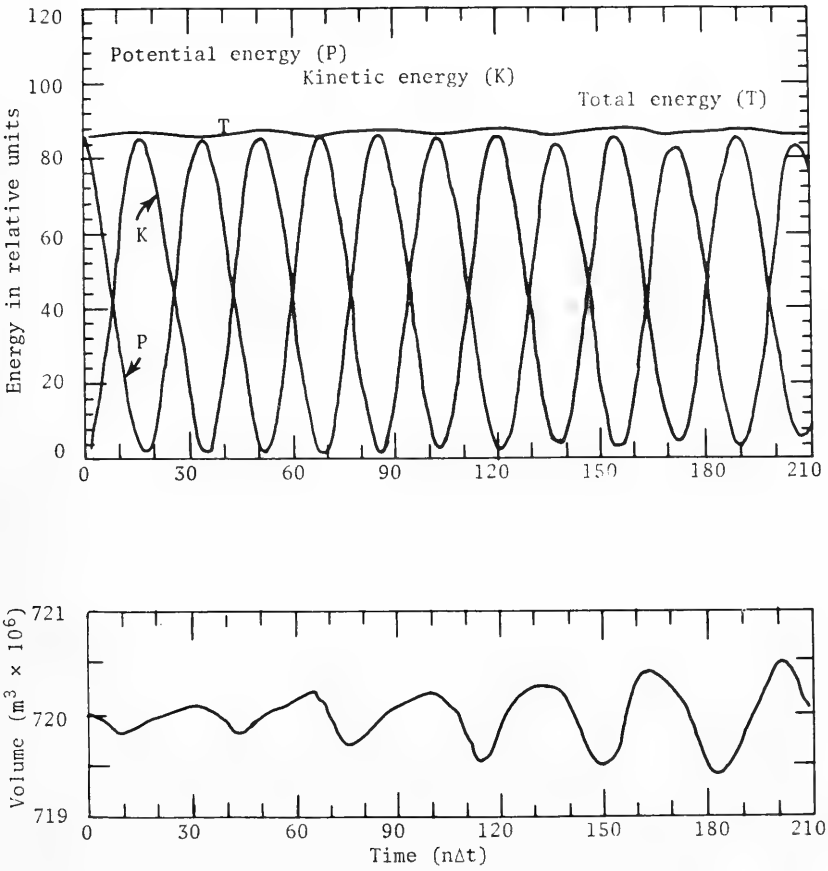

Figure G-2. Volume, potential, kinetic, and total energies for uninodal seich test case.

Rotational effects on the seiching mode were checked by specifying the Coriolis parameter as 0.75 σ_o, 1.00 σ_o, and 1.25 σ_o where σ_o is the angular frequency of the fundamental mode. The computed frequencies, σ , were compared with those obtained by Rao (1966) and Platzman (1972).

Table G-1 gives the comparison with Rao's and Platzman's results.

Table G-1. Comparison of computed values of σ/σ_o with those obtained by Rao (1966) and Platzman (1972).

f/σ_o	σ/σ_o		Average computed σ/σ_o	% error
	From Rao (1966)	From Platzman (1972)		
0.75		0.769	0.76	1.1
1.00	0.723	0.721	0.75	4.0
1.25	0.686	0.683	0.71	3.9

Although the errors occurring with $f/\sigma_o \geq 1.00$ are large, these values of f/σ_o represent stern tests of the algorithm. It is definitely encouraging that no evidence of instability is indicated in the simulated hydrographs.

APPENDIX H

WIND DEFORMATION PROCEDURE

Assuming that the wind-stress components $(\tau_{S*}^{(SYM)}, \tau_{T*}^{(SYM)})$ are known in the stretched shelf coordinate system from the application of a symmetric wind field model, the problem in part is to identify a region for a given hurricane and coastline where it is appropriate to alter these stresses to reflect the influence of land. The proposed deformation equations are applied only at points which are located within this region. Existing charts of hurricane winds and the investigation by Graham and Nunn (1959) provide the basis for the empirical deformation formulas. In this manner, the analytical representation obviates the detailed input of a massive sequence of digitized wind field data that conforms with the observations near the coast as well as offshore.

The wind-stress components, $\tau_{S*}^{(SYM)}$ and $\tau_{T*}^{(SYM)}$, are altered at a point for which $Y_I > Y_D$ according to the relationship:

$$\tau_{S*} = \tau_{S*}^{(SYM)} \cdot I_f \ , \tag{H-1}$$

and

$$\tau_{T*} = \tau_{T*}^{(SYM)} \cdot (I_f)^m \ , \tag{H-2}$$

where m is a constant chosen to be 2 and I_f is an influence factor given by:

$$I_f = 1 - D_f [\ (Y_I - Y_D)/\bar{R}_h]^2 \ , \tag{H-3}$$

where $\bar{R}_h$ is a constant taken as the average radius to maximum winds of the hurricane, D_f is a distortion factor, Y_D is the shortest distance the point is from land, and Y_I is the distance the influence region extends from the coast relative to the point in question (Figure H-1). In general, Y_I should depend on X_D, the distance the point in question is from a centrally located point along the coast (x_c, y_c). This latter point is generally assigned the coordinates of intersection of the hurricane track with the coastline. From Figure H-1, the distances X_D and Y_D are given by:

$$X_D = \pm [\ (x_s - x_c)^2 + (y_s - y_c)^2]^{\frac{1}{2}} \ , \tag{H-4}$$

and

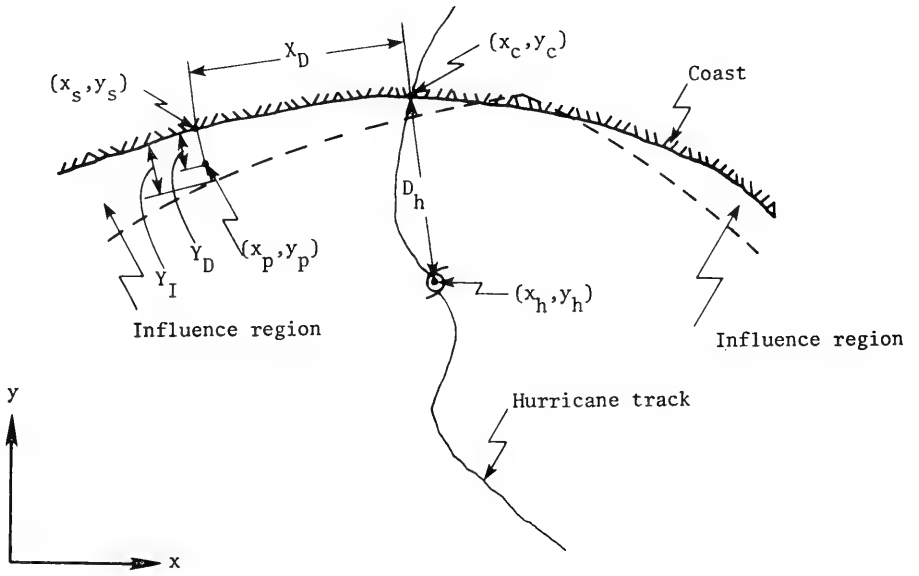

Figure H-1. Conceptual design of influence region showing the relationship between D_h , X_D , Y_D , and Y_I .

$$Y_D = [(x_p - x_s)^2 + (y_p - y_s)^2]^{\frac{1}{2}} , \qquad \text{(H-5)}$$

where (x_s,y_s) is a point along the coast determined by the intersection of a line normal to the coast and passing through the point in question (x_p,y_p). The sign convention is that X_D is positive if the point in question is to the right of the hurricane track and negative if it lies on the left. In general, the influence region is defined by:

$$Y_I = [\, F_I(X_D) + S_f \,] \cdot R_f , \qquad \text{(H-6)}$$

where F_I is the influence function of X_D, S_f is a shift factor which permits the influence line to be moved normal to the coast, and R_f is a range factor. The influence function attempts to relate the degree of distortion in the wind isovels relative to the tract of the hurricane and the shape of the coastline. The extent of the land influence is given by Y_I, which depends on S_f and R_f. These coefficients as well as D_f are considered to be related to the distance of the hurricane from the point where it crosses the coast.

Additional investigation is required to establish a generalized procedure based on physical principles for deforming the winds in a manner which faithfully reproduces the observations. Consequently, each storm is parameterized individually to accomplish the task. The relationships used for deforming the winds of Hurricane Carla are:

$$F_I = | X_D - \bar{R}_h | /7 , \qquad \text{(H-7)}$$

$$D_f = .1 [\, 1 + e^{-.05(D_h/\bar{R}_h - 2)^2}] , \qquad \text{(H-8)}$$

$$S_f = \tfrac{1}{2} [\, .5 - \frac{1}{\pi} \tan^{-1} (D_h/2\bar{R}_h)]\, \bar{R}_h , \qquad \text{(H-9)}$$

$$R_f = \begin{cases} 1.5 & , \text{if } D_h < -5\bar{R}_h \\ .5 + e^{-.025(D_h/\bar{R}_h + 5)^2} & , \text{if } D_h \geq 5\bar{R}_h \end{cases} \qquad \text{(H-10)}$$

where $\bar{R}_h$ is taken as approximately 37 kilometers and

$$D_h = \pm [\, (x_c - x_h)^2 + (y_c - y_h)^2]^{\frac{1}{2}} . \qquad \text{(H-11)}$$

The sign convention is that D_h is positive if the hurricane is over water and negative if the storm is over land. For Hurricane Camille,

these relations are:

$$F_I = \begin{cases} (X_D + 6\bar{R}_h)/1.5 \text{ , if } X_D \leq -3\bar{R}_h \\ |X_D|/1.5 \text{ , if } -3\bar{R}_h < X_D < 0 \\ |X_D|/7 \text{ , if } X_D \geq 0 \end{cases} \quad \text{(H-12)}$$

$$D_f = 0.2 \text{ ,} \quad \text{(H-13)}$$

$$S_f = 0.5 \text{ ,} \quad \text{(H-14)}$$

and

$$R_f = 1.0 \text{ .} \quad \text{(H-15)}$$

The Hurricane Gracie wind fields were not deformed because the winds are presented in digital form. Any deformation obtained would be dependent upon a subjective analysis which requires additional developmental work. Moreover, the selection of Gracie was made on the knowledge that the results would possibly be compared with those obtained by other investigators using symmetric wind fields.

APPENDIX I

SYMBOLS AND DEFINITIONS

B_n, C_n	Transformation coefficients
C_D	Nondimensional wind-drag coefficient
D	Depth of water
D_f	Distortion factor for deforming the wind
D_h	Distance of hurricane from the coast
D_m	Maximum expected depth of water at any point within computing grid
D_o	Depth of water relative to mean sea level
E	Error function
f	Coriolis parameter
F	Scale factor associated with the orthogonal curvilinear coordinate system
F_I	Influence function for deforming the wind
g	Acceleration due to gravity
H	Water level relative to mean sea level
H_B	Hydrostatic elevation of the sea surface corresponding to the departure of the atmospheric pressure from a constant
I_f	Influence factor for deforming the wind
IM,JM	Number of computational grid points along the S* and T* axes
k	Wave number = π/λ
$k_{m,n}$	Wave number of free wave in the annulus

K_o	Nondimensional bottom-drag coefficient
N	Number of Fourier-type transformation coefficients in the series
P	Atmospheric pressure
P_∞	Far field pressure
P_o	Central pressure of the hurricane
Q_{S*}, Q_{T*}	Volume transport per unit width in the S* and T* directions
r, θ	Polar coordinates
r_h	Distance from the hurricane center to any point
R_f	Range factor for deforming the wind
R_h	Distance from the hurricane center to the region of maximum winds
S_f	Shift factor for deforming the wind
S_n, S_p	Distance normal to the seaward boundary and along the coast
S*,T*	Coordinates of the stretched shelf coordinate system
T	Long wave travel time
V_R	Maximum winds of the hurricane
W^c, W^S	Weighting factors for the coast and seaward boundary curves
W_{10}	Windspeed at an elevation of 10 meters above the water surface
x,y	Rectilinear coordinates

x_c, y_c	Coordinates of landfall of the hurricane
x_h, y_h	Position of hurricane center
x_p, y_p	A point in the influence region
x_s, y_s	A point along the coast determined by the intersection of a line normal to the coast and passing through (x_p, y_p)
X^c, Y^c, X^s, Y^s	Coordinates of the coast and seaward boundary curves to be mapped
Y_I	Extent of the land influence for deforming the wind
Z	Plane of (x,y)
β	Extent of η $(\pm)$ in the ζ-plane
Δ	Arc length
Δt	Surge algorithm time increment
ξ	The alongshore curvilinear coordinate of the shelf coordinate system
γ^c, γ^s	Prorating factors for the length of the transform-generated curves
λ	Half the horizontal extent of the region to be mapped in the Z or ζ-plane
μ, ν	Functions transforming ξ and η to the stretched shelf coordinate system (S*,T*)
ϕ	Ingress angle
ρ_A, ρ_W	Density of air and water
σ^2, σ^2_n	Total and n^{th} contribution to the "curvilinearity" variance
σ_{S*}, σ_{T*}	Bottom resistance stress divided by ρ_W in the S* and T* directions

τ_{S^*}, τ_{T^*}	Wind stress divided by ρ_W in the S* and T* directions
θ	Angle between the ξ and x axes
η	The offshore curvilinear coordinate of the shelf coordinate system (ξ,η)
ζ	Plane of (ξ,η)

Wanstrath, John J.

Storm surge simulation in transformed coordinates / by John J. Wanstrath, Robert E. Whitaker...[et al.]. – Fort Belvoir, Va. : U.S. Coastal Engineering Research Center, 1976.

2 v. : ill. (Technical report – U.S. Coastal Engineering Research Center ; no. 76-3) (Contract – U.S. Coastal Engineering Research Center ; DACW72-73-C-0014)

CONTENTS : v.1. Theory and application. - v.2. Program documentation.

Includes bibliographies.

Report discusses a two-dimensional time-dependent numerical storm surge model using orthogonal curvilinear coordinates. Model is used in simulating storm surge induced by selected hurricanes.

1. Storm surges. 2. Computer programs. 3. Hurricane Camille, 1969. 4. Hurricane Carla, 1961. 5. Hurricane Gracie, 1959. I. Title. II. Whitaker, Robert E., joint author. III. Series : U.S. Coastal Engineering Research Center. Contract DACW72-73-C-0014).

TC203 .U581tr no. 76-3 627 .U581tr

Wanstrath, John J.

Storm surge simulation in transformed coordinates / by John J. Wanstrath, Robert E. Whitaker...[et al.]. – Fort Belvoir, Va. : U.S Coastal Engineering Research Center, 1976.

2 v. : ill. (Technical report – U.S. Coastal Engineering Research Center ; no. 76-3) (Contract – U.S. Coastal Engineering Research Center ; DACW72-73-C-0014)

CONTENTS : v.1. Theory and application. - v.2. Program documentation.

Includes bibliographies.

Report discusses a two-dimensional time-dependent numerical storm surge model using orthogonal curvilinear coordinates. Model is used in simulating storm surge induced by selected hurricanes.

1. Storm surges. 2. Computer programs. 3. Hurricane Camille, 1969. 4. Hurricane Carla, 1961. 5. Hurricane Gracie, 1959. I. Title. II. Whitaker, Robert E., joint author. III. Series : U.S. Coastal Engineering Research Center. Contract DACW72-73-C-0014).

TC203 .U581tr no. 76-3 627 .U581tr

Wanstrath, John J.

Storm surge simulation in transformed coordinates / by John J. Wanstrath, Robert E. Whitaker...[et al.]. – Fort Belvoir, Va. : U.S. Coastal Engineering Research Center, 1976.

2 v. : ill. (Technical report – U.S. Coastal Engineering Research Center ; no. 76-3) (Contract – U.S. Coastal Engineering Research Center ; DACW72-73-C-0014)

CONTENTS : v.1. Theory and application. - v.2. Program documentation.

Includes bibliographies.

Report discusses a two-dimensional time-dependent numerical storm surge model using orthogonal curvilinear coordinates. Model is used in simulating storm surge induced by selected hurricanes.

1. Storm surges. 2. Computer programs. 3. Hurricane Camille, 1969. 4. Hurricane Carla, 1961. 5. Hurricane Gracie, 1959. I. Title. II. Whitaker, Robert E., joint author. III. Series : U.S. Coastal Engineering Research Center. Contract DACW72-73-C-0014).

TC203 .U581tr no. 76-3 627 .U581tr

Wanstrath, John J.

Storm surge simulation in transformed coordinates / by John J. Wanstrath, Robert E. Whitaker...[et al.]. – Fort Belvoir, Va. : U.S. Coastal Engineering Research Center, 1976.

2 v. : ill. (Technical report – U.S. Coastal Engineering Research Center ; no. 76-3) (Contract – U.S. Coastal Engineering Research Center ; DACW72-73-C-0014)

CONTENTS : v.1. Theory and application. - v.2. Program documentation.

Includes bibliographies.

Report discusses a two-dimensional time-dependent numerical storm surge model using orthogonal curvilinear coordinates. Model is used in simulating storm surge induced by selected hurricanes.

1. Storm surges. 2. Computer programs. 3. Hurricane Camille, 1969. 4. Hurricane Carla, 1961. 5. Hurricane Gracie, 1959. I. Title. II. Whitaker, Robert E., joint author. III. Series : U.S. Coastal Engineering Research Center. Contract DACW72-73-C-0014).

TC203 .U581tr no. 76-3 627 .U581tr

Wanstrath, John J.

Storm surge simulation in transformed coordinates / by John J. Wanstrath, Robert E. Whitaker...[et al.]. – Fort Belvoir, Va. : U.S. Coastal Engineering Research Center, 1976.

2 v. : ill. (Technical report – U.S. Coastal Engineering Research Center ; no. 76-3) (Contract – U.S. Coastal Engineering Research Center ; DACW72-73-C-0014)

CONTENTS : v.1. Theory and application. - v.2. Program documentation.

Includes bibliographies.

Report discusses a two-dimensional time-dependent numerical storm surge model using orthogonal curvilinear coordinates. Model is used in simulating storm surge induced by selected hurricanes.

1. Storm surges. 2. Computer programs. 3. Hurricane Camille, 1969. 4. Hurricane Carla, 1961. 5. Hurricane Gracie, 1959. I. Title. II. Whitaker, Robert E., joint author. III. Series : U.S. Coastal Engineering Research Center. Contract DACW72-73-C-0014).

TC203 .U581tr no. 76-3 627 .U581tr

Wanstrath, John J.

Storm surge simulation in transformed coordinates / by John J. Wanstrath, Robert E. Whitaker...[et al.]. – Fort Belvoir, Va. : U.S. Coastal Engineering Research Center, 1976.

2 v. : ill. (Technical report – U.S. Coastal Engineering Research Center ; no. 76-3) (Contract – U.S. Coastal Engineering Research Center ; DACW72-73-C-0014)

CONTENTS : v.1. Theory and application. - v.2. Program documentation.

Includes bibliographies.

Report discusses a two-dimensional time-dependent numerical storm surge model using orthogonal curvilinear coordinates. Model is used in simulating storm surge induced by selected hurricanes.

1. Storm surges. 2. Computer programs. 3. Hurricane Camille, 1969. 4. Hurricane Carla, 1961. 5. Hurricane Gracie, 1959. I. Title. II. Whitaker, Robert E., joint author. III. Series : U.S. Coastal Engineering Research Center. Contract DACW72-73-C-0014).

TC203 .U581tr no. 76-3 627 .U581tr

Wanstrath, John J.

Storm surge simulation in transformed coordinates / by John J. Wanstrath, Robert E. Whitaker...[et al.]. – Fort Belvoir, Va. : U.S. Coastal Engineering Research Center, 1976.

2 v. : ill. (Technical report – U.S. Coastal Engineering Research Center ; no. 76-3) (Contract – U.S. Coastal Engineering Research Center ; DACW72-73-C-0014)

CONTENTS : v.1. Theory and application. - v.2. Program documentation.

Includes bibliographies.

Report discusses a two-dimensional time-dependent numerical storm surge model using orthogonal curvilinear coordinates. Model is used in simulating storm surge induced by selected hurricanes.

1. Storm surges. 2. Computer programs. 3. Hurricane Camille, 1969. 4. Hurricane Carla, 1961. 5. Hurricane Gracie, 1959. I. Title. II. Whitaker, Robert E., joint author. III. Series : U.S. Coastal Engineering Research Center. Contract DACW72-73-C-0014).

TC203 .U581tr no. 76-3 627 .U581tr

Wanstrath, John J.

Storm surge simulation in transformed coordinates / by John J. Wanstrath, Robert E. Whitaker...[et al.]. – Fort Belvoir, Va. : U.S. Coastal Engineering Research Center, 1976.

2 v. : ill. (Technical report – U.S. Coastal Engineering Research Center ; no. 76-3) (Contract – U.S. Coastal Engineering Research Center ; DACW72-73-C-0014)

CONTENTS : v.1. Theory and application. - v.2. Program documentation.

Includes bibliographies.

Report discusses a two-dimensional time-dependent numerical storm surge model using orthogonal curvilinear coordinates. Model is used in simulating storm surge induced by selected hurricanes.

1. Storm surges. 2. Computer programs. 3. Hurricane Camille, 1969. 4. Hurricane Carla, 1961. 5. Hurricane Gracie, 1959. I. Title. II. Whitaker, Robert E., joint author. III. Series : U.S. Coastal Engineering Research Center. Contract DACW72-73-C-0014).

TC203 .U581tr no. 76-3 627 .U581tr